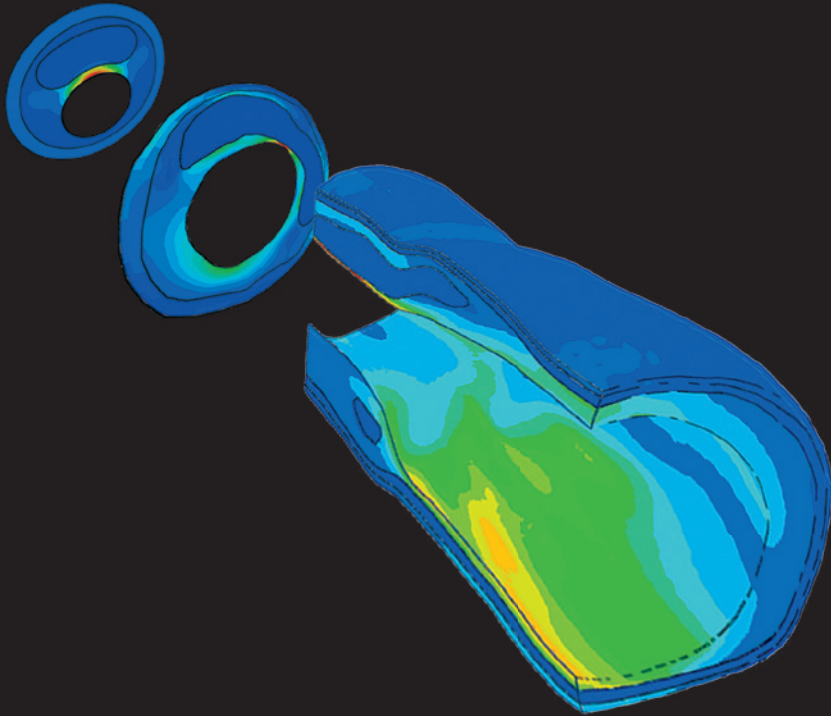# BIOMECHANICAL MODELING

OF ATHEROSCLEROTIC PLAQUES

FOR RISK ASSESSMENT

Ali Çağdaş Akyıldız

BIOMECHANICAL MODELING OF ATHEROSCLEROTIC PLAQUES FOR RISK ASSESSMENT

Ali Çağdaş Akyıldız

BIOMECHANICAL MODELING
OF ATHEROSCLEROTIC PLAQUES
FOR RISK ASSESSMENT

Biomechanische Modelvorming
van Atherosclerotische Plaques
ten behoeve van Risico Analyse

Thesis

to obtain the degree of Doctor
from the Erasmus University Rotterdam
by command of the rector magnificus
Prof. Dr. H. G. Schmidt
and in accordance with the decision of the Doctorate Board.

The public defense shall be held on
Wednesday the 23rd of October 2013 at 13.30
by

Ali Çağdaş Akyıldız

born in Istanbul, Turkey

ERASMUS UNIVERSITEIT ROTTERDAM

Doctoral Committee

Promotor: Prof.dr.ir. A.F.W. van der Steen

Co-promotor: Dr.ir F.J.H. Gijsen

Committee members: Prof.dr. A. van der Lugt

Prof.dr.ir. E.H. van Brummelen

Prof.dr. J. Dankelman

dedicated to the ones that show

empathy to all the others

List of Abbreviations

2D   Two dimensional
3D   Three dimensional
AHA   American Heart Association
AI   Alignment index
BI   Backward Incremental
CTA   Computed Tomography Angiography
ECA   External carotid artery
EE   Eindige Elementen
FE   Finite Element
FEA   Finite Element Analysis
ICA   Internal carotid artery
IVUS   Intravascular Ultrasound
IMA   Intima-Media-Adventitia
IMT   Intima-Media thickness
IS   Initial stress
IR   Ideal random
LRNC   Lipid rich necrotic core
MRI   Magnetic Resonance Imaging
ORO   Oil Red O
PFA   Preferred fiber alignment
RF   Radiofrequency
SC   Structured collagen
UC   Unstructured collagen
US   Ultrasound

Contents

Angina Pectoris

…
And let's face it
within the last ten years
the only thing I've been able to offer
to my impoverished country
is just an apple, doctor, a red apple
I call my heart.
neither <u>atherosclerosis</u>, nor nicotine, nor prison,
that's the reason, doctor, that's the reason
for this angina pectoris.
…

Nazim Hikmet (1948)

Chapter 1

General Introduction

1.1   Atherosclerosis

A healthy arterial wall comprises three layers: the adventitia, the media and the intima (Figure 1.1, left side). The adventitia is the outermost layer, mainly composed of collagen. The media underlies the adventitia and is the middle layer in the arterial wall. It is made up of concentrically arranged smooth muscle cells and collagen fibers. The intima is the innermost layer. It is a thin sheet of endothelial cells attached to a basal membrane.

Atherosclerosis is a systemic, inflammatory disease of the arterial system characterized by local thickening of vessel walls [1]. Thickened arterial segments are called atherosclerotic plaques (Figure 1.1, right side). During atherogenesis - progression of an atherosclerotic plaque- the major changes take place in the intima due to infiltration of lipids and inflammatory cells from the luminal side, smooth muscle cell migration and proliferation, extracellular matrix deposition, and intraplaque hemorrhage. From a thin cell layer, the intima transforms into a thick layer (Figure 1.1) with the possible structural components being smooth muscle cells, collagen and elastin fibers, and lipids. Besides changes in the intima, atherosclerosis causes differentiation in the media and adventitia layers. Fibrosis, atrophy and inflammation may take place in the media and adventitia during atherogenesis [2].

Clinical events induced by atherosclerosis are the major cause of morbidity and mortality worldwide [3]. In coronary arteries, atherosclerotic plaques are the underlying reason of both stable and unstable angina, and acute myocardial infarction [4]. In carotid arteries, they may lead to transient ischemic attacks
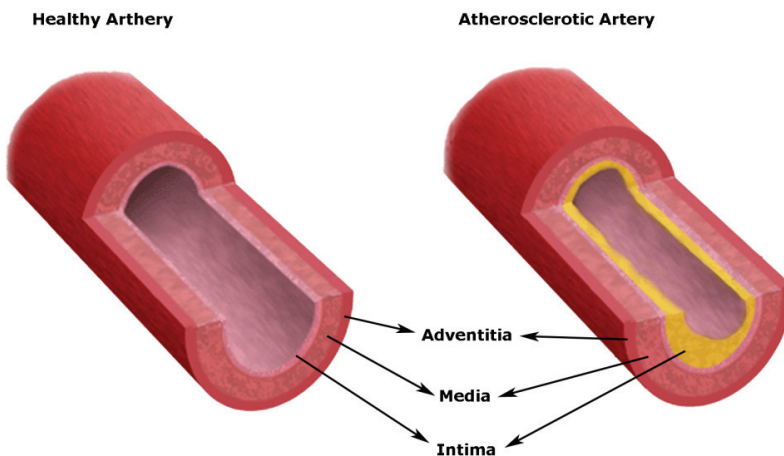

Healthy Arthery   **Atherosclerotic Artery**

Adventitia

Media

Intima

Figure 1.1: Longitudinal cross-section of a healthy (left) and an atherosclerotic artery (right)

and stroke [5], and in iliac arteries, to peripheral artery disease [6]. Each year, more than 12 million people die from cardiovascular events triggered by atherosclerosis [7].

1.2   Atherogenesis and Plaque Classification

Atherosclerosis is a progressive disease, which may start at very early ages in human life. As coronary artery disease is one of the leading causes of death [7], atherogenesis in coronary arteries were studied widely. Based on a series of post-mortem pathological studies, a classification scheme with 8 plaque types was developed by Stary and coworkers [8], and adopted by the American Heart Association (Figure 1.2, only first 6 lesion types are shown). Even though the scheme was proposed for coronary arteries, it represents the successive stages of atherosclerosis for all vascular territories.
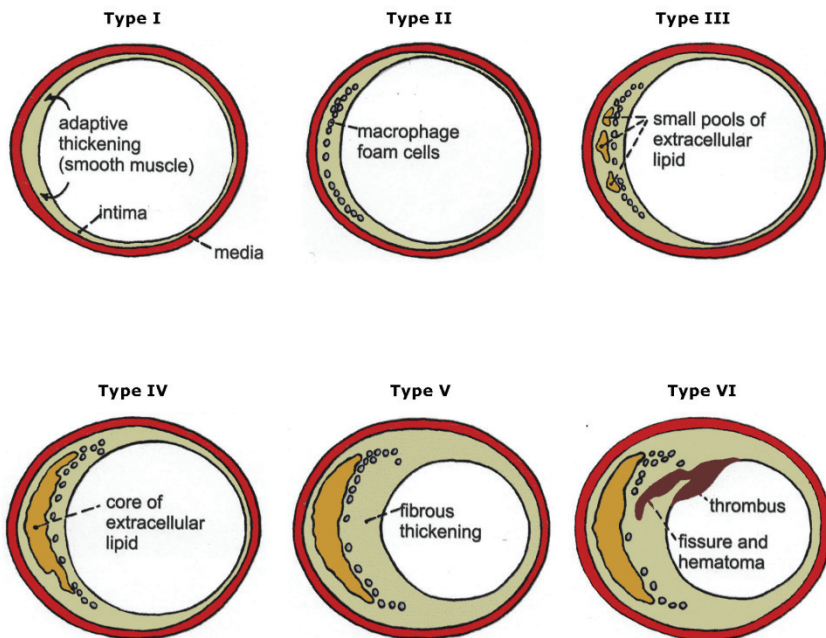
Figure 1.2: Atherosclerotic plaque classification of American Heart Association for coronary arteries. Images are adapted from [9].

Type I and II plaques are the early stages of atherosclerosis. Adaptive intimal thickening, mainly consisting of smooth muscle cells, occurs in Type I plaques. Type II plaques differ from Type I plaques by the presence of macrophages and foam cells. Type III plaques are considered as the intermediate stage of atherosclerosis. Extracellular lipids are present between the smooth muscle cells that form the main component of the pathologically thickened intima. The media

and adventitia are still largely unaffected by the disease. In Type IV (called atheroma) and Type V plaques (called fibro-atheroma), the diseased intima is characterized by the presence of a lipid rich necrotic content, referred to as lipid core or as necrotic core if death cells are present, which contains free cholesterol esters. Foam cells cover the core and a proteoglycan rich cap, often containing macrophages, separates the lipid core from the lumen. Type IV plaques do not contain excessive amounts of smooth muscle cells or collagen. Type V plaques are characterized by an increase in intima volume, mainly due to increased synthesis of fibrous tissue (primarily collagen) and smooth muscle cells. The intima might contain organized thrombi. Media and adventitia in type V plaques are often disrupted or disarranged. If a Type IV or Type V plaque develops a surface defect or intra-plaque bleeding, it is generally referred to as a ruptured plaque or Type VI plaque. These plaques might further progress into calcified plaques (Type VII), or fibrotic plaques (Type VIII) (not shown in Figure 1.2). In calcified plaques, part of the intima is fibrous with large calcifications. Underlying atheroma might still be present in these plaques. Fibrotic plaques do not contain a lipid core and are characterized by the presence of fibrous tissue.

1.3   Vulnerable Plaques and Plaque Rupture

Atherosclerotic plaques that are prone to rupture are referred to as vulnerable plaques. The acute manifestations of atherosclerosis are associated with the rupture of the cap of vulnerable plaques [10]. Cap is the part of the intima that covers the lipid core (which is also referred to as lipid pool, necrotic core or lipid rich necrotic core by the biomechanics society) and separates it from the lumen. Cap rupture exposes the lipid core of the plaque to the blood flow and triggers thrombolytic events.

As more than 70% of cardiovascular diseases are caused by vulnerable plaques, characterization of these plaques is a very active research field. Most previous studies focused on image-based identification of specific geometric plaque features, including cap thickness (e.g. [11]), lipid core size (e.g. [12]), and presence of intra-plaque hemorrhage (e.g. [13]), and investigated the association of these features with plaque rupture and vulnerable plaques.

Postmortem histopathological studies showed that majority of ruptured plagues were uncalcified and nonstenotic, and resemble Type IV plaques in the American Heart Association classification scheme [14]. These studies identified vulnerable plaques as the plaques with a relatively large lipid core and a thin fibrous cap [15-18]. However, not all plaques with these characteristics rupture. Moreover, not all ruptured plaques have these characteristics. Thus, adequate characterization of vulnerable plaques is yet not available.

From mechanical point of view, a plaque cap ruptures when the local stresses in the cap exceed the cap strength. Biomechanical models that compare cap stresses to cap strength may be of additional value for rupture risk assessment [19]. Previous numerical studies showed the correspondence of high stress regions in the cap to rupture locations [20, 21]. Therefore, even the cap stresses alone might serve as a rupture risk predictor.

1.4   Stresses in Atherosclerotic Plaques

Blood vessels and atherosclerotic plaques experience two types of loading conditions: blood pressure and shear force due to blood flow. It has been shown that shear stresses due to the blood flow are important for plaque initiation and development [19, 22, 23]. Since shear stresses are three orders of magnitude smaller than the stresses induced by blood pressure [24], their mechanical role in cap rupture is negligible and therefore, cap rupture is considered to be the result of the stresses induced by blood pressure.

Due to the complex and heterogeneous morphology of atherosclerotic plaques, obtaining plaque and cap stresses induced by blood pressure is trivial and requires advanced methods. A method frequently used to obtain plaque stresses is the finite element (FE) analysis (Figure 1.3). Assessment of the stresses in atherosclerotic plaques with FE models relies on three important parameters: accurate representation of the loading, boundary and initial conditions, geometric features of atherosclerotic plaques, and the material properties of the plaque components.

FE plaque models and stress analyses in most biomechanical studies are based on geometries obtained from histology or in vivo imaging, including magnetic resonance (MR) and noninvasive ultrasound (US) imaging for carotid arteries and intravascular US and optical coherence tomography for coronaries. In histology images, the plaque is usually pressure fixed to prevent the collapse of the lumen, and in vivo images are obtained at a certain blood pressure. Thus,
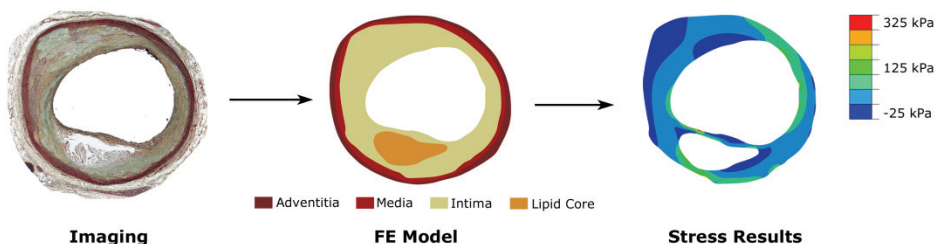

Figure 1.3: Finite element (FE) modeling of an atherosclerotic plaque to obtain plaque and cap stresses

both in vivo images and pressure fixed histology images provide a   geometry that is under an intraluminal pressure. Stresses at this initial loading state are called initial stresses. Until recently, computational models of atherosclerotic plaques neglected initial stresses since no numerical methods were available to determine initial stresses in atherosclerotic plaques.

Among many geometric features of atherosclerotic plaques, influence of cap thickness has been investigated most extensively in biomechanical studies. It was demonstrated that cap stresses increase exponentially with decreasing cap thickness [25-27].   However, large variation in cap thickness of ruptured plaques [28] indicate that cap thickness is not the only relevant geometric feature. This was illustrated in a parameter study by Ohayon et al. with idealized plaque models [29]. They showed that necrotic core size also has a significant influence on cap stresses, and might be as critical for plaque rupture as the cap thickness. Yet, studies with detailed description of plaque geometry and large numbers of geometric parameters are necessary to deepen our understanding of which geometric plaque features are risk indicators for high cap stresses.

Material properties of plaque components are also important input parameters for FE models. As the media and adventitia are less affected by atherosclerosis, it can be expected that the material properties of these layers do not differ from healthy state. On the other hand, intima transforms from a homogeneous thin layer into a heterogeneous thick layer during atherogenesis. The constituents of the intima are different for different plaque types. It is expected that the material properties of the intima strongly depends on its structure and content. Experimental studies on atherosclerotic intima properties are very limited and the reported intima stiffness values span a wide range, differing from each other by order(s) of magnitude [30-37]. The limited data compromise the reliability of finite element models. Thus, new experimental studies are necessary to reveal the material properties of atherosclerotic intima.
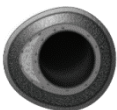
1.5   Thesis Objective and Outline

The objective of this thesis is to determine the requirements of FE plaque models to compute plaque and cap stresses for future rupture risk assessment, to establish the influence of plaque geometry and material properties on cap stresses, and to estimate the material properties of atherosclerotic plaques.

The first part of the thesis focuses on the assessment of the requirements for reliable stress computations with FE models. A numerical technique, the Backward Incremental (BI) method, is implemented in chapter 2 to compute the initial stresses and zero-pressure geometry of plaques. The effect of neglecting the initial stresses on plaque and cap stresses is investigated. Atherosclerotic plaques are 3D structures and image based plaque models generally have a relatively low axial resolution. The influence of axial sampling resolution on computed plaque and cap stresses are evaluated in chapter 3**.**

The second part of the thesis investigates the influence of plaque geometry and material properties on cap stresses. In chapter 4, effect of the plaque geometry and the intima material properties on plaque stresses is discussed, using idealized 2D plaque geometries. Influence of plaque geometry is further evaluated in chapter 5 with finite element models based on realistic plaque geometries, obtained from human coronary histology images.

The third part of the thesis focuses on the material properties of atherosclerotic plaques. First, experimental studies that investigated atherosclerotic intima properties are reviewed in chapter 6. Large range of intima stiffness reported in these studies is discussed by classifying them with respect to the loading direction and loading type applied in the experiments. In chapter 7, mechanical compressive properties of carotid plaques in axial direction are examined with a recently developed experimental technique, micro indentation combined with confocal microscopy. To investigate the mechanical intima properties in other directions, a more physiological testing technique, inflation tests, is combined with inverse FE analysis and applied to atherosclerotic iliac arteries in chapter 8. The last chapter of the thesis provides a summary and a general discussion.

Chapter 2

Initial Stress in Biomechanical Models of Atherosclerotic Plaques

2.1   Introduction

Atherosclerosis is a potentially life threatening arterial disease, in which plaques form in the vessel walls, especially in areas of low and oscillatory flow [38]. Some of these plaques develop into vulnerable plaques, characterized by thin fibrous caps, covering large necrotic cores and the presence of macrophages [39]. The caps of these plaques are susceptible to rupture, exposing the lipid-rich core to the blood, triggering a thrombolytic response. This thrombus formation can lead to instantaneous blockage of the artery and instigate a stroke or myocardial infarction [4, 40].

For atherosclerotic plaques at risk, physicians may opt for resection or balloon or stent angioplasty. Whether this is deemed necessary is nowadays mainly based on the percentage of lumen narrowing as seen on X-ray angiography for plaques in the coronary arteries [41] or based on ultrasound plaque imaging and Doppler velocity measurements in the carotid arteries [42]. Additionally, computed tomography angiography (CTA) or magnetic resonance imaging (MRI) is used to characterize plaque components and composition in 3D [43, 44]. Lumen narrowing may not be the most obvious parameter to assess the risk of cap rupture, as in most cases expansive remodeling of the vessel occurs [45]. Consequently, these vulnerable plaques are not characterized by a significant lumen stenosis before they rupture and cause an event [46, 47]. From a mechanical point of view, rupture of a cap will occur when the stresses in the cap exceed the strength of the cap. Determining stresses in the cap of atherosclerotic plaques using patient specific models may therefore be a more suitable approach to assess risk of cap rupture [25, 48]. Based on the complete geometry of the plaque, the blood pressure of the patient, and the mechanical properties of the plaque constituents, the stress in the cap can be determined using the finite element method.

Most biomechanical analyses on plaques on carotid arteries are performed utilizing non-invasive MRI data [49-52]. For coronary plaques, the geometry is mainly based on post-mortem histological data [48] or intravascular ultrasound (IVUS) [25]. During imaging or processing, the plaques were pressurized, either by the in vivo blood pressure (MRI and IVUS) or by perfusion fixating the vessel with formalin at a certain pressure prior to histological preparation [53]. This leads to a certain initial stress state, which is neglected when cap stresses are computed directly based on the measured geometry. The computed cap stresses may be affected by this limitation. A preshrinkage method has been proposed earlier [54] to shrink the in vivo plaque geometry prior to the stress calculations to estimate the zero-stress state. This method requires manual adaptations to fit

the geometry of the simulation to the geometry as derived by imaging. The Backward Incremental (BI) method was previously used to account for the effect of initial stress (IS) on the stress distribution in the wall of aneurysms [55]. This method requires no manual input and the derived geometry from the simulations closely fits the geometry as measured with imaging. The aim of the present study is to apply the BI method to atherosclerotic plaques and to identify the effect of the initial stress state on the plaque stress distributions.

2.2 Methods

2D patient-specific plaque models were created based on histological data of diseased coronary arteries. The arteries were perfusion fixed with formalin at 100 mmHg before histological preparation. In total, fifty cross-sections of 5 µm were obtained from nine different plaques, from coronary arteries of seven patients. Between the sections there was a minimum interval of 200 µm. Modified Movat pentachrome staining was performed to distinguish between plaque components (Figure 2.1, A). In the cross-sections, the lumen, necrotic core, intima, and media were manually delineated (Figure 2.1, A and B).
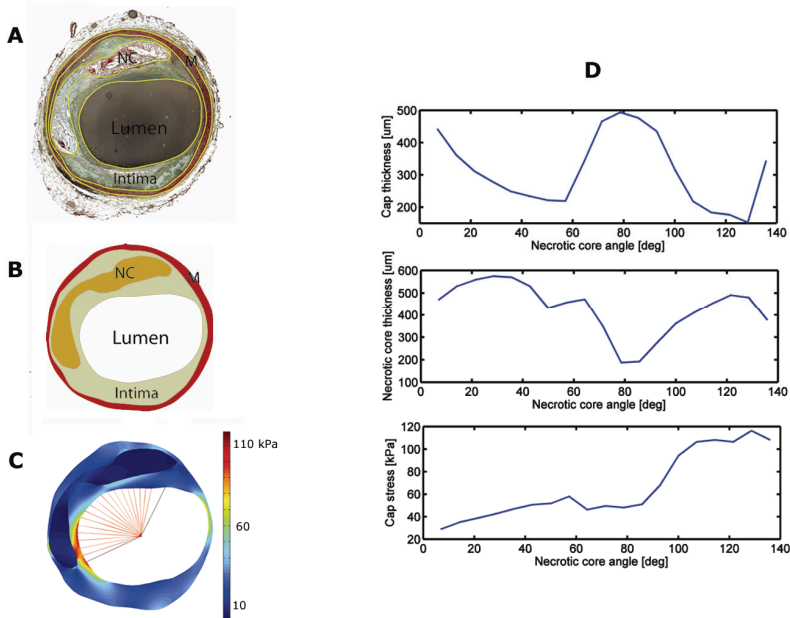

Figure 2.1: A) Histological cross-section with corresponding manual delineations of the lumen, intima, media (M), and necrotic core (NC). B) Corresponding segmentations for the finite element model. C) Typical stress map with the angular segments (red lines). D) Minimum cap thickness, maximum necrotic core thickness, and peak cap stress over all segments are determined per plaque.

If more than one necrotic core was present, only the largest necrotic core was delineated for the stress analyses, which enables the evaluation of the effect of IS with respect to geometrical features, like cap and necrotic core thickness.

Meshing of the plaques and computing the stresses were performed using Abaqus Standard 6.9 (Simulia Dassault Systems, Providence, RI, USA). Meshing was done using 4-node bilinear quadrilateral plane strain elements, and the element size was chosen such that at least three elements were present over the thickness of the cap. Rigid body motions and rotations were suppressed by partly restraining two nodes of the model. The neo-Hookean hyperelastic material model [56], given as $W=C (I_1 - 3) + (J_{el} - 1)^2/D$ was used for all components. Here, *W is* the strain energy density function, I_1 the first invariant of the deformation tensor, and J_{el} the elastic volume strain. The parameter *D* represents the amount of incompressibility of the material, and is set to 10^{-5} kPa^{-1} for all components, corresponding to almost complete incompressibility. The parameter *C* represents half of the shear modulus and is set to 250 kPa for the media, 50 kPa for the intima and 5 kPa for the necrotic core, corresponding to values previously reported in literature [30, 36, 57].

IS was computed using an in-house written Python script, based on the BI method as described previously [55]. The intraluminal pressure was increased in 15 steps to the fixation pressure of 13.3 kPa (100 mmHg). Each step, a standard stress analysis was performed and the stresses were thereafter applied node-wise as initial stress boundary condition in the subsequent pressure step. The IS was applied to the initial geometry, which implicitly ignores the deformations between the pressure steps. After the IS state was reached, a peak systolic pressure of 18.7 kPa (140 mmHg) was applied in 5 steps, and the stresses and deformations were computed. From the IS state, also the zero-pressure geometry was determined by reducing the luminal pressure to 0 kPa. Schematically, the BI method may be represented as:

$\Omega_0 = \Omega_{measured}$
$\mathbf{F}_{0,0} = \mathbf{I}$
$\boldsymbol{\sigma}_0 = 0$
for n = 1:20

$(\mathbf{F}_{n-1,n}, \delta\boldsymbol{\sigma}_n) = f(\Omega_{n-1}, \mathbf{F}_{0,n-1}, \boldsymbol{\sigma}_{n-1}, p_n, G)$
if (n < 15) then $\Omega_n = \Omega_{n-1}$
if (n ≥ 15) then $\Omega_n = \Omega_n(\mathbf{F}_{n-1,n}, \Omega_{n-1})$
$\mathbf{F}_{0,n} = \mathbf{F}_{0,n-1} \cdot \mathbf{F}_{n-1,n}$
$\boldsymbol{\sigma}_n = \boldsymbol{\sigma}_{n-1} + \delta\boldsymbol{\sigma}_n$
end for
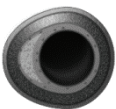
Here, Ω_n is the geometry at pressure step n, $\mathbf{F}_{a,b}$ is the deformation tensor between steps *a* and *b*, $\mathbf{I}$ is the unity tensor, $\boldsymbol{\sigma}_n$ is the stress tensor, p_n is the pressure and G represents the material parameters.The geometries at the IS state and zero pressure state were compared quantitatively by evaluating area change of the lumen area and the lumen circumferential shrinkage, as was previously defined by [54].

The peak plaque stress as computed with IS was compared to the peak plaque stress as computed with the conventional straightforward analysis without IS. Additionally, the cap of the plaque covering the necrotic core was identified and the peak cap stress was determined with and without IS. Therefore, the center of the lumen and the edges of the necrotic core were automatically detected and the necrotic core angle was defined as the angle between the lines connecting the central lumen point and each of the edges of the necrotic core (Figure 2.1, C). The necrotic core is thereafter divided in 20 segments and for each segment, the minimum cap thickness, maximum necrotic core thickness, and peak cap stress was determined (Figure 2.1, D). Per plaque, the minimum cap thickness, maximum necrotic core thickness, and necrotic core angle were determined and related to the peak cap stress, to evaluate whether the relationships between geometrical features and peak cap stress were altered when IS was accounted for. A t-test was used for comparison between groups, while a paired t-test was used when the effect of IS was evaluated plaque-specifically. A p-value < 0.05 was considered significant. All parameters were tested for normality with the Shapiro-Wilk test and none deviated significantly from a normal distribution.

2.3   Results

Figure 2.2 shows two representative examples of plaque models with the corresponding systolic geometries with and without IS. Also, the zero pressure geometry is displayed. The systolic geometries as computed without IS are clearly more inflated than with IS. The average lumen area of the histological geometries was 3.3 ± 1.6 mm^2. The systolic lumen areas with and without IS were significantly different, being 3.8 ± 1.6 mm^2 and 4.9 ± 2.2 mm^2, respectively (p<0.01). The average increase in lumen area between histological and systolic geometries was 18% ± 6% with IS, and 54% ± 14% without IS (p<0.001). The average lumen area of the zero pressure geometries was 2.2 ± 1.2 mm^2, which was 32% ± 11% smaller than the histological geometry. Figure 2.2 clearly shows the strong non-uniform lumen contour deformation between the zero pressure and histological geometries. The lengths of the lumen contours were determined and circumferential shrinkage varied between 5% and 16%, with an average of 11% ± 4%.
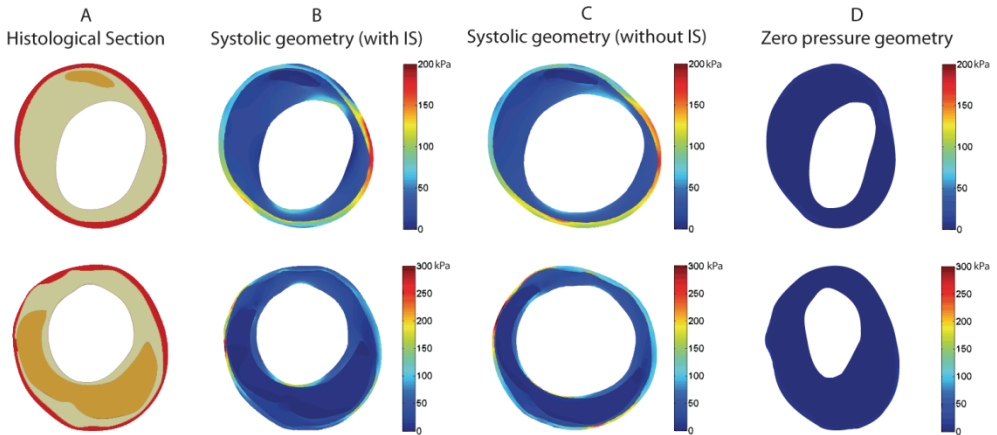
Figure 2.2: Examples of two plaque models with a small (top) and large (bottom) necrotic core. A) the histological geometries (media in red, necrotic core in orange and intima in khaki). The systolic geometries as computed with (B) and without (C) initial stress are shown with the stress colour map. D) Zero pressure geometries

Peak stress analysis

Figure 2.3 shows the percent change in peak von Mises stress due to the IS as function of the peak stress without IS for the whole plaques (Figure 2.3, A) and for the caps only (Figure 2.3, B). The change in peak plaque stress after accounting for IS varied strongly between plaques from -40% to +48% (average ± SD: +5% ± 20%). On group average, the peak plaque stress was 229 kPa (range 95 – 460 kPa) without IS and 235 (85 – 492) kPa with IS (p=0.42). The change in peak cap stress ranged from -55% to +52% (average ± SD: -4% ± 18%). The group average peak cap stress was 92 ± 63 kPa (range 22 – 318 kPa) without IS and 87 ± 56 kPa (24 – 270 kPa) with IS (p=0.09).

Geometrical analysis

The minimum cap thickness, maximum necrotic core thickness, necrotic core angle and maximum cap stress with and without IS were determined for each plaque. Figure 2.4 shows the absolute peak cap stress in relation to the minimum cap thickness without (Figure 2.4, A) and with IS (Figure 2.4, B). Cap thickness varied between 16 and 727 µm, with a median of 213 µm. The mean and standard deviation peak cap stress for the plaques with cap thickness below and above the median cap thickness are also indicated in Figure 2.4. For sections with a cap thickness below 213 µm, the peak cap stress without IS was 121 ± 71 kPa. For sections with a cap thickness above 213 µm, the peak cap stress was significantly lower at 63 ± 33 kPa (p<0.01). With IS, thin caps were still associated to higher peak cap stress, although the differences were smaller. The peak cap stresses were 105 ± 55 kPa and 66 ± 48 kPa for a cap thickness below and above 213 µm, respectively (p=0.01).
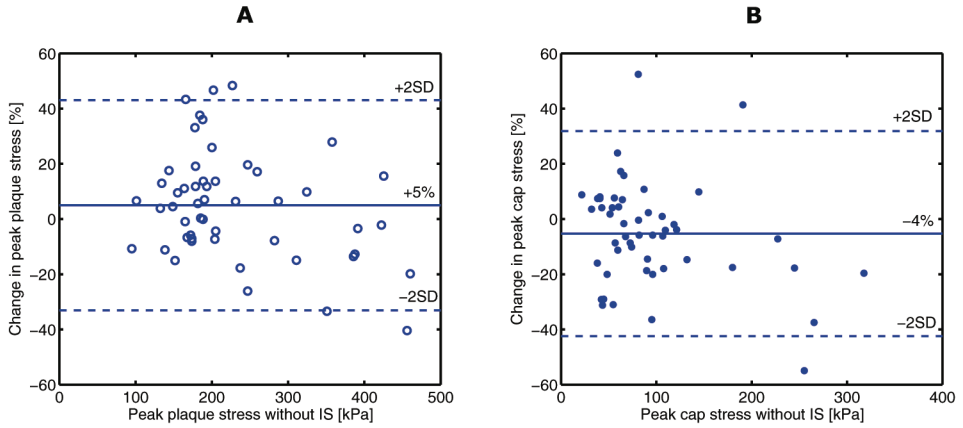
Figure 2.3: Percent change in peak stress due to the initial stress as function of the peak stress without initial stress for the whole plaque (A) and for the cap (B). The average change is indicated with solid lines and the dashed lines indicate ± 2 SD.

Figure 2.4: Peak cap stress without (A) and with (B) initial stress in relation to minimum cap thickness. Mean and standard deviations are indicated for plaques with a cap thickness below and above the median cap thickness of 213 μm, indicated with the dashed line.

Figure 2.5 displays the absolute peak cap stress without IS (Figure 2.5, A and C) and with IS (Figure 2.5, B and D) with respect to the necrotic core thickness (Figure 2.5, A and B) and the necrotic core angle (Figure 2.5, C and D). The peak cap stress for necrotic cores thinner than the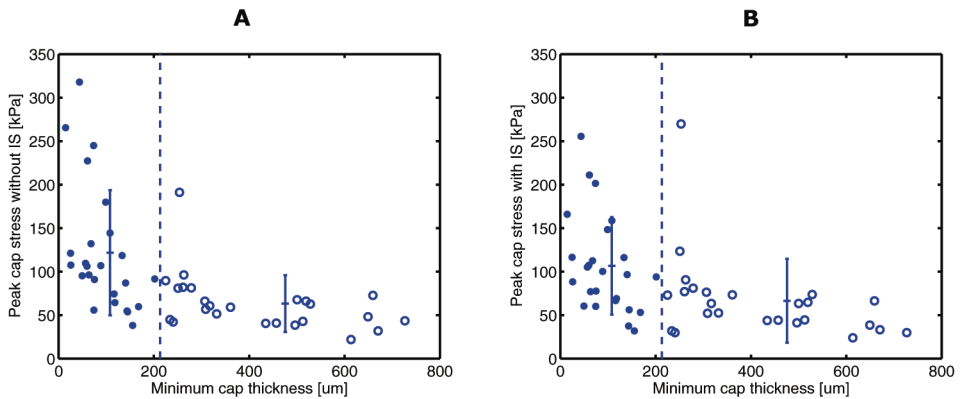 group median (499 μm) is on average borderline significantly lower than for necrotic cores thicker than 499 μm, both without (71±28 kPa versus 100±70 kPa, p-value 0.05) and with IS (76±45 kPa versus 109±73 kPa, p-value 0.06). The group median necrotic core angle is 66 °. The average peak cap stress for necrotic core angles below and above 66° are not significantly different (79±51 kPa and 105±70 kPa without IS (p-value 0.15); 80±51 kPa and 91±59 kPa with IS (p-value 0.45), respectively).
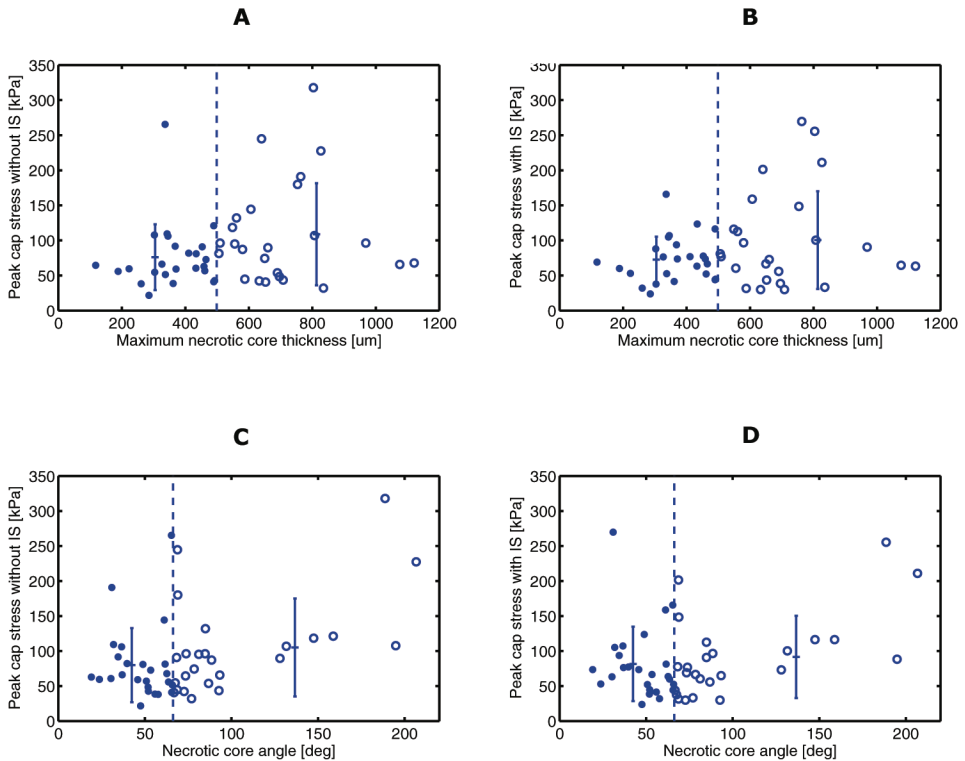

Figure 2.5: Peak cap stress without (A, C) and with (B, D) initial stress in relation with maximum necrotic core thickness (A, B) and necrotic core angle (C, D). Mean and standard deviations are indicated with a value below and above the median value as indicated with the dashed line (499 μm for necrotic core thickness, and 66° for necrotic core angle).
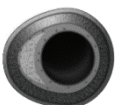
Figure 2.6 shows the percent change in peak cap stress due to IS with respect to the minimum cap thickness (Figure 2.6, A), the maximum necrotic core thickness (Figure 2.6, B) and the necrotic core angle (Figure 2.6, C). For plaques with a cap thickness below the median of 213 um, the change in peak cap stress due to IS was -10±15% (p<0.01). For caps thicker than 213 μm, the peak cap stress did not change (1±20%, p-value 0.76). A necrotic core thicker than the median thickness of 499 μm was associated with a decrease in peak cap stress (-9±17%, p-value = 0.01), while no change was found for thin necrotic cores (-1±20%, p-value 0.88). Plaques with necrotic core angles above 66° showed a decrease in peak cap stress (-12±13%, p-value < 0.01), while for necrotic core angles below 66°, the peak cap stress did not change (3±20%, p-value 0.94).

Figure 2.6: Change in peak cap stress due to IS in relation to (A) minimum cap thickness, (B) maximum necrotic core thickness, and (C) necrotic core angle. Mean and standard deviations are indicated for plaques with a value below and above the median value as indicated with the dashed line (213 μm for cap thickness, 499 μm for necrotic core thickness, and 66° for necrotic core angle).
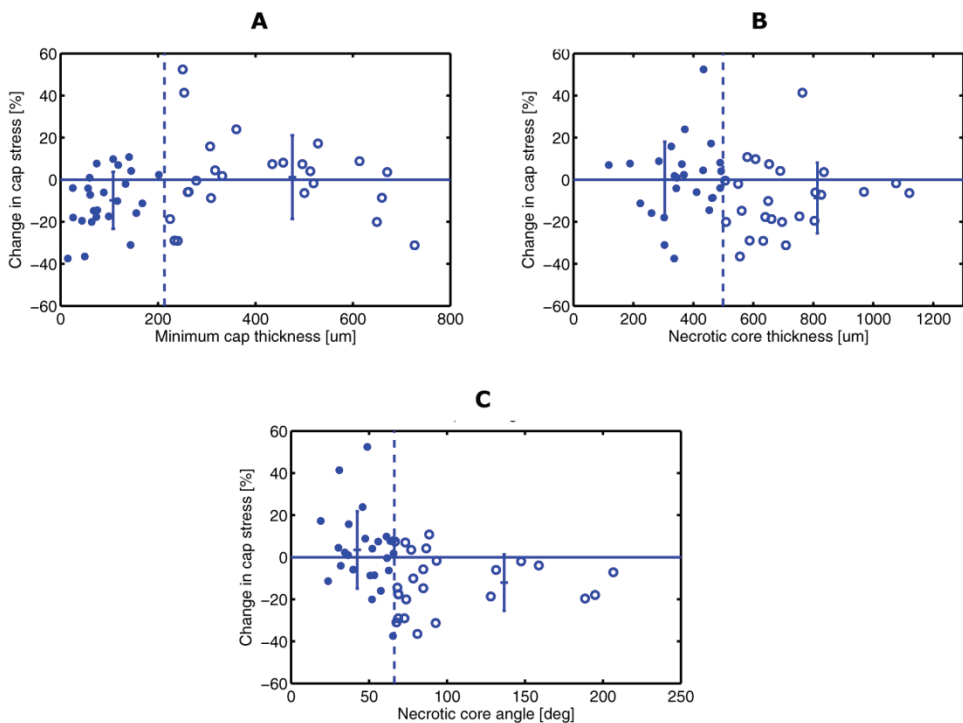
2.4   Discussion

Stress analyses on atherosclerotic plaques are more and more performed with the ultimate goal of using stress as prognostic parameter for plaque rupture. The plaque models are in most cases based on pressurized geometries and IS that are present due to the pressure are usually ignored. The results from this study show that ignoring these IS can have a different effect on the resulting stresses for different plaque geometries. Although on average the effect of IS is close to zero (+5% and -4% for the whole plaque and for the cap, respectively), a strong variation is observed, ranging from -40% to +48% for the whole plaque and from -55% to +52% for the cap.

The observed non-uniform deformation of the lumen contour from histological to zero pressure geometries impedes the use of a uniform shrinkage method, as previously proposed [54]. This method requires manual adaptations to fit the results to the IS, which may have an effect on the resulting plaque stresses. In that study, lumen circumferential shrinkage was determined based in vivo and ex vivo MRI with values ranging from -5% to +17% and average of +8 ± 6% [54]. By applying the BI method, no manual adaptations are required. Therefore, the results are more reproducible. The lumen circumferential shrinkage in the present study ranged between 5% and 16%, with an average of 11 ± 4%. Although the average shrinkage in our study is somewhat higher, the range of values coincides well.

The effect of IS on the peak cap stress showed a dependency on the cap thickness, and on the necrotic core thickness and angle. Plaques with a thin cap and a thick or wide necrotic core showed an average decrease of peak cap stress, while for thicker caps and thin and narrow necrotic cores no general change was observed. This may be explained by the fact that in the first group, the caps are more deformed when IS is omitted in the computations. When IS is incorporated, this deformation is partly suppressed, resulting in a decrease in peak cap stress. Despite the general relation between geometrical features and effect of IS on peak plaque stress, a considerable variation in effect is found. Therefore, for an individual plaque the effect of IS on the peak cap stress cannot be determined without performing stress computations with IS.

Generally, the geometrical features still have the same effect on the peak cap stress, both with and without IS. Peak cap stresses increase for thinner fibrous caps and thicker necrotic cores, as was also found in other studies [27, 29, 36]. Also for a larger necrotic core angle slightly higher peak cap stresses were found, confirming previous results [29]. This indicates that the effect of IS is
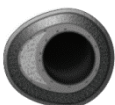
less important when geometrical characteristics are studied in relation to peak cap stresses.

Some limitations of this study need to be mentioned. First of all, only 2D models were created based on perfusion fixed histological sections. Although the effect of IS in 3D will be comparable [55], other factors may also play an important role in computing the absolute plaque stresses, like axial pre-stretch. Additionally, each 2D model was treated as an independent entity, while in fact each patient provided multiple histological slices. A minimum distance of 200 µm between each histological slice was maintained, ensuring enough geometrical variation, that the slices may be treated as independent of each other.

In the models, the adventitial layer and calcifications were not included. Especially the calcifications may play an important role in the stress distribution in a plaque [48, 58, 59], but it may be assumed that calcifications have a minor effect on the general plaque deformation pattern, and therefore on the conclusions of this study. Also the presence of any residual stresses that normally are present in arteries is neglected in the present study, as there is no adequate way to determine the residual stresses in atherosclerotic vessels.

Although small, some stresses were still present in the zero pressure geometry. For all computed zero pressure geometries, the maximum stress is in the order of 10-15 kPa, representing 3-6% of the peak stresses at systolic pressure. This may be caused by the implementation of the IS in the computations and future work will include reducing these residual stresses in the zero pressure state.

The material models of the three constituents were assumed to be isotropic and homogeneous, which is a simplification of the real mechanical behavior. As normal forward computations are performed in each pressure step, more complex models [49, 60, 61] can also be used in combination with the BI method. The advantage of using more sophisticated material models in biomechanical plaque analyses is not completely clear yet and some controversy exists on the choice of parameters used in the models. We therefore chose to use simplified material models.

2.5 Conclusion

When IS are accounted for in atherosclerotic plaque stress analyses, the general relations between geometrical features and peak cap stress remain intact. However, on a patient-specific basis, accounting for IS has a different effect on the absolute cap stress for each plaque. Incorporating IS may therefore improve the accuracy of future atherosclerotic plaque-specific rupture risk analyses based on cap stress.
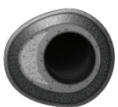
Chapter 3

Influence of Axial Image Resolution on Atherosclerotic Plaque Stress Computations

This chapter is based on:

3.1   Introduction

Atherosclerosis is characterized by plaque formation in the arterial wall [28]. Plaque rupture may lead to thromboembolism, possibly causing acute myocardial infarctions and ischemic strokes [4, 40]. Rupture prone plaques, termed vulnerable plaques, generally consist of a large necrotic core separated from the lumen by a thin macrophage infiltrated fibrous cap [15, 39].

To improve clinical decision making for medical treatment much attention has been focused on understanding vulnerable plaque rupture. The biomechanical approach treats plaque rupture as an event of mechanical failure, where stresses in the cap lead to its rupture if they exceed the cap strength [19, 26, 62, 63]. Finite element analysis (FEA) is often used to provide insight into the stress distribution in plaques and the dependence of plaque stress on morphological and geometrical factors such as cap thickness, necrotic core size, luminal curvature and microcalcifications [64-71]. In addition to contributing to understanding of plaque rupture [44], biomechanical modeling also shows potential for non-invasive identification of vulnerable plaques using novel risk-stratification criteria [72].

Reliable stress assessment using FEA critically depends on accurate reconstruction of the plaque geometry. The plaque geometry is typically obtained from a range of in vivo or ex vivo imaging methods including magnetic resonance imaging (MRI) [51, 52, 68, 73] , computed tomography (CT) [71], optical coherence tomography (OCT) [74], intravascular ultrasound (IVUS) [25, 75, 76] and histology [48, 64, 77-79]. In the case of 2D FEA simulations, plaque components are delineated in cross sectional images, and a plane strain analysis is performed. For 3D simulations, cross sectional images are predominantly obtained from MRI volume data which typically consist of anisotropic voxels with an in-plane resolution being in the order of 5 - 10 times higher than the axial resolution (voxel dimensions of 0.2 - 0.6 mm in-plane vs. 1 mm - 2 mm axial) [80]. The 3D geometry is reconstructed by axially stacking cross sectional segmented contours with a distance which will be referred to in this study as the axial sampling resolution. For contours derived from volume image data, the axial sampling resolution is equal to the axial voxel dimension while for contours based on histology it is equal to the slice distance. Upon stacking the contours, interpolation is used to generate the 3D arterial geometry.

This study aims to quantify the influence of axial sampling resolution on computed peak plaque and cap stresses using FEA. This will be done by performing stress simulations on a set of histology based atherosclerotic arterial segments. Each segment will be reconstructed in 3D using a high axial
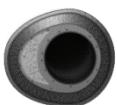
resolution and a low axial resolution. For each segment also 2D simulations will be performed and compared to the 3D models.

3.2   Methods

<u>Histology and segmentation</u>

To investigate the influence of axial sampling resolution on computed stresses, we needed a data set of diseased arteries with a sufficiently high resolution that can serve as a gold standard. We used a histological set of human coronary arteries with an axial slice distance of 0.5 mm. We selected 4 arterial segments with a length of 3 mm (7 slices). The selection criteria were such that each segment had at least one large necrotic core and at least one thin cap. Before sectioning, the arteries were decalcified and perfusion fixated with formalin at 100 mmHg and stained with a Movat pentachrome staining to enable segmentation of the plaque components. Manual segmentation of the lumen, necrotic cores, media and adventitia layers was performed (Figure 3.1).
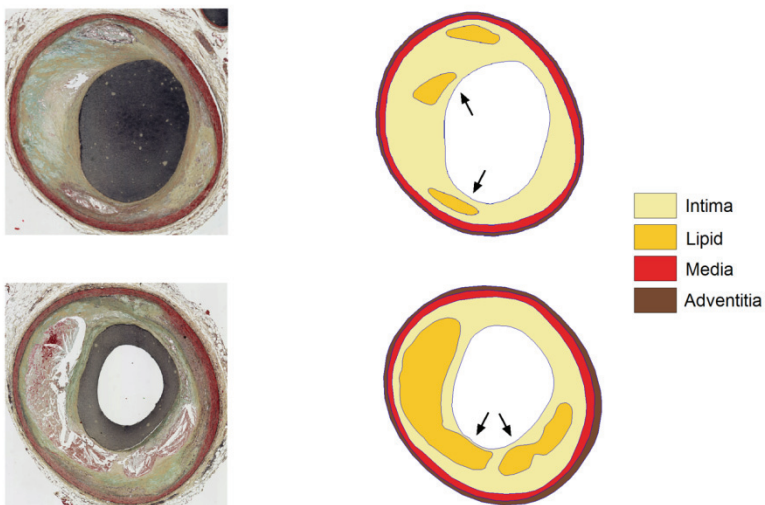
Figure 3.1: Histological cross sections and their delineated contours. Cap regions are indicated by black arrows.

<u>Geometry reconstructions</u>

To reconstruct the 3D geometries, the slices were stacked vertically by alignment of the luminal center of gravity. For each arterial segment, a reference geometry using all 7 histological slices spaced 0.5 mm apart was created, referred to as the high sampling (HS) model. A low sampling (LS) geometry was created to mimic the in vivo imaging situation which had only 4 slices spaced 1.0 mm apart. The most extreme case of low sampling would be the use of only a single slice, thus resulting in a 2D formulation. To investigate

and compare results of this lowest possible sampling resolution to the HS models, four 2D models were created from the same four slices used for the LS geometry (Figure 3.2). Non-uniform rational basis spline interpolation in Gambit (Fluent Inc., ANSYS, Canonsburg, Pennsylvania) was used to interpolate between slices. To avoid reading out values at the boundary of the simulated domain, an additional top and bottom end slice were added to each 3D model before geometrical interpolation.
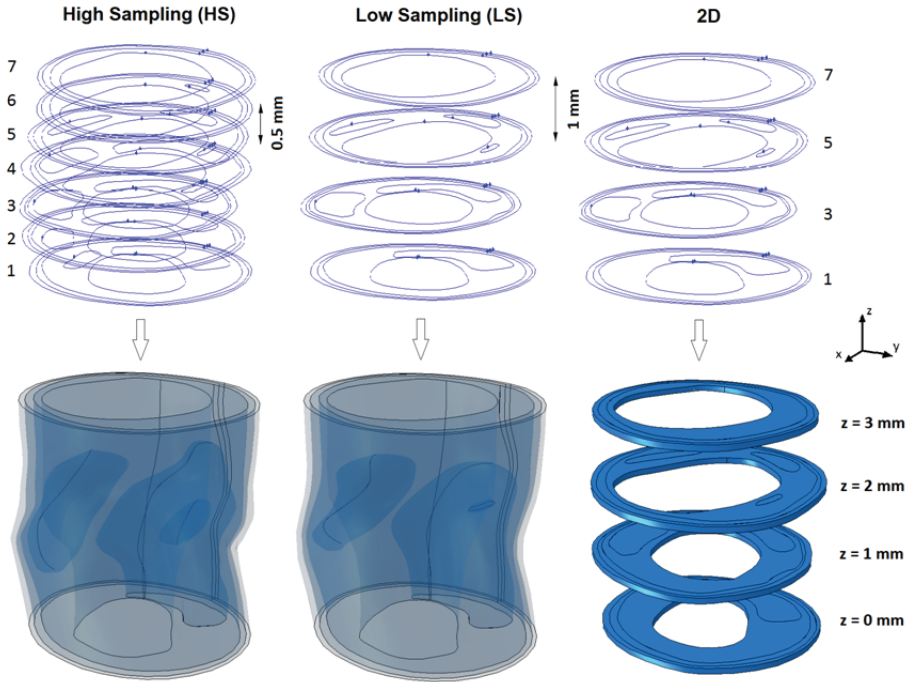
Figure 3.2: Geometry reconstruction procedure (segment 4 used as example). Contours shown in top panel result in the models in the bottom panel. HS uses all 7 histological cross sections (slice distance 0.5 mm) to re-create the 3D artery geometry, whereas for LS only 4 cross sections are used. 2D simulations are performed on the same 4 cross sections as used for LS.

Material properties and computational analysis

All tissues were assumed to be homogeneous, hyperelastic and incompressible. The intima and lipid core tissues were assumed to be isotropic and modeled with the Neo-Hookean material model. The media and adventitia tissues were modeled with an anisotropic material model [81]. The same material constants were used as in Akyildiz et al. and are listed in Table 3.1 [64].
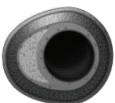
Table 3.1: Material constants of the plaque components

Tissue type	Material Constant(s)
Media	μ = 2.24 kPa, k_1 = 65.76 kPa, k_2 = 76.87, ϕ = 50.89° and κ = 0.27
Adventitia	μ = 5.86 kPa, k_1 = 2069.42 kPa, k_2 = 394.28, ϕ = 52.54° and κ = 0.20
Lipid	C = 0.167 kPa
Intima	C = 167 kPa

All FEA were performed using Abaqus (Version 6.11.1, Dassault Systèmes Simulia Corp., Providence, RI, USA). The models for the 2D simulations were meshed with four-node linear hybrid elements (~100.000 elements). For 3D simulations, four-node linear hybrid tetrahedral elements were used. All 3D meshes were created using an iterative adaptive remeshing procedure allowing for small elements in high stress regions while keeping the total mesh size below 2 million elements. All models contained at least 3 layers of elements in every thin cap and yielded mesh independent solutions. The initial stress was calculated using the Backward Incremental method [78, 82]. A static intraluminal pressure of 15 kPa (~110 mmHg) was applied as the loading condition for all models. The 2D models were based on a plane strain assumption whereas the boundary conditions for the 3D models consisted of restraining the z-component of the deformation at the axial boundaries.

Analysis

The maximum principal stress, stress-P1 [kPa], was used as the stress scalar quantity in this study [51]. Quantitative comparisons were performed only at cross sections matching the slices used to create the HS models. Four out of seven of these slices are shared in all models (HS, LS and 2D) while the other three represent interpolated cross sections for the LS models and do not occur as 2D models (Figure 3.2). The peak plaque stress refers to the maximum stress in a cross sectional plane at a particular z-height. The peak cap stress specifically refers to the maximum stress in a cap region in a plane. Computed stresses for HS were compared to LS and 2D cases using Bland Altman plots which plot the relative difference (in %) as a function of the mean of two values. Mean slice curvatures in the z-direction (axial) were numerically calculated from the 3D FEA mesh, by inverting the radius of the osculating circle through 3 vertically interpolated aligned mesh nodes around the slice and averaging for the entire lumen wall circumference. A non-parametrical 1-tailed Mann–Whitney U test was used for comparison between groups of data where a p-value lower than 0.01 was considered significant.

3.3   Results

Qualitative stress distribution

Longitudinal stress plots are shown in Figure 3.3. Within the reference geometry of each arterial segment, the HS case, we found a highly heterogeneous stress distribution along the luminal wall. High stresses were found in the cap regions, regions of high luminal curvature and in thin vessel walls at the plaque shoulder areas. Low stresses were found in the soft necrotic cores and at thick intima regions. Overall peak stresses varied largely, from 205 kPa (segment 1) to 380 kPa (segment 3). When observing the LS cases, we first noticed axial smoothing of geometrical plaque features (indicated by the white arrows) leading to local vessel wall thickening or thinning. From a qualitative perspective, lower axial sampling did not appear to influence the general stress distribution except for the case of segment 3 (grey arrow). At this location, local geometrical changes were observed in both the curvatures of the geometrical plaque features and in the thickness of the arterial wall.
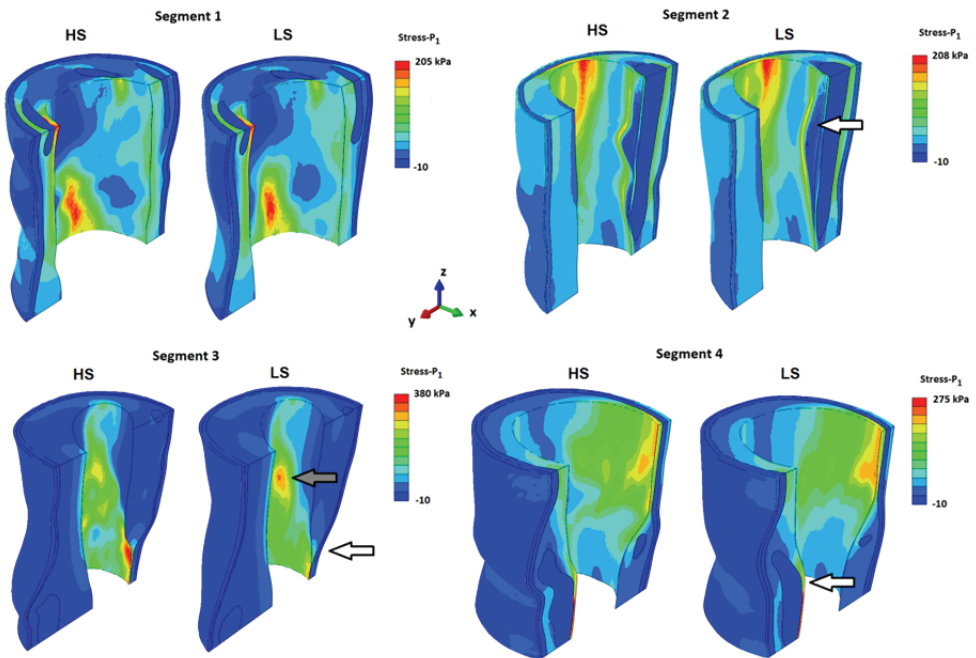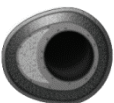

Figure 3.3: Plaque stress-P_1 distribution shown on longitudinal cuts through each segment for the HS and LS case. Arrows mark regions of interest.

Peak plaque stress

An example of the stress distribution in a shared cross section is shown in Figure 3.4. The cross section contained one necrotic core with a thin cap leading to a highly heterogeneous stress distribution. The peak plaque stress was found in a region where the in-plane luminal wall curvature is relatively high and the vessel wall is thin. For lower sampling, the qualitative stress distribution and the location of peak plaque stress remained the same. The computed magnitude of the peak plaque stress was influenced however by lower sampling: for LS the peak plaque stress was higher (186 kPa vs. 180 kPa) and for 2D also higher (195 kPa vs. 180 kPa). We observed a similar trend for all other cross sections: the qualitative stress distribution, as well as the location of peak plaque stress, was unaffected by lower sampling, but the magnitude of peak plaque stress was significantly influenced. In Figure 3.5, plots show the relative difference of peak plaque stress computed from the HS model from that of both the LS and 2D models as a function of their averaged value. For the 16 shared cross sections from LS geometries, the magnitude of the peak plaque stress compared to that of the HS models deviated +4.9 ± 11.9% (p=0.34, range [-8%, +34%]). For the 12 interpolated cross sections from the LS geometries the difference with the HS geometries was larger: -9.7 ± 12.1% (p=0.29, range [-30%, +15%]). For the 16 2D cases the difference was +1.2 ± 19.8% (p=0.46, range [-33%, +47%]). The mean in the latter case was small, which indicates that there was no systematic bias. Although statistical tests showed no significance, the error and range (19.8% and 47% respectively) were large, indicating a significant decrease in the accuracy of calculated peak plaque stresses when performing 2D simulations instead of 3D HS.
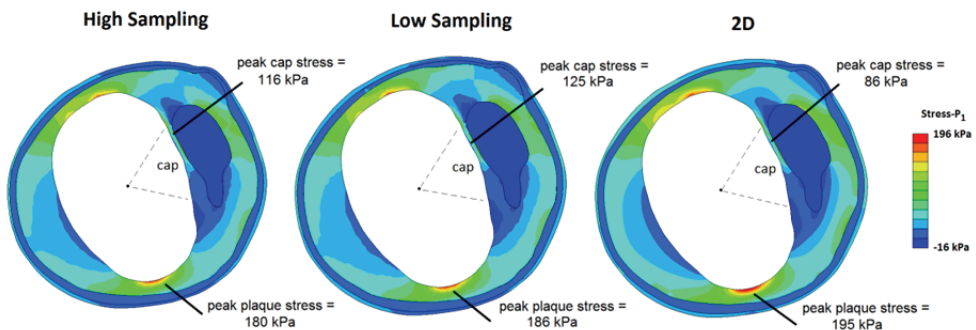
Figure 3.4: Example of a cross sectional stress distribution resulting from all three sampling cases (slice 7 from segment 2, cap thickness 44 μm)

A

B

C
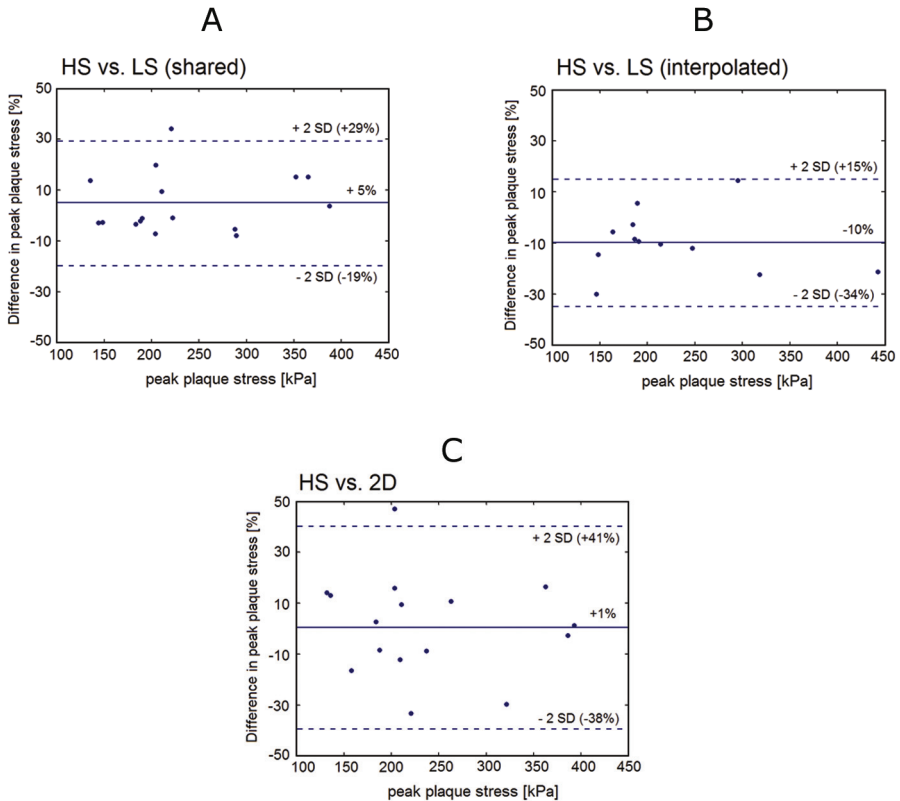
Figure 3.5: Bland Altman plots showing the relative difference in peak plaque stress for shared slices of LS compared to HS (A), interpolated slices of LS to HS (B) and 2D to HS (C) as a function of the average peak plaque stress

Peak cap stress

The magnitude of the peak cap stress in the example cross section in Figure 3.4 also changed for lower axial sampling. For LS, the peak cap stress was 8% higher (125 vs. 116 kPa) and for 2D it was 26% lower (86 kPa vs. 116 kPa). This again followed the general trend that the accuracy of the calculated peak cap stress significantly decreased for lower sampling, but without a clear systematic bias. In Figure 3.6, the relative difference in peak cap stress is plotted as a function of cap thickness for all caps present in the shared cross sectional slices studied. From the 17 cap regions identified, it was found that the peak cap stress in the LS case deviated +6 ± 15.5% (p=0.37, range [-17%, +34%]) from the HS case, and in the 2D case it deviated -1.2 ± 24.0% (p=0.45, range [-41%, +50%]). As seen in the plots, minimum cap thickness is not a predictor of whether LS models will either under- or overestimate the peak cap stress, but as the right graph in Figure 3.6 shows, smaller cap thicknesses lead to a larger range in errors in calculated stresses for 2D models.
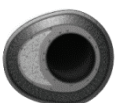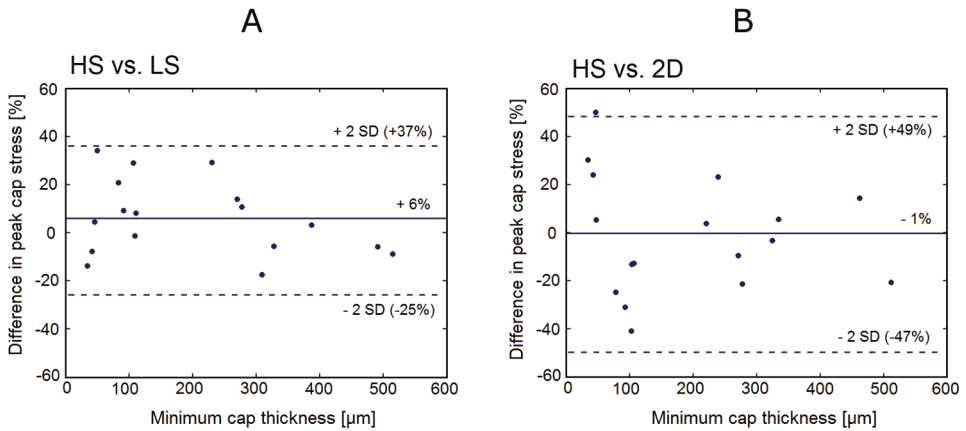
Figure 3.6: Relative difference in peak cap stress for shared slices of LS compared to HS (A), and 2D compared to HS (B) as a function of minimum cap thickness

Cap thickness – Peak cap stress relationship

Although lower sampling caused significant changes in the absolute magnitude of peak stresses, we questioned whether parametrical relationships, such as the relationship between peak cap stress and minimum cap thickness, were influenced by lower sampling. In Figure 3.7, we plot this relationship for the HS, LS and 2D models, which reveals that the relationship was unaffected by lower sampling. For thin caps (mean thickness of 71 µm), the mean peak cap stress for HS was 139 ± 57 kPa and for thick caps (mean thickness of 349 µm) 62 ± 27 kPa (p<0.01). For LS, this same change was observed: thin caps 120 ± 42 kPa and thick caps 60 ± 19 kPa (p<0.01). Finally, for 2D simulations there was also a significant difference between both groups: thin caps 123 ± 44 kPa and thick caps 61 ± 26 kPa (p<0.01).
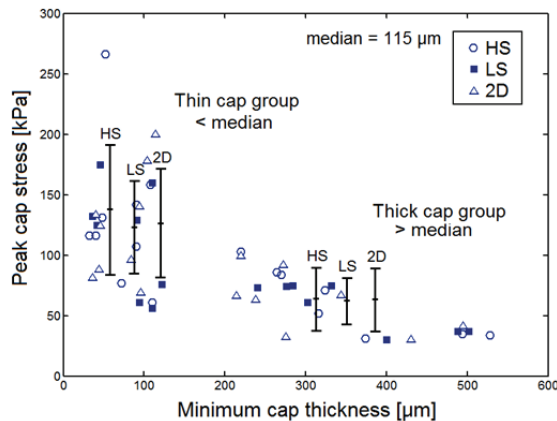
Figure 3.7: Peak cap stress as a function of minimum cap thickness for all three sampling cases

Luminal wall curvature – Peak plaque stress relationship

To gain insight into why lower sampling leads to a wide, but unbiased, spread in peak plaque and cap stresses, we quantified the effect of axial sampling resolution on average luminal wall z-curvature per cross section studied. Luminal wall axial curvature was chosen since it is the most obvious parameter influenced by axial sampling resolution. In Figure 3.8 shows the computed difference in average luminal z-curvature per slice between HS and LS geometries against the difference in computed peak plaque stress. Slice mean luminal z-curvature magnitudes were found to be in the range of $1.4\text{-}3.9\text{x}10^{-4}$ μm^{-1} (mean $2.4\text{x}10^{-4}$ μm^{-1}), which are a factor 10 lower than typical in plane (x, y) curvatures (found to be in the order of $1\text{x}10^{-3}$ μm^{-1}). Comparing LS to HS, the mean difference in curvature was -8 ± 34%, range [-51%, +70%] which indicates that luminal wall z-curvature on average tends to decrease for lower sampling. However, a positive or negative change in luminal wall z-curvature could not be correlated to an under- or overestimation in peak plaque stress.
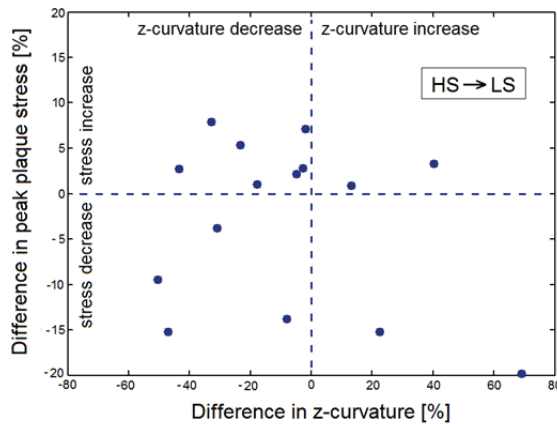
Figure 3.8: Difference in peak plaque stress as a function of difference in slice mean luminal wall z-curvature when comparing LS to HS

3.4   Discussion

Biomechanical FEA is an increasingly used method to study vulnerable plaque rupture risk [19], thus it is vital that its constituents and their effects on model outcomes are well understood. This study focused on the geometry reconstruction step and quantified the influence of axial sampling on peak stresses. Results showed that lower sampling had a small influence on the qualitative stress distribution in plaques and on the location of peak stresses. The 3D qualitative stress distribution was found to be unaffected, suggesting that an axial sampling resolution of 1 mm is sufficient to capture the general
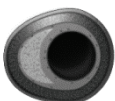
geometrical features of atherosclerotic arterial segments. However, regarding the accuracy of calculated peak cap stresses, lower sampling did have a profound influence. Although lower sampling did not lead to a systematic bias in computed peak cap stresses (+6% and +1% for HS vs. LS and HS vs. 2D), it did lead to a larger error in calculated values (15.5% for HS vs. LS up to 24.0% for HS vs. 2D).

In order to understand the geometrical changes induced by lower sampling and their correlation with over- or underprediction of peak stresses, geometrical analyses were performed. While lower axial sampling led to geometrical axial smoothing, a decrease in axial curvature failed to correlate with lower peak stresses as would, at first hand, be expected from a mechanical perspective. Furthermore, the cap thickness turned out to be an inadequate predictor for a bias in computed peak stress differences. It was also observed that lower sampling models did not include some small necrotic cores and other local morphological plaque features present in HS models, due to the resolution limit of 1.0 mm. It can be noted that LS models typically lead to an underestimation in lipid core axial length, illustrated in Figure 3.2. This underestimation can be up to 1 slice distance (1.0 mm) and could be significant if the missed geometrical information revealed a thin cap. With regard to spline interpolation, lower sampling can lead to both a locally thinner or thicker cap or vessel wall and a higher or lower axial curvature, either increasing or decreasing peak stresses. Combined, these geometrical effects lead to a complex interplay of parameters altered by lower sampling which causes a larger, but unbiased, error in computed peak stresses in shared slices. This error was larger for interpolated slices, implying that stresses in solely non-interpolated cross sections should be considered for 3D plaque stress computations.

The most extreme form of under sampling would be the use of single slice information, thus resulting in a 2D model. The comparison of 2D models with 3D resulted in the observation that absolute stress values from 2D simulations deviated significantly from the HS models, up to 48% for peak cap stresses. In a study by Ohayon et al., a similar discrepancy in peak stress was found when comparing 2D simulations to 3D based on intravascular ultrasound data from one coronary arterial segment [83]. Biased stress overprediction and difference in peak stress location for 2D models in that study could be attributed to the use of a fine and a coarse mesh for 2D and 3D models respectively, whereas our study employed a similar mesh density for both models. An additional difference is that this study used decalcified tissue, which might be a smoothing factor. Although the 2D to 3D model comparison is valuable for this particular study on axial sampling resolution, it is impotant to note that this comparison cannot be

translated directly to in vivo 2D and 3D stress simulations. This is because this study did not take any circumferential or axial residual stresses for 3D and 2D models into account. Residual stresses have been shown to have a crucial impact on peak plaque and cap stresses as well as on comparisons between 2D and 3D models [79, 84, 85]. Residual stresses are thus a vital constituent for accurate plaque stress modeling in vivo. Unfortunately, residual stresses are currently unobtainable from in vivo data used for non-invasive FEA-based plaque vulnerability studies for which this study would be of relevance [19]. To truly investigate the outcome of 2D and 3D model comparisons w residual stresses using more than one arterial segment should be subject of further studies.

This work showed the possibility of using histology for 3D biomechanical plaque models, allowing contours based on a high axial and in-plane resolution and enabling the inclusion of thin media and adventitia layers, all in contrast to using in vivo imaging data such as MRI. The use of histology, however, also led to certain limitations of this study. Decalcification was applied during histological processing and therefore, our study could not include macro- or microcalcifications into the models. The possible effects of decalcification on the outcome of this study remain unknown and should be investigated in future research by for instance utilizing additional micro-CT imaging. It has been shown that the presence of microcalcifications in the cap can increase the peak cap stress 2 to 5 fold, which is significantly larger than stress magnitude changes reported in this study [70, 71]. A minimum axial resolution of 6.7 µm would be required for adequate reconstruction of microcalcifications to evaluate their effect on local peak cap stresses [71]. This resolution is beyond the currently available non-invasive imaging modalities. In case of microcalcifications, the results of this study still provide valuable insight into the cap background stress. Furthermore, axially aligned stacking of the cross sectional contours neglected the lumen centerline curvature, which might influence results. However, it is reasonable to assume that this curvature is low compared to axial changes of geometrical plaque features and is thus of little influence on the plaque stresses.

3.5   Conclusion

Axial sampling resolution was found to have a minor influence on general stress distributions and on the peak plaque/cap stress locations. The relationship between peak cap stress and minimum cap thickness was found to be unaffected by lower sampling. Lower sampling did, however, have a major influence on the accuracy of the computed magnitude of peak plaque/cap stresses. Therefore, it can be concluded that high sampled 3D models are required for accurate plaque vulnerability assessment using stress magnitude as a measure for rupture risk.
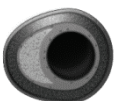
Chapter 4

Effects of Intima Stiffness and Plaque Morphology on Peak Cap Stress

4.1   Introduction

Atherosclerosis is a cardiovascular disease that is characterized by local thickening of the vessel wall, or plaque formation. A subset of atherosclerotic plaques, called vulnerable plaques, is characterized by lipid accumulation in the vessel wall, with a thin fibrous cap separating the necrotic core from the lumen (Figure 4.1) [39]. Rupture of the cap of a vulnerable plaque in a coronary artery is the underlying cause of the majority of acute myocardial infarctions and sudden coronary deaths [4, 86].

Rupture of a cap occurs when the mechanical stress in the cap exceeds its strength. The determinants of the stress distribution in a plaque are the loading conditions, the plaque geometry and the material properties of the plaque constituents. Variations in these factors affect the stress values and the stress distribution in the cap significantly. Therefore, detailed investigations of these features are essential to reveal biomechanical risk factors for plaque rupture.

The possible role of local mechanical stress as a predictor for plaque rupture [63, 87, 88] instigated many studies to explore the effects of various geometric plaque features on the cap stresses. Some studies concentrated on real plaque geometries obtained from intravascular ultrasound [25, 89], magnetic resonance
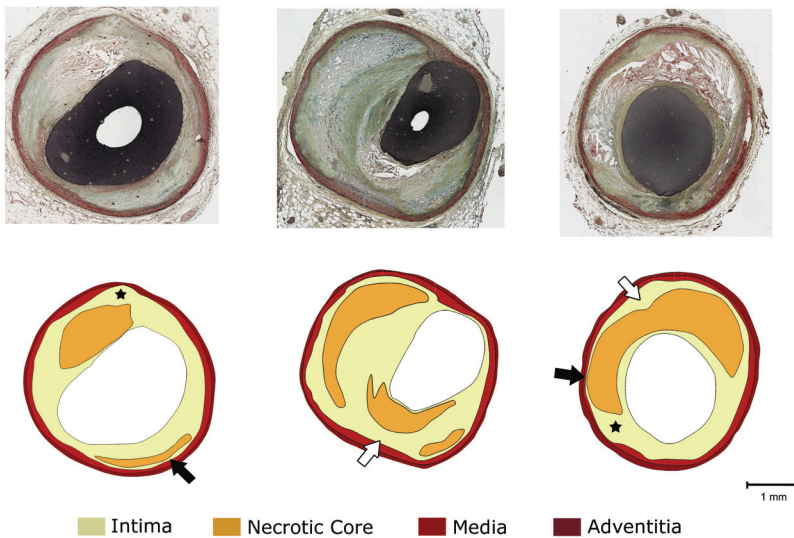

Figure 4.1: Examples of coronary artery plaques having different geometric features: histological cross-sections (upper panel), and corresponding color-coded, manually drawn contours (lower panel). White arrows indicate a thick layer, black arrows indicate a thin layer of intima between the media and the necrotic core. Black star shows media degradation.
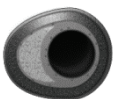
[85, 90], or histology images [20, 21, 48, 91, 92] whereas others used idealized geometries [26, 29, 76, 93]. The influence of the cap thickness has been investigated most extensively. In several computational studies, it was demonstrated that the stresses in the cap increase exponentially with decreasing cap thickness [26, 85, 89]. However, the large variation of cap thickness of ruptured plaques [28] indicates that cap thickness is not the only relevant geometric plaque feature. This was illustrated in a comprehensive parameter study by Ohayon et al. [29]. They showed that the size of the necrotic core also has a significant influence on cap stresses, and speculated that the thickness of the lipid core may be as critical for plaque rupture as the cap thickness.

It is likely that besides cap thickness and necrotic core thickness, other geometric features play a role in plaque rupture. Structures behind the necrotic core, including intima, media and adventitia tissue, might influence cap stresses as well. These plaque components have diverse morphological structures. The thickness of the intima tissue can vary greatly. Some necrotic cores are separated from the media by a thick layer of tissue, while others almost touch the media (Figure 4.1). The thickness of the media also shows great variation: at some locations, the media is severely compromised or even completely degraded (Figure 4.1).

The material properties of plaque components are determined by their composition, which might vary greatly among different plaques. The intima tissue is especially heterogeneous: it consists of extracellular proteoglycan-rich matrix material, smooth muscle cells, inflammatory cells, collagen etc. [28]. Since these components are present in different amounts in different plaques, the material properties of the intima tissue may vary greatly. Experimental studies on atherosclerotic plaque material properties have mostly reported high intima stiffness with the Young's moduli (E) between 500 kPa and 1000 kPa, even up to 2300 kPa [31, 34, 35, 76, 94-96]; E=1000 kPa has frequently been used in the numerical studies [20, 25, 26]. However, Lee et al. measured much lower E values: an average of 41 kPa for the nonfibrous and 82 kPa fibrous atherosclerotic intima tissues [97]. This finding has been supported by a recent study that used an advanced testing method and reported a mean E value of 33 kPa[30].

The aim of our study was to investigate the influence of the variation of intima material properties and of geometric variations of different plaque components on cap stresses. A parametric study was carried out to explore the individual and combined effects of possible biomechanical determinants of plaque rupture.

4.2   Methods

Two dimensional (2D) idealized geometries of varying cap thickness, necrotic core thickness and angle, intima thickness behind the necrotic core, adventitia thickness, and local regression depth in the media tissue were generated to mimic the different geometric features of atherosclerotic plaque cross-sections. Different stiffness values for the intima were used in the models such that the stiffness range reported in literature [30, 31, 34, 35, 94, 96, 97] was covered to explore its influence on peak cap stress.

Idealized geometries

The symmetric idealized baseline geometry (Figure 4.2.A) was constructed based on in vivo imaging studies [15, 25, 26, 98-101] and morphometric analysis of histology images obtained from 10 atherosclerotic human coronaries. The structure comprises five different geometric components: cap, necrotic core, intima, media and adventitia. The cap was defined as the region of the intima separating the necrotic core and the lumen. By varying the geometric parameter values (Table 4.1) a large set of different 2D idealized plaque models was obtained. The lumen diameter was kept constant in all models. The thickness of each geometric component, except the media layer, was altered uniformly. The thickness of each geometric component, except the media layer, was altered uniformly. The media layer of an atherosclerotic plaque often shows local regression rather than uniform thinning. To model local media regression (Figure 4.1, black star), the thickness of the media layer was reduced at the center or shoulder region (Figure 4.2.B).The necrotic core angle was defined as given in Figure 4.2.A.

Figure 4.2: Left: A computational model showing different geometric structures. α= Necrotic core angle, a= Adventitia thickness, b= Media thickness, c= Intima thickness behind the necrotic core, d= Necrotic core thickness, e= Cap thickness. Right: A model with local media regression in the center. (S= Shoulder, M= Midcap)
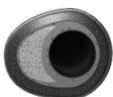
Material properties

Four different tissue types were used as plaque constituents: intima, necrotic core, media, and adventitia. Intima material properties were also applied to the cap. All tissue types were assumed to be incompressible and homogenous.

For the intima and necrotic core, the neo-Hookean material model [56] was employed, which is defined by the strain energy density function $W_{NH}=C(I_1-3)$, I_1 being the first invariant of the left Cauchy-Green tensor. The only material constant in the model is C [N/m^2]. For small deformations, C can be derived from the Young's modulus, E [N/m^2], by $C=E/6$. In the remainder of this paper, we will report E values to facilitate the comparison with E values in literature.

Table 4.1: Baseline values and ranges of the geometric features used in computational models. Thickness of all sections but the media was altered uniformly. For the media section, the values are the thickness values at the location of media regression.

Geometric feature	Baseline Value	Value Range (:Increment)
Lumen radius	1.25 mm	-
Cap thickness	0.05 mm	0.05 - 0.25 (:0.05) mm
Necrotic core thickness	1.20 mm	0.60 - 1.40 (:0.2) mm
Necrotic core angle	30°	10° - 40° (:10°)
Thickness of intima behind the necrotic core	0.50 mm	0.30 - 0.70 (:0.1) mm
Media thickness	0.25 mm	0.05 - 0.25 (:0.05) mm
Adventitia thickness	0.15 mm	0.10 - 0.20 (:0.05) mm

Since the intima can be relatively thick, the choice for its properties is especially important. To cover the wide intima stiffness range reported in literature, three different shear moduli for the intima were used in the current study: a high value (E=1000 kPa) [31] to mimic stiff intima experimental results, a low value (E=33 kPa) [30] for soft intima experimental results and an intermediate value (E=500 kPa). The models generated using these three different intima stiffness values were labeled as stiff, intermediate and soft intima models. The isotropic neo-Hookean model was used for the intima since anisotropic, nonlinear material parameters for atherosclerotic human coronary intima are not available yet. The necrotic core was modeled as a very soft tissue (E=1 kPa) [36].

For the media and adventitia, the anisotropic material model of Gasser et al. [81], which describes the strain energy density function for a composite material reinforced by two families of fibers, was used:

$$W_{aniso} = \mu(I_1-3)+k_1/k_2[\exp(k_2[\kappa(I_1-3)+(1-3\kappa)(I_4-1)]^2]-1$$

where μ, k_1, k_2 and $\kappa \in [0,1/3]$ are the model parameters. The model parameter values were obtained by fitting the material model to the experimental human coronary data [96] with the help of MATLAB (R2006b, The Mathworks Inc.). I_1 and $I_4=\lambda_\theta^2\cos^2\varphi+\lambda_z^2\sin^2\varphi$ are invariants with φ being the angle between the fibers and circumferential direction in the individual layers. All material parameter values used in the present study are listed in Table 4.2.

Table 4.2: Material constants of the plaque components

Tissue	Material Constants
Media	μ=2.24 kPa, k_1=65.76 kPa, k_2=76.87, φ=50.89° and κ=0.27
Adventitia	μ=5.86 kPa, k_1=2069.42 kPa, k_2=394.28, φ=52.54° and κ=0.20
Necrotic core	E= 1 kPa
Intima	E_{stiff} = 1000 kPa, E_{inter} = 500 kPa, E_{soft} = 33 kPa

Computational analysis

The finite element analyses were performed with ABAQUS (Version 6.9.1, Dassault Systemes Simulia Corp., Providence, RI, USA). The models were meshed with three-node and four-node linear, hybrid elements. Element size was chosen such that at least 5 layers of elements were present in the cap layer. The models contained approximately 100k elements. Large deformation formulation and plane strain assumption, allowing for out of plane stress build up, were used for all computational models. Appropriate boundary conditions were used to suppress rigid body motion. Static intraluminal pressure of 15 kPa (~110 mmHg) was applied as the loading condition. Postprocessing of the simulations was performed with MATLAB. The peak von Mises stresses in the cap were computed for midcap and shoulder regions (Figure 4.2.B) separately. The 99-percentile stress [102] was used as cap stress parameter and 1% of the highest stresses was excluded. Numerical simulations with finer meshes displayed negligible changes in the stress distribution.
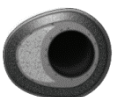
4.3   Results

An example of the numerical results is shown in Figure 4.3 where the computed stress map of a plaque half cross-section is presented. The peak cap stresses in the models mainly occurred in the midcap region. However, the difference between the peak cap stresses in the shoulder region and the midcap was small and never exceeded 5%. Generally, the results for all simulations were identical when using maximum principal stresses instead of von Mises stresses. In the remaining part of the paper, only the peak stresses in the midcaps are presented.

Figure 4.3: Contour map of von Mises stresses in half cross-section of a plaque model with intermediate intima stiffness. The highest stresses are in the cap and the peak stress values in the midcap and shoulder region are similar.
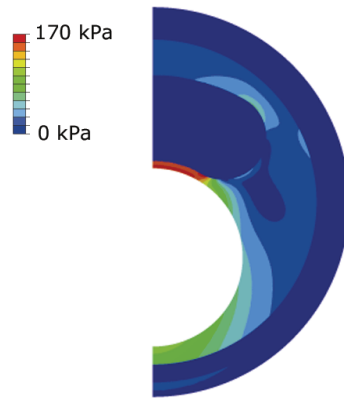
Overall, more than 1000 simulations were performed to evaluate single and combined effects of geometric plaque parameter variations for the three intima models. The geometric variation we investigated will be illustrated by discussing two relevant examples in detail (Figure 4.4 and Figure 4.5). The main findings are presented in Table 4.3 and will be summarized at the end of the section.

The influence of the cap thickness on peak cap stress for the three different intima models is shown in Figure 4.4. For the baseline geometry, the peak cap stress for the soft intima changed non-linearly from 84 to 127 kPa (+50%) when the cap thickness decreased from 0.25 to 0.05 mm. The intermediate intima model showed the highest peak cap stress among the three intima models for all cap thickness values and the peak cap stress increased from 85 to 259 kPa (+205%) with decreasing cap thickness. For the stiff intima, the peak cap stress was slightly lower than the intermediate intima, increasing from 77 to 231 kPa (+200%). For the models with a thin cap, peak cap stress for the soft intima was lower than the stiff and intermediate intima models, while for the models with a thick cap, similar peak cap stresses were observed for all intima models.

Figure 4.4: Influence of the cap thickness and intima stiffness on peak cap stress for baseline geometry. Constant parameter values for the models: necrotic core thickness=1.2 mm, intima thickness behind necrotic core =0.5 mm, adventitia thickness=0.15 mm, media thickness=0.25 mm, necrotic core angle=30˚. Peak cap stress values and the undeformed geometries of some models are attached to the associated columns. The Young's modulus (*E*) values for the intima: 33 kPa for soft, 500 kPa for intermediate and 1000 kPa for stiff

Thicker necrotic core elevated the peak cap stress as well (Figure 4.5). For the soft intima, the peak cap stress was much lower than for the other two intima models irrespective of the necrotic core size. The stiff and intermediate models showed comparable results. For the soft intima, the peak cap stress increased almost linearly from 71 to 142 kPa (+100%), for the intermediate intima, from 156 to 296 kPa (+90%) and for the stiff intima, from 159 to 254 kPa (+60%) when the necrotic core thickness was varied from 0.6 to 1.4 mm in the baseline geometry.

The maximum effects of all varied geometric parameters on peak cap stress for different intima models are summarized in Table 4.3. Varying the necrotic core angle of the baseline geometry from 10˚ to 40˚altered the peak cap stress by -6% for the stiff intima model and by -7% for the intermediate intima model. However, the change was -55% for the soft intima model. Due to change in the thickness of the intima layer behind the necrotic core from 0.3 to 0.7 mm, the peak cap stress decreased by 22% for the stiff intima model and 29% for the intermediate stiff model. By contrast, the peak cap stress was elevated by 27%

for the soft intima model. For the stiff and intermediate intima models, change in the adventitia thickness from 0.1 to 0.2 mm had almost no effect on the peak cap stress (-1%) and for the soft intima model, the peak cap stress changed only by -5%. Local regression of the media layer did not change the peak cap stress more than 1% in any of the intima models studied (data not shown).
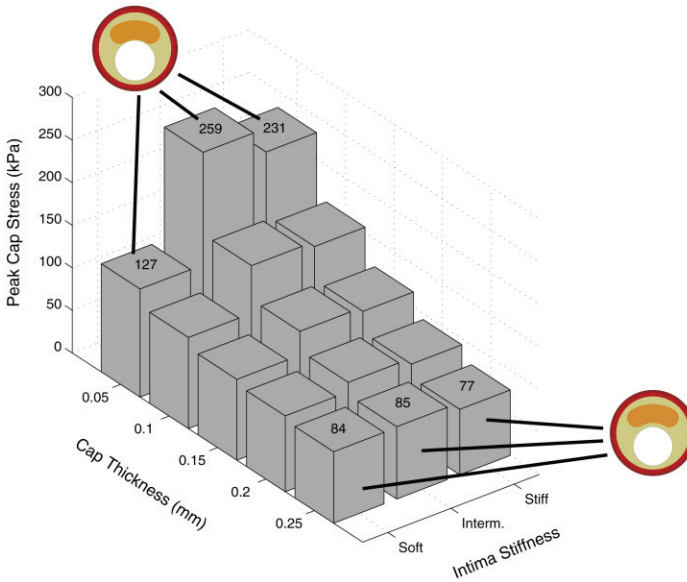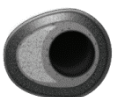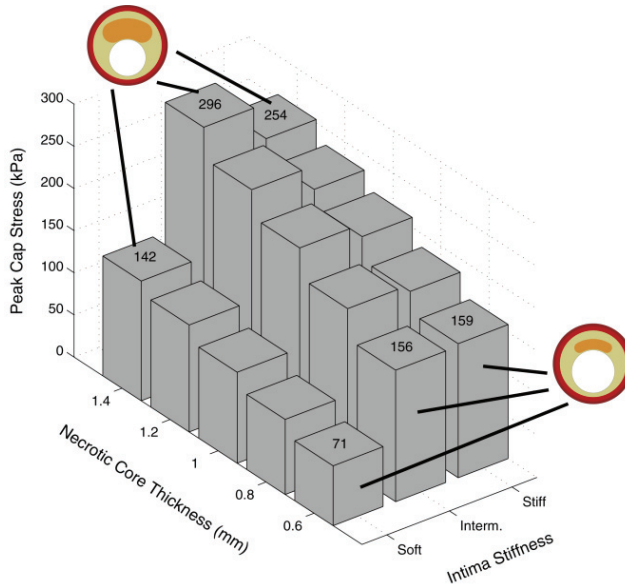

Figure 4.5: Influence of the necrotic core thickness and intima stiffness on the peak cap stress for the baseline geometry. Constant parameter values for the models: cap thickness=0.05 mm, intima thickness behind the necrotic core =0.5 mm, adventitia thickness=0.15 mm, media thickness=0.25 mm, necrotic core angle=30°. Peak cap stress values and the undeformed geometries of some models are attached to the associated columns. The Young's modulus (*E*) values for the intima: 33 kPa for soft, 500 kPa for intermediate and 1000 kPa for stiff

Table 4.3: Percentage changes in the peak cap stress due to alterations in the geometric features for all intima models. The baseline values of the geometric features were: cap thickness=0.05 mm, necrotic core thickness=1.2 mm, necrotic core angle=30°, intima thickness behind the necrotic core =0.5 mm, media thickness=0.25 mm and adventitia thickness=0.15 mm. The range and direction of the variation are displayed for each feature.

Intima Stiffness	Cap thickness (mm)	Necrotic core thickness (mm)	Necrotic core angle	Intima thickness (mm)	Adventitia thickness (mm)
	0.25→0.05	0.6→1.4	10°→40°	0.3→0.7	0.1→0.2
Stiff	+200 %	+60 %	- 6 %	-22 %	-1 %
Intermediate	+205 %	+90 %	- 7 %	-29 %	-1 %
Soft	+ 55 %	+100 %	-55 %	+27 %	-5 %

4.4 Discussion

Insights into biomechanical factors that influence cap stresses of vulnerable plaques are important for rupture risk prediction. The morphology of an atherosclerotic plaque and the material properties of its components are important determinants of the stress distribution in the plaque cap. The present study showed that the stiffness of the intima of a plaque has a profound influence on the resulting cap stresses. It also revealed that, in addition to the thickness of the plaque cap and necrotic core, other morphological plaque features as necrotic core angle and intima thickness behind the necrotic core are of great importance for cap stresses.

The experimental studies reported stiffness values ranging from 30 kPa up to 2000 kPa for atherosclerotic intima [31, 34, 35, 76, 94-96]. All previous computational studies used stiffness values in the upper range of the reported values for intima. In some studies [20, 26, 92] the impact of the material stiffness of intima on peak plaque stress has been investigated. However, even the lowest stiffness values in these papers were much higher than 30 kPa. Recent studies [30, 103] that focused on measuring the material properties of intima tissue have confirmed a previous study from Lee et al. [97] indicating that low stiffness values for the intima might be more appropriate. To the authors' knowledge, this is the first study that used intima stiffness values in the lower range of the reported experimental values [30, 97] and investigated how cap stresses are affected by intima stiffness.

For the stiff and intermediate intima models, the main load bearing plaque structure was the intima. Therefore, the stresses in the intima were higher than the stresses in the media and adventitia layers. For the soft intima models, the media and adventitia were relatively stiffer than the intima and contributed to supporting the overall load. Consequently, stresses in the media and adventitia increased while the ones in the intima and cap decreased. Hence, the soft intima models usually showed much lower peak cap stresses than the stiff and intermediate intima models.

Intima stiffness also altered the effects of geometric variations of the plaque morphology on peak cap stress. For the stiff and intermediate intima models, cap thickness was the most essential geometric plaque parameter within the investigated parameter range. A thinner cap elevated the peak cap stress dramatically, which is in line with the previous studies [26, 89, 104]. Necrotic core thickness was also an important geometrical feature, and an increase in the necrotic core thickness resulted in higher stresses, confirming the findings of Ohayon et al [29]. Since the intima was the main load bearing structure, a
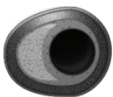
thicker intima behind the necrotic core contained the deformation of the cap, thus the peak cap stress was reduced.

Since the media and adventitia were the load bearing structures for the soft intima models, the effect of reducing cap thickness was much less pronounced. The necrotic core thickness appeared to be the most influential morphological plaque parameter. A thicker intima layer increased the peak cap stress because deformations of the necrotic core and cap were much larger due to the larger soft intima behind the necrotic core. Furthermore, necrotic core angle emerged as an important geometric parameter in the soft intima models, being equally important as the cap thickness. This finding can be attributed to the difference of the circumferential length of the cap in the midcap region. We observed that the displacement of the central part of midcap region in radial direction was comparable for all the necrotic core angles. The length of the cap for smaller necrotic core angles was smaller than the length of the cap for the larger necrotic core angles. When subjected to comparable radial displacements, the smaller cap length for the smaller necrotic core angles induced higher strains and therefore higher stresses.

Plaque rupture is an interplay between the cap stress in the cap and local cap strength. To assess the risk of plaque rupture in clinical setting, both need to be determined. We showed that the stresses in the cap of a vulnerable plaque strongly depend on material properties of the intima and the geometric features of the individual plaque components. Currently, intima-media thickness (IMT) is used as a clinical measure to both detect and track the progression of atherosclerosis. IMT corresponds to the sum of the thickness values of the cap, necrotic core, intima behind the necrotic core, and media in the present study. IMT has been shown to correlate with the presence of coronary disease, and predict cardiovascular events [105] , and a larger IMT was observed more in unstable angina patients than in the stable angina patients [106]. However, we could not find any relation between IMT and peak cap stress in the current study (data not shown). The results of this study support the need for more detailed quantitative imaging of the individual plaque components for stress assessment in coronary plaques. A combination of an intravascular ultrasound derived imaging technique [107] and optical coherence tomography (OCT) [11] could potentially provide the necessary quantitative geometric data for various plaque components, including cap thickness and necrotic core size. Rupture risk assessment also requires local information about cap strength. Several factors influence tissue strength, including local macrophage density [108]. The presence of macrophages can be detected in vivo by means of OCT [109]. Although further clinical validation of these advanced invasive imaging

techniques is required, they might be combined in clinical imaging tools for rupture risk assessment.

A main limitation of the study is the relatively simple material model used for the intima section. Anisotropic, nonlinear material properties were used for media and adventitia. However, intima tissue was assumed to be isotropic since no data are available for anisotropic material parameters for atherosclerotic human coronary intima. Atherosclerotic lesions are often highly complex structures with irregular geometries (Figure 4.1). Due to the smooth tissue interfaces and component morphologies in idealized geometries, no local stress concentrations were observed in this study. This explains the similar stress results in shoulder and midcap regions in contrast to some previous studies that used real plaque geometries [20, 21, 92]. Idealized geometries allowed isolating the effects of the investigated geometric features. In the current study, 2D models were used and stress results might be different than those of 3D models. However, Tang et al. [49] reported similar stress distribution maps for 2D and 3D finite elements models of atherosclerotic plaques. 2D models are easier to construct, require less computational effort, and are therefore effective for parametric analysis. Initial stresses were not incorporated in the computations. For the computations with realistic geometries, initial stresses should be taken into account since this leads to physiologically more realistic strains and stresses. It is likely that including initial stresses would not change the main findings of this study since idealized geometries were used and relative changes were evaluated. Residual stresses were not incorporated in the models either. Ohayon et al. showed that residual stresses in atherosclerotic plaques change stress values, but not the distribution within the structure [79]. Thus, it is likely that incorporating residual stresses would not change the main findings of this study. Another limitation is that calcifications within atherosclerotic plaques were disregarded although they are present in atherosclerotic lesions [39]. Although large calcifications might lower the plaque stresses [48], several studies have shown that microcalcification might induce local stress concentrations and elevations [58, 110]. If and how the impact of calcification on cap stresses is altered by intima stiffness and geometric features warrant further studies.

4.5 Conclusion

For stiff and intermediate intima models, cap thickness was the most important morphological risk factor. For soft intima models, necrotic core thickness and necrotic core angle had a bigger impact on peak cap stress. We therefore need to enhance our knowledge of intima material properties if we want to derive critical morphological plaque features for risk evaluation.
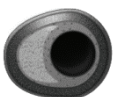
Chapter 5

Influence of Plaque Geometry on Peak Cap Stress in Human Coronary Arteries

5.1   Introduction

Approximately one third of all deaths worldwide are due to cardiovascular diseases [111]. Among cardiovascular diseases, the top two causes of mortality are stroke and coronary heart disease. Coronary heart disease might result in fatal heart attack [3] and more than 70% of fatal heart attacks are initiated by rupture of atherosclerotic plaques in coronary arteries [112].

Plaque rupture is the term used for the disruption of an atherosclerotic plaque cap. This exposes lipid rich necrotic core content underneath a plaque cap to blood which triggers intraluminal thrombosis. This might subsequently lead to a stroke or heart attack. Some atherosclerotic plaques, called vulnerable plaques, are more prone to rupture than others, known as stable plaques. Postmortem studies have shown that a thin cap and a large lipid rich necrotic core are the most common morphological features in vulnerable plaques [15, 18, 112]. Yet, not all vulnerable plaques with a thin cap and a large lipid rich necrotic core rupture. This indicates the need of further exploration of vulnerable plaque features.

From a mechanical point of view, a plaque cap ruptures when cap strength is exceeded by the local stress at a certain location within the cap. There are three important determinants of cap stresses: 1) intraluminal blood pressure, 2) material properties of plaque constituents, and 3) plaque morphology. The possible role of local mechanical stress as a predictor for plaque rupture [63, 76, 87, 88] instigated some studies, which explored the effects of various geometric plaque features on cap stresses. Decrease in cap thickness has been shown to increase peak cap stress exponentially [26, 85, 89]. Increases in necrotic core thickness and lumen curvature elevate cap stresses as well [29, 68, 113]. However, all these studies explored only a few geometric features of atherosclerotic plaques. Recently, our group studied the effect of plaque morphology on cap stresses incorporating a large number of geometric features where idealized plaque geometries were used [64]. We found that intima thickness and necrotic core angle were important factors as well. In a more recent paper, Dolla et al. [114]   confirmed the complex and interdependent influence of geometric plaque features by employing six plaque features, also using idealized plaque geometries. Although these studies have provided great insights for our understanding on atherosclerotic plaque biomechanics, they were limited to idealized plaque geometries. A study that employs detailed, realistic plaque geometries and a large set of geometric features to study the effect of plaque morphology on cap stresses is missing. The current study aims to evaluate the influence of morphology by using ten geometric plaque features
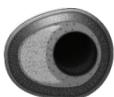
and realistic finite element (FE) models of atherosclerotic human coronary cross-sections. FE models were generated from histology images, which provide the most detailed geometrical and morphological information compared to other imaging modalities. Moreover, a statistical model to estimate peak cap stress from the most influential geometric features and a new geometric surrogate to stratify atherosclerotic coronary plaques for possible improvement in clinical rupture risk assessment were proposed.

5.2 Methods

Finite Element Analysis

Two dimensional finite element models (ABAQUS Standard 6.11, Dassault Systemes Simulia Corp., Providence, RI, USA) with large deformation formulation and plane strain assumption were generated from 77 histology cross-sections. Since the histology images were obtained from arteries fixed at 100 mmHg, the backward incremental method [78] was incorporated into the finite element simulations to compute the initial stresses present on the histology images (Figure 5.1). Subsequently, a peak systolic pressure of 140 mmHg was applied. The stress results reported in this paper are maximum principal stresses at this systolic pressure.
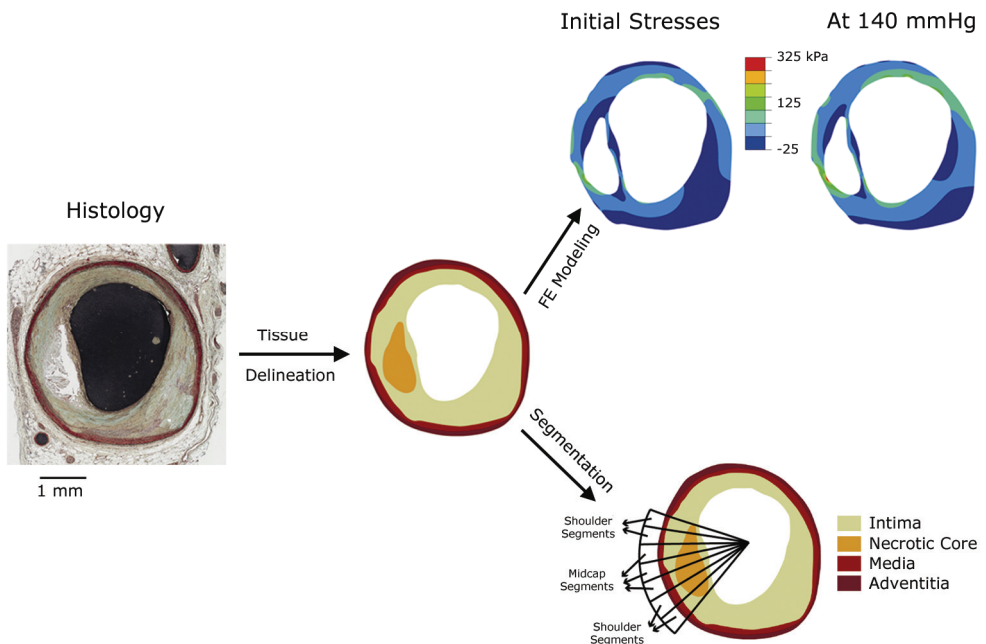
Figure 5.1: From histology to data analysis. Intima, necrotic core (NC), media, and adventitia were delineated on histology images. The obtained geometries were used for finite element simulations. Cap regions were divided into midcap and shoulder segments.

The nonlinear mechanical behavior of media and adventitia was modeled by fitting incompressible, hyperelastic Yeoh models [56] to the uniaxial tension test results obtained from human coronary vessels [57]. The Yeoh model is characterized by a strain energy density function, W_{Yeoh} :

$$W_{Yeoh} = C_1 (I_1-3) + C_2 (I_1-3)^2 + C_3 (I_1-3)^3$$

where I_1 is the first invariant of the left Cauchy-Green deformation tensor. C_1, C_2 and C_3 [kPa] are the material constants. For intima and necrotic core, a neo-Hookean material model [56] with a strain energy density function, W_{NH}, was employed:

$$W_{NH} = C (I_1-3)$$

and the material constants were obtained from literature [57, 64]. All plaque constituents were assumed to be incompressible. The values of the material constants are listed in Table 5.1.

Table 5.1: Material constants of plaque components

Tissue	Material Constants (kPa)
Media	$C_1=6.3$, $C_2=25$, $C_3=255$
Adventitia	$C_1=2.4$, $C_2=80$, $C_3=345$
Intima	$C = 166$
Necrotic core	$C= 0.166$

Data Analysis

The delineated histology cross-sections were further used to identify the values of geometric features in cap regions (Figure 5.1). Each region was divided into three areas: two shoulder areas and a midcap area. They were further divided into smaller segments with an angle of 5° (Figure 5.1). The peak cap stress and 9 geometric parameters were determined for entire cap region and for each segment. The nine geometric parameters are: 1) lumen radius, 2) cap thickness, 3) necrotic core thickness, 4) intima thickness behind the necrotic core, 5) media thickness, 6) adventitia thickness, 7) total intima-media-adventitia (IMA) thickness, 8) lumen curvature, and 9) necrotic core curvature. An additional geometric parameter for entire cap region was the necrotic core angle. An in-house written MATLAB (R2010a, The MathWorks Inc.) script was used to measure maximum, minimum and mean values of the geometric parameters.

Statistical analyses were performed with SPSS (release 17.0). All data (peak cap stress and geometric parameters) were checked for normality using Shapiro-Wilk test. Since the data were not normally distributed, nonparametric tests
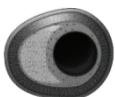
were employed for statistical analysis. For multivariate regression analysis, log-transformation was used to improve the normality and the model fit. A statistical significance was considered if p<0.001.

Two types of analyses were conducted: segmental analysis and cap analysis. With the segmental analysis, influence of geometric parameters in a segment on peak cap stress in the same segment was examined in order to explore the local geometry effects. First, nonparametric Spearman's correlations were calculated to investigate the relationships between each geometric parameter and the peak cap stress in segments, and between geometric parameters themselves. Secondly, a multivariate regression analysis with backward elimination method was performed, treating local peak cap stress as the dependent variable and the geometric parameters as independent variables. For cap analysis, a multivariate regression analysis was employed to predict peak cap stress in a plaque cross-section using global geometric plaque parameters.

Stress Stratification Model Based On Geometric Parameters

A model based on geometric parameters was sought to stratify plaques with respect to their peak cap stresses. First, plaques were classified as high, medium and low stress plaques based on the finite element results using two threshold values. Peak cap stress of 300 kPa was the threshold for the medium stress-high stress classification. This value has been reported as the minimum cap strength for human coronary plaques in a computational study [20] and widely used in other studies [67, 89, 115, 116]. Low stress-medium stress threshold was selected as 140 kPa since some studies reported this value as the lower limit of plaque strength [33, 57, 94, 108]. After grouping the plaques as high, medium and low stress plaques, a mathematical surrogate employing the important geometric plaque parameters from multivariate regression plaque analysis was sought to identify these plaque groups.

5.3 Results

Geometric Parameters and Stress Results

The investigated human coronary plaques had diverse geometries. Table 5.2 shows the median and quartile values of the most relevant geometric parameters. The minimum cap thickness had a median of 190 μm [1st quartile (Q_1):3rd quartile (Q_3) = 65:400 μm]. The maximum necrotic core thickness had a median of 508 [297:598] μm. The median value of lumen radius was 922 [780:1075] μm.

Table 5.2: Geometric parameter values for cap analysis. Th: Thickness, NC: Necrotic Core, IMA: Intima-Media-Adventitia, Curv: Curvature, Q_1: First quartile, Q_3: Third quartile

Geometric Parameter	Median [Q_1:Q_3]
Min. Cap Th.	190 [65:400] μm
Max. NC Th.	508 [297:598] μm
Min. Intima Th.	100 [47:191] μm
Min. Media Th.	63 [25:83] μm
Min. Adventitia Th.	55 [34:88] μm
Min. IMA Th.	282 [220:422] μm
Max Lumen Radius	922 [780:1075] μm
NC Angle	55 [35:75] °
Max. Lumen Curv.	3.4 [2.6:5.8] mm^{-1}
Max. NC Curv.	31 [21:55] mm^{-1}

Finite element simulations revealed that stress distribution and peak stress values strongly depend on plaque geometry. Figure 5.2 illustrates how stress results were influenced by distinct geometrical features. In Figure 5.2.A, a representative example for plaques with a smooth necrotic core and a smooth lumen shape is shown. For this type of plaques, peak stresses in shoulder regions were mostly at the lumen border (140 and 120 kPa in the representative example in Figure 5.2.A) and in midcap region at the necrotic core border (230 kPa in Figure 5.2 .A). Lowest stresses in the entire cap were found at the luminal side in the midcap regions (10 kPa in Figure 5.2.A). Figure 5.2.B demonstrates that for plaques with irregular lumen or necrotic core shape, peak stress locations shifted towards the irregularities (430 kPa in Figure 5.2.B). Figure 5.2.C illustrates that the stresses in the shoulder of a cap were elevated if a thin intima layer in the nondiseased part of a vessel adjacent to a cap shoulder was present (475 kPa in Figure 5.2.C). Peak stresses in shoulder (median [Q_1:Q_3] = 88 [49:176] kPa) and midcap regions (102 [65:172] kPa) were not significantly different (p-value=0.16).
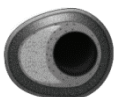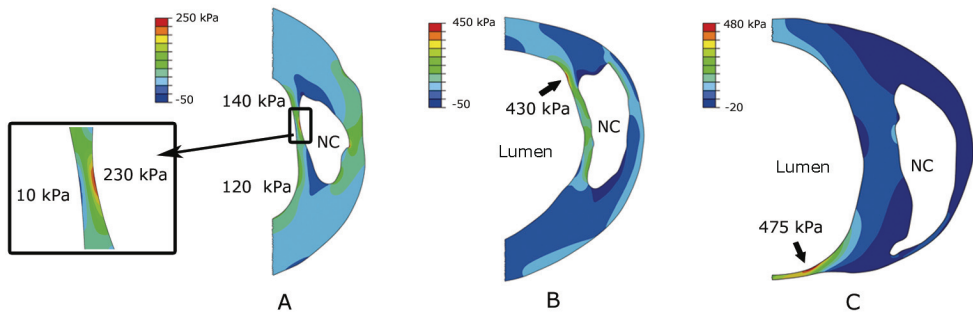
Figure 5.2: Finite element analysis results showing maximum principal stress (in kPa) within the intima of atherosclerotic coronary plaques. A: In plaques with smooth lumen and necrotic core (NC) shapes, higher stresses were observed at the lumen border in the shoulders and at the NC border in the midcap region. Very low, even negative stresses were present at the lumen border in midcap. B: Irregularities on the lumen or NC border caused stress concentrations. C: High stresses were present in a thin intima region adjacent to a plaque shoulder, which increased the cap stresses.

Segmental Analysis

Segmental bivariate analysis aimed to quantify the effect of local morphology on local peak cap stress. The analysis showed that local values of four geometric plaque parameters significantly correlated to local peak cap stress: minimum cap thickness, minimum media thickness, maximum lumen curvature, and maximum lumen radius (Table 5.3). Minimum cap thickness showed the strongest correlation to stress (ρ=-0.59) and was in a negative fashion. Maximum lumen radius showed a positive, moderate correlation (ρ=0.47). Maximum lumen curvature (ρ=0.17) and minimum media thickness (ρ=0.14) were also positively but weakly correlated to local peak cap stress. Maximum necrotic core thickness, which has been shown in earlier studies to be an important factor for cap stress, did not show a significant correlation to local stress. There were also significant and strong correlations between the geometric plaque parameters (data not shown) indicating that the influence of a geometric feature might be confounded by other geometric parameters. Therefore, we performed multivariate regression analysis on segmental results. Using backward elimination method, a model with three geometric plaque parameters was obtained (Table 5.4). These geometric parameters were the ones that had the strongest correlations to stress in the bivariate analysis. In the model (R-value=0.73) thinner cap, larger lumen and larger lumen curvature elevated local peak stress. Minimum media thickness, which showed statistically significant correlation, was not significant in multivariate analysis.
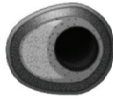
Table 5.3: Nonparametric Spearman's correlation coefficients for segmental analysis. Th: Thickness, NC: Necrotic Core, Adv: Adventitia, IMA: Intima-Media-Adventitia, Curv: Curvature. An asterisk indicates a significant correlation (p<0.001)

	Min Cap Th.	Max NC Th.	Min Intima Th.	Min Media Th.	Min Adv. Th.	Min IMA Th.	Max Lumen Curv.	Max NC Curv.	Max Lumen Radius
Peak Segment Stress	-0.59 *	0.01	0.06	0.14 *	-0.07	0.09	0.17 *	0.09	0.47 *

Table 5.4: Multivariate regression model for segmental analysis (R=0.73) and cap analysis (R=0.79). MinCapth: Minimum cap thickness, MaxLumRad: Maximum lumen radius, MaxLumCurv: Maximum lumen curvature, Unstand: unstandardised, Stand: standardized, Coeff: coefficient. All p-values <0.001. Peak cap stress in kPa, minimum cap thickness and maximum lumen radius are µm, and maximum lumen curvature in mm^{-1}. Segmental analysis uses local, cap analysis uses global values.

$\log_{10}(\text{PeakCapStress})$

	Segmental Analysis			Cap Analysis		
	Unstand. Coefficient	95% CI	Stand. Coefficient	Unstand. Coefficient	95% CI	Stand. Coefficient
Constant	2.17	[2.00; 2.33]	-	0.97	[0.02; 1.92]	-
$\log_{10}$ (MinCapTh)	-0.28	[-0.31;-0.26]	-0.66	-0.40	[-0.50;-0.32]	-0.67
$\log_{10}$ (MaxLumRad)	0.38	[0.32; 0.43]	0.37	0.71	[0.40; 1.02]	0.34
$\log_{10}$ (MaxLumCurv)	0.06	[0.04; 0.08]	0.13	-	-	-

<u>Cap Analysis</u>

Multivariate regression analysis was used to predict the global peak cap stress in plaques from geometrical parameters. Minimum cap thickness and maximum lumen radius were the only significant geometric parameters in the final statistical model (R=0.79):

$log_{10}(PeakCapStress) = 0.97-0.4*log_{10}(MinCapTh)+0.71*log_{10} (MaxLumRad)$

with peak cap stress (PeakCapStress) in kPa, minimum cap thickness (MinCapTh) and maximum lumen radius (MaxLumRad) in μm. Thinner cap and larger lumen radius increased peak cap stress. Lumen curvature, which was one of the important parameters in the segmental multivariate analysis, did not have a significant effect in cap analysis. Table 5.4 shows the standardized and unstandardized coefficients, and 95% confidence intervals of the geometric parameters.

<u>Stress Stratification Model Based on Geometric Parameters</u>

Stratification of atherosclerotic coronary plaques based on the most important geometric parameters from the multivariate regression analysis -minimum cap thickness and maximum lumen radius- is shown in Figure 5.3. Plaques with the peak cap stress above 300 kPa were identified as high stress plaques (n=9, indicated with asterisks in Figure 5.3), below 140 kPa as low stress plaques (n=39, indicated with circles in Figure 5.3), and between 300 and 140 kPa as medium stress plaques (n=29, indicated with plus-signs in Figure 5.3). The lowest maximum lumen radius to minimum cap thickness ratio amongst the high stress plaques was 6.5. This value was used to define the border between the high ratio and medium ratio regions in Figure 5.3. The lowest ratio amongst the medium stress plaques was 2.5 and defined the border between the medium and low ratio regions. By definition, all high stress plaques were in high ratio region. Eighty percent of the medium stress plaques were located in high ratio region and the rest in medium ratio region. Fifty percent of the low stress plaques were in low ratio region, 30% were located in medium ratio region and 15% were in high ratio region. The high ratio region contained all three stress types. Twenty-five percent of the plaques in this region were high stress plaques, 60% were medium stress plaques and 15% were low stress plaques.
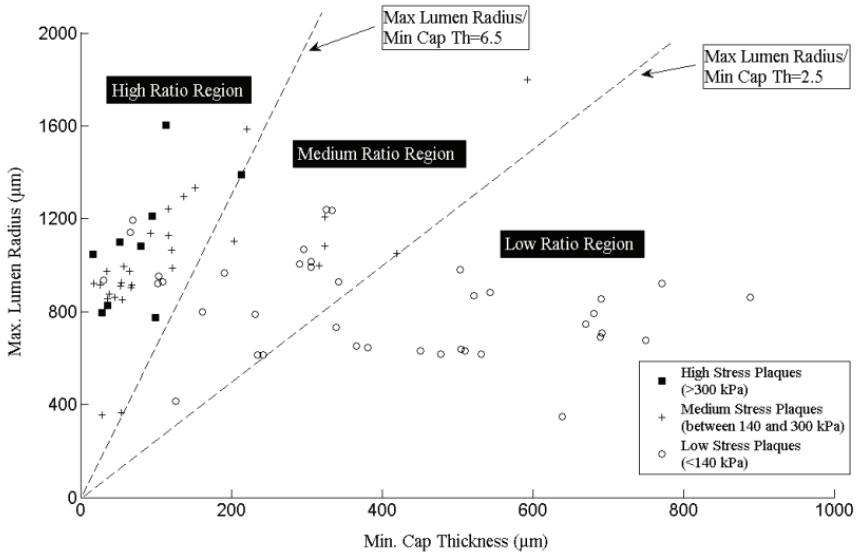
Figure 5.3: Stratification of high, medium, and low stress plaques based on the ratio of maximum lumen radius to minimum cap thickness. The data points show the finite element stress results. A square indicates peak cap stress above 300 kPa, a plus indicates between 300 kPa and 140 kPa, and a circle indicates below 140 kPa.

5.4   Discussion

Cap stresses in atherosclerotic plaques are strongly influenced by geometry. Most of the previous studies that investigated the effect of plaque morphology on cap stresses focused on only one or two geometric plaque features. However, atherosclerotic plaques are geometrically complex structures and we can therefore anticipate that many plaque features influence cap stresses. To have an extensive investigation of influence of plaque morphology, a number of geometric features have to be employed in such studies. Other studies that used a larger number of geometric features were limited to idealized geometries. To overcome these limitations, the current study employed 77 realistic plaque cross-sections to study the effect of ten geometric plaque features. To our knowledge, this is the first study that utilized such a large number of geometric features and detailed, realistic FE models of human coronary plaques obtained by histology.

Histology provides high resolution images and captures even small geometric features that are not possible to obtain with most other imaging techniques. This study showed that such small geometric features (e.g. a thin region or lumen irregularity in a cap) might influence cap stress values and distribution. It was also shown that the adjacent intima region might be of great importance for cap stresses. A thin intima layer adjacent to cap can elevate stresses in the shoulder
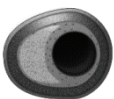
region. This might be a possible explanation for why most of the coronary plaques rupture in the shoulder region [117].

Significant correlations between geometric parameters in the segmental bivariate analysis indicated that the effect of a geometric parameter on peak cap stress might be confounded by other geometric parameters. Therefore, we conducted a multivariate analysis on the segmental level, which showed that a thin cap is an important risk factor for high cap stresses, confirming the findings of previous studies [26, 64, 85, 89]. Necrotic core thickness has been shown to be another important factor for cap stresses by some earlier computational studies with idealized geometries [29, 64]. However, in the present study no significant effect of necrotic core thickness on peak cap stress was found. This can be attributed to the more complex structure of the realistic plaque geometries compared to idealized geometries. From a mechanical point of view, large necrotic core should increase cap stress but the effect of a thin intima might obscure this effect. Local lumen radius was an important factor for local peak cap stress and in line with the Laplace Law; a larger radius leads to higher stresses. This finding might shed light on why plaque rupture mostly occurs in the proximal part of coronaries [101]. Teng et al. [118] have shown that high local lumen curvature, an indication of irregularity on lumen shape, results in stress concentration regions in carotid arteries. Present study showed the same effect of lumen curvature in coronaries. In a recent study, we investigated the influence of the plaque structures behind necrotic core using idealized plaque geometries. The study showed that media and adventitia had almost no influence whereas intima behind the necrotic core had a slight effect. This was because the load due to the intraluminal blood pressure is carried mostly by the intima. These findings were confirmed by the present study.

Prediction of global peak cap stress is of great importance for rupture risk assessment in atherosclerotic plaques. FE models allow computing the plaque and cap stresses. However, even the simplest models require processing and computational times that are beyond the limits that they can be used in the clinic. Therefore, we sought for an alternative model that can predict peak cap stress. We used multivariate regression analysis where global peak cap stress is estimated from geometrical parameters. The calculated R-value of the model was 0.79 and is a reasonably good fit considered the complex geometries of atherosclerotic plaques and the possible nonlinearity in the influence of plaque geometry on cap stresses. The geometric features in the model -the minimum cap thickness and maximum lumen radius- can be measured by optical coherence tomography, making this model suitable for an evaluation in a clinical setting.

The current criterion for clinical treatment decision in coronary artery disease is stenosis degree. However, two thirds of acute coronary events occur in mildly stenosed arteries [4, 53]. Thus, better risk prediction models have to be developed. Minimum cap thickness is a well-accepted geometric risk factor, although it is not clinically used for risk prediction yet. This study showed that maximum lumen radius is also an important geometric plaque feature for cap stress. The proposed model based on the ratio of maximum lumen radius to minimum cap thickness to stratify plaques with respect to peak cap stress, combines these two important risk factors making a step forward for better stress prediction. With the threshold ratio values presented in this paper to define the high, medium, and low ratio regions; the model detects low stress plaques accurately. Future studies with extended data sets will help to determine these threshold values more precisely and eventually, to identify both high and low stress plaques more correctly. This ratio model can be potentially used to improve the risk prediction in clinical intervention decisions.

In order to have a representative database for the study, four histology cross-sections were selected from each atherosclerotic coronary on average. To make sure that the cross-sections from a coronary could be treated independently, we selected them such that they were at least 0.2 mm apart from each other and showed different morphologies. For further expansion on the clinical applicability of the results of this study, more patients should be included.

A limitation of this study is that the plaques investigated did not contain any calcification. Although the stabilizing effect of macro-calcifications has shown [48], indicating that plaques without calcification might be more of vulnerable type, micro-calcification may cause stress concentrations [110, 119]. This warrants further investigation. Another limitation is that the anisotropic material properties of media and adventitia available in literature were not employed in the finite element computations. As no significant influence of these layers on cap stresses was observed, it may be expected that anisotropic models for media and adventitia would not affect the main conclusions of this study. The correct intima stiffness is essential for stress computations in atherosclerotic plaques and for identification of geometric features influential on peak cap stress [64]. Although Young's modulus values as low as 33 kPa have been reported for atherosclerotic intima [30, 97], larger values around 1000 kPa are mostly to be found in literature [33, 35, 37, 94, 95, 120]. Therefore, we used stiff intima material properties in the finite element simulations. This study employed 2D models for the analysis, which are a simplification of real, 3D plaque structure. However, Nieuwstadt et al. [121] has shown that 2D models are accurate enough for evaluation of the influence of geometrical features on cap stresses.
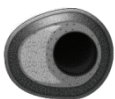
The finite element simulations did not incorporate intraluminal flow. However, the shear stresses induced by blood flow are three orders of magnitude lower than the wall stresses due to the blood pressure [24].

5.5   Conclusion

Atherosclerotic plaques are geometrically complex structures and previously developed geometrical risk factors based on idealized geometries are of limited use. Using realistic geometries, we showed that local peak cap stress is mainly influenced by local measures of minimum cap thickness, maximum lumen radius and maximum lumen curvature. With the statistical model proposed, the global peak cap stress can be estimated by the former two. Moreover, the ratio of minimum cap thickness to maximum lumen radius can be potentially used for stress stratification of coronary plaques.
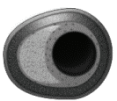
Chapter 6

Mechanical Properties of Human Atherosclerotic Intima Tissue

6.1   Introduction

Atherosclerosis is the most important pathology in the arterial system. In coronary arteries, it is the underlying cause of both stable and unstable angina, and acute myocardial infarctions [4]. Atherosclerotic plaques in carotid arteries may lead to stroke [5], and in the iliac arteries they are the main cause of peripheral artery disease [6]. Acute manifestations of atherosclerotic disease are associated with rupture of the cap of vulnerable plaques [10] and identification of these rupture-prone plaques is therefore a very active research field. Most studies are geared towards image-based identification of specific plaque features including cap thickness [11], lipid pool size [12], and the presence of intra-plaque hemorrhage [13]. These plaque features are surrogate markers for peak mechanical stresses in the cap, which is generally regarded as an important parameter to predict cap rupture [122]. Biomechanical modeling of atherosclerotic plaques is essential to further deepen our understanding of which plaque features are essential for cap stresses [12, 27, 64, 123], and therefore relevant targets for image-based diagnosis. Moreover, if reliable data on mechanical strength of the cap is available, biomechanical models potentially can be used for the identification of rupture prone plaques [66].

Application of biomechanical plaque models relies on various input parameters, including accurate representation of geometrical plaque features, appropriate loading and boundary conditions, and the material properties of the relevant plaque components. Although imaging geometrical plaque features and obtaining appropriate boundary conditions also represent a challenge in a clinical setting, we want to focus on the material properties in this review. Since the intima occupies the larger part of the volume of an atherosclerotic plaque, the choice for the material properties of this component is critical. This review contains three parts. In the first part, we focus on the composition of intimal tissue of various atherosclerotic plaque types. The difference in composition of the plaques is most likely the key factor that explains the enormous diversity of the experimental data that we discuss in second part. Implications of the spread in the experimental data are discussed in the third part.

6.2   Atherosclerotic Intima Pathology: Mechanical Perspective

Properties of atherosclerotic intima components

A healthy arterial wall comprises three layers: the adventitia, the media and the intima. During the progression of atherosclerosis, the major changes in the arterial wall take place in the intima. A healthy intima is a thin layer of endothelial cells attached to a basal membrane. Several processes are
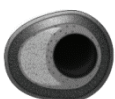
responsible for intima thickening during lesion development, including infiltration of lipids and inflammatory cells from the luminal side, smooth muscle cell migration and proliferation, extracellular matrix buildup, and intraplaque hemorrhage. The main structural components of atherosclerotic intima are smooth muscle cells, collagen, elastin, and lipids. Biomechanical behavior of atherosclerotic intima tissue is determined by the properties of the individual components and its internal structure.

The mechanical properties of smooth muscle cells depend on various factors including their phenotype (contractile or synthetic) and the extent of their activation. The behavior of contractile smooth muscle cells is non-linear, anisotropic and depends on vascular tone [124]. The smooth muscle cells in a diseased intima are predominantly synthetic and are less stiff than the contractile ones. Stiffness values as low as 10 kPa were reported for rat aorta smooth muscle cells [125, 126]. These low stiffness values can be attributed to a low amount of filaments in synthetic smooth muscle cells. The absence of filaments probably might also lead to more isotropic properties, although these were not measured.

Collagen types I, III, IV and V are present in the diseased intima. Collagen type I is dominant, while deposits of collagen type IV are frequently observed in the shoulder region of plaques [127]. The stiffness of the individual collagen fibers was estimated at 1 GPa [128], but no distinction was made between different collagen types. The contribution of collagen to the load bearing capacity of the intima also depends on their distribution and cross-linking. Rats with reduced collagen cross-linking showed lower stiffness for the thoracic aorta [129]. Due to the high stiffness of collagen, the amount and organization of collagen in atherosclerotic plaques can be expected to have a marked influence on the overall mechanical behavior of plaques.

The healthy vascular wall comprises of several layers of elastin. Elastin layers play an important role in the elastic behavior of the vessel wall as response to the variation in blood pressure over the cardiac cycle. It is estimated that the elastic modulus of arterial elastin is in the order of 0.5-1.0 MPa [128, 130]. However, only very low amounts of elastin are found in atherosclerotic intima tissue, and elastin is mainly located in the medial layer of the artery and in the cap of the plaque. Elastin can therefore be considered as a minor contributor to the mechanical behavior of atherosclerotic intima.

The major components of a lipid pool are water, phospholipids, cholesterol esters, cholesterol crystals, and other lipids [131]. Liquid cholesterol esters transform to a crystalline form over time, possibly leading to stiffening of the

lipid pool [132]. This may increase the structural stability of the plaque and decrease the probability of cap rupture [36]. Experimental data on the mechanical properties of lipid pools are not available. Shear measurements performed on synthetic models of lipid pools with various lipid compositions yielded low storage moduli ranging from 50 to 300 Pa, depending on the amount of cholesterol crystals [36].

No experimental data on bulk calcifications in plaques are available. Ebenstein et al. used nano-indentation tests to determine the properties of calcified plaques [133]. The majority of calcified samples showed stiffness values between 100 MPa and 10 GPa, whereas some had values as high as 21 GPa. The average stiffness was 0.7±2.2 GPa, indicating large calcifications can be regarded as rigid inclusions. Calcified inclusions in atherosclerotic intima tissue might therefore strongly influence the mechanical properties of a plaque, and especially increasing the heterogeneity of the properties over the lesion.

Besides the aforementioned components, various other cellular components including inflammatory cells, foam cells and red blood cells are present in the intima. As individual cells are generally mobile, they are not expected to contribute to the structural integrity of the intima. However, a large cluster of macrophages or large intraplaque hemorrhage may locally influence the mechanical properties of intima tissue.

Atherosclerotic plaque classification

As coronary artery disease is one of the leading causes of death [7], atherosclerotic plaque formation, growth and rupture in coronary arteries was studied widely. Based on a series of post-mortem pathological studies, a classification scheme was developed by Stary and coworkers [134-136]. Using additional pathological studies focusing on vulnerable plaques [28], the original classification scheme was adapted [8] and adopted by the American Heart Association (AHA). They proposed a classification scheme with 8 lesion types, representing the successive stages of atherosclerosis. The classification scheme is based on coronary and aortic specimen. Atherosclerotic plaques develop from early lesions or fatty streaks (type I and type II lesions) into intermediate lesions, or pre-atheroma (type III lesions). In intermediate lesions, extracellular lipids are present between the smooth muscle cells that form the main component of the pathologically thickened intima. The media and adventitia are still largely unaffected by the disease. In atheroma and fibro-atheroma (type IV and V lesions), the diseased intima is characterized by the presence of a lipid core, which contains free cholesterol esters. Foam cells cover the core and a proteoglycan rich cap, often containing macrophages, separates the lipid core
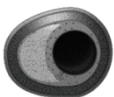
from the lumen. Type IV lesions do not contain excessive amounts of smooth muscle cells or collagen. Type V lesions are characterized by an increase in intima volume, mainly due to increased synthesis of fibrous tissue (primarily collagen) and smooth muscle cells. The intima might contain organized thrombi. The media and adventitia in type V plaques are often disrupted or disarranged. If a type IV or type V lesion develops a surface defect or intra-plaque bleeding, it is generally referred to as a ruptured lesion (type VI lesion). These lesions might further progress into calcified lesions (type VII), or fibrotic lesions (type VIII). In calcified lesions, part of the intima is fibrous with large calcifications. Underlying atheroma might still be present in these lesions. Fibrotic lesions do not contain a lipid core and are characterized by the presence of fibrous tissue.

From a mechanical perspective, the intimal tissue of the type III lesions might still be considered to be fairly homogeneous and isotropic. It can also be anticipated that the intima is fairly soft due to the absence of structured elastin layers and the presence of lipid droplets. The homogeneity of the material properties of an atherosclerotic intima is most certainly lost when it progresses into a type IV lesion. The diseased intima of a type IV lesion is likely to show heterogeneous properties. Due to the absence of large amounts of collagen and smooth muscle cells, and the presence of a lipid core, it is probably soft with no distinct anisotropy. Type V lesions might show a great variety in mechanical behavior. The fibro-atheroma may behave similar to the type IV lesion, but an incremental build-up of collagen and smooth muscle cells might lead to stiffer and anisotropic properties. Calcified lesions (type VII) are inhomogeneous, with very stiff calcified inclusions. Fibrous lesions might be fairly homogenous and due to the absence of a lipid core, reasonably stiff. The effect of the degradation of the media and the adventitia on the overall mechanical behavior of the plaque is hard to estimate and largely depends on the load bearing capacities of the diseased intima. Overall, we see a shift from soft atherosclerotic intima (types II and IV) towards moderately stiff (types VI and VI) and finally to even stiffer intima (types VII and VIII) as atherosclerosis progresses. Types VII and VIII are also likely to have isotropic material behavior, while plaque types V and VI might be considered fairly anisotropic. Almost all plaque types have a heterogeneous component distribution, except types II and VIII (Table 6.1).

Atherosclerotic plaque type distribution in vascular territories

The occurrence of stroke is related to the presence of atherosclerotic plaques in the internal carotid artery [137]. The clinical observation that surface irregularities and the presence of ulcerations are strong predictors of recurrent events [138] indicates that plaque rupture is a clinically relevant event for this vascular territory. To prevent this from happening, lumen obstructing plaques
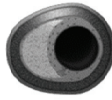
Table 6.1: Relative stiffness, homogeneity and anisotropy of the different plaque types, based on plaque content and composition
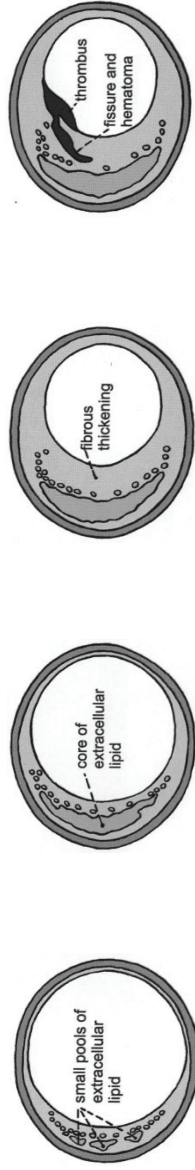
Plaque Type	III	IV	V	VI	VII	VIII
Description	Pre-Atheroma	Atheroma	Fibro-atheroma	Ruptured lesion	Calcified	Fibrous
SMC	-	-/+	+	-/+ or +	-/+	-/+
Collagen	-	-/+	+	-/+ or +	-/+	+
Stiffness	-	-	-/+	- or -/+	+	+
Homogeneity	-/+	-	-	-	-	-/+
Anisotropy	-	-/+	+	-/+ or +	-/+	-/+

SMC: Smooth muscle cells.

The "-" indicates absence or low amount, "+" indicates presence or high amount, and "-/+" indicates intermediate amount. The drawings are adapted from [9]

are often removed during a procedure called carotid endarterectomy [139]. Plaque specimens obtained from these procedures were studied and compared to coronary plaques, and many similarities were found [140, 141]. The main difference in plaque composition between the two vascular territories was that more intra-plaque hemorrhage was observed in carotid plaques: in symptomatic patients, 65% of the carotid plaques showed signs of intra-plaque hemorrhage [141]. The resulting accumulation of red blood cells seemed to be an important source of lipid-related plaque growth [142]. The prevalence of calcifications was comparable to coronary plaques, although more calcified nodules were present. From a morphological perspective, carotid plaques have thicker caps and often multiple small necrotic cores [140]. From a clinical perspective, these small necrotic cores might be responsible for ulceration: the 'cavities' at the luminal side might originate from a ruptured cap covering a small necrotic core. They are frequently found in carotid arteries but seldom seen in coronaries, a fact that might also be related to the size of the arteries and the different flow conditions.

A comparison between plaques from coronary, carotid, and femoral arteries from autopsies was performed by Dalager et al. [143]. Histological evaluation was done on the specimens and they were graded according to the AHA classification. Sections from coronary arteries had the highest incidence of plaque (≈50%), mainly type IV or V plaques (51%), followed by type VIII fibrous plaques (45%) (Figure 6.1.A). Overall, carotid arteries had fewer plaques (30%) and contained more foam cells and intermediate lesions (59%) than coronary plaques. Almost all carotid plaques were lipid-rich type IV or V plaques. Fewer plaques were found in femoral arteries (20%) and the majority of femoral plaques were fibrous, type VIII (52%).
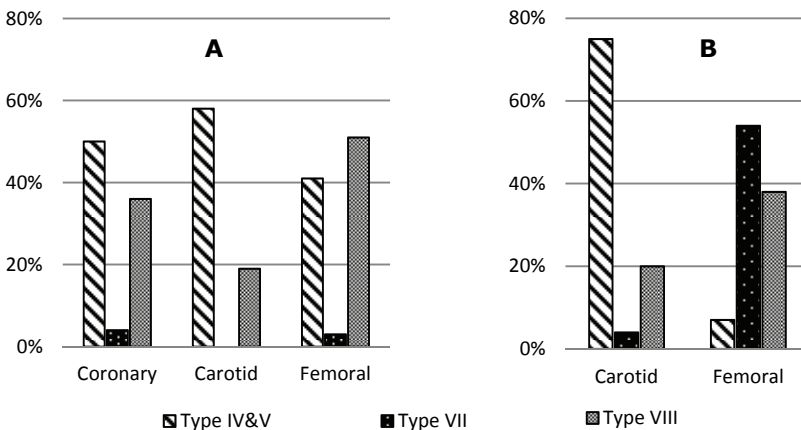
Figure 6.1: Incidence of atherosclerotic plaques reported by A) Dalager et al. [143] and B) Herrison et al. [144] with respect to vascular territories and AHA classification

Herisson et al. used endarterectomy specimens to demonstrate the differences between advanced carotid and femoral plaques (Figure 6.1.B) [144]. They showed that 75% of the carotid plaques qualified as fibrous cap atheroma (type IV and V) compared to only 7% of the femoral plaques. Femoral plaques contained more calcium, less cholesterol and were less inflamed than carotid plaques. They found more calcified plaques (type VII) in the femoral arteries than Dalager et al. [143], probably due to decalcification procedure followed in the latter study.

In a recent natural history study, van Dijk et al. investigated the peri-renal region of 260 apparently healthy individuals [145]. They found that aortic plaques develop into predominantly type IV and V during the fourth decade. They concluded that the main features of aortic plaques resemble the coronary plaques, although aortic plaques are larger. In young individuals, the abdominal and thoracic aorta contained more lesions than the right coronary artery [146]. The plaque burden increased over time in all arteries, but raised lesions – presumably more advanced plaque types- became more dominant in the right coronary artery when compared to the aorta. Publication date of this study precluded application of the AHA classification scheme.

To summarize, the composition of atherosclerotic plaques, especially the clinically most relevant ones, is complex and heterogeneous. Moreover, plaques are dynamic structures and their composition, and thus their type, changes over time. Since the mechanical properties are interlinked with plaque composition, they also will highly depend on plaque type. Experimental studies on plaque biomechanics would therefore greatly benefit from incorporating classification schemes, like the one introduced by AHA, in their analysis. One has to keep in mind that the classification schemes are descriptive and qualitative by nature, and that plaque types from different vascular territories might exhibit subtle but mechanically significant differences.

6.3   Experimental Data on Atherosclerotic Intima Properties

A variety of studies evaluated the mechanical properties of atherosclerotic intima tissue. Eleven studies met our inclusion criteria: the intima tissue should originate from advanced plaques, sufficient details on stress and strain should be provided, and intima tissue should be tested rather than the entire vessel wall. We grouped these studies with respect to the vascular territory (coronary, carotid, aorta, and iliac/femoral arteries) and applied loading protocol (uniaxial tension or unconfined compression). Protocol details (specimen storage, temperature the tests were done at, preconditioning, etc.) of the studies are summarized in Table 6.2.
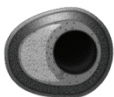
Table 6.2: Details of the papers reviewed

Authors (Year)	Vessel Type	Test Type	Test direction	Number of Patients	Number of Samples and Description in the Study	Sample Size	Testing Temperature	Testing Time	Preconditioning
Born&Richardson (1990)	Coronary	Tension	Circ. and axial	25	5 of 25 plaques were reported.	3-4x0.5 mm	Room temperature	Immediately after autopsy	No
Maher et al. (2009)	Carotid	Tension	Circ.	10	16 plaque samples (8 calcified, 4 echolucent, 4 mixed)	4x1 mm	NF	Within 2 hours after endarterectomy	10 times up to 10% strain
Lawlor et al. (2011)	Carotid	Tension	Circ.	14	14 whole plaques (preop.: 5 hard, 6 mixed, 2 soft, 1 n/a)	Length > 4xWidth	NF	Within 2 hours after endarterectomy	No
Maher et al. (2009)	Carotid	Comp.	Radial	11	44 plaque samples (16 calcified, 5 echolucent, 23 mixed)	4 mm in diameter	NF	Within 2 hours after endarterectomy	10 times up to 10% strain
Barrett et al. (2009)	Carotid	Comp.	Radial	8	11 plaques	Indenter radius=0.5mm	NF	Within 3 hours after endarterectomy	NF
Loree et al. (1994)	Aorta	Tension	Circ.	21	26 fibrous caps (12 cellular,9 hypocellular,5 calcified)	5x5x1,2 mm	4° C	Within 36 hours after death (Refrigrated @ 4°C)	3 cycles
Lendon et al. (1993)	Aorta	Tension	NF	NF	6 plaque caps (2 ulcerated, 2 non-ulcerated, 2 intima)	1.5x7 mm	NF	NF	NF
Lee et al. (1991)	Aorta	Comp.	Radial	14	27 fibrous caps (7 cellular, 9 hypocellular, 11 calcified)	3.5 mm in radius	Room temperature	Within 16 hours after death	Allowed to creep for 30 min.
Lee et al. (1992)	Aorta	Comp.	Radial	22	43 atheroma caps (18 fibrous, 14 nonfibrous, 11 calcified)	3.5 mm in radius	Room temperature	NF	Allowed to creep
Holzapfel et al. (2004)	Iliac	Tension	Circ. and axial	8	9 circumferential, 9 axial fibrous cap 4 circumferential, 4 axial fibrotic intima	Length: 7-17 mm Width: 2-6 mm Thickness: 0.2-1.7 mm	37° C	Within 48 hours after autopsy (Refrigrated @ 4°C)	5 cycles
Topoleski et al. (1997)	Aortailiac	Comp.	Radial	6	24 samples from nonulcerated lesions	5x5mm	37° C	Within 12-48 hours of death	Repeatability/ recoverability
Salunke et al. (2001)	Aortailiac	Comp.	Radial	NF	18 samples from nonulcerated lesions (5 calcified, 7 fibrous, 6 atheromatous)	5x5mm	37° C	Within 12-48 hours of death	Repeatability/ recoverability

n/a: Not applicable. NF: Not found, Comp: Compression, Circ: Circumferential, preop.: preoperatively

Table 6.3: Calculated tangential stiffness (in kPa) of average tensile properties

Stretch	Born& Richardson (1990) Coronary Circ. and axial n=5	Maher et al.* (2009) Carotid Circ. n=16	Lawlor et al.** (2011) Carotid Circ. Hard n=5	Mixed n=6	Soft n=2	All n=14	Loree et al. (1994) Aorta Circ. Hypo-cellular n=9	Cellular n=12	Calcified n=5	All n=26	Lendon et al. (1993) Aorta Direction not available Non-ulcerated Cap n=2	Ulcerated Cap n=2	Adjacent Intima n=2	All n=6	Holzapfel et al. (2004) Iliac Circ. Cap n=9	Medial Intima n=4	Axial Cap n=8	Medial Intima n=4	All n=25
1.00	[10]	200	110	500	0	250	270	90	330	200	0	75	0	25	130	500	100	390	220
1.05	500	890	170	530	20	290	4900	1100	3000	2700	380	100	20	170	1600	$10*10^3$	4200	$11*10^3$	$5*10^3$
1.10	1900	2300	270	630	80	380	$16*10^3$	3500	6500	8200	1500	170	75	590	4700	$36*10^3$	$15*10^3$	$41*10^3$	$19*10^3$
1.15	[4200]	4300	430	800	180	530	$35*10^3$	7300	$11*10^3$	$17*10^3$	3400	290	170	1300	9300	$78*10^3$	$32*10^3$	$[88*10^3]$	$40*10^3$
1.20	[7400]	7100	630	1000	310	740	$60*10^3$	$13*10^3$	$16*10^3$	$28*10^3$	6100	460	300	2300	$16*10^3$	$140*10^3$	$56*10^3$	$[150*10^3]$	$70*10^3$
1.25	$[12*10^3]$	$10*10^3$	890	1300	490	1000	$93*10^3$	$19*10^3$	$[22*10^3]$	$43*10^3$	9500	670	470	3600	$23*10^3$	$[210*10^3]$	$87*10^3$	$[240*10^3]$	$110*10^3$
1.30	$[17*10^3]$	$15*10^3$	1200	1700	700	1300	$130*10^3$	$27*10^3$	$[28*10^3]$	$60*10^3$	$14*10^3$	930	680	5100	$33*10^3$	$[300*10^3]$	$[120*10^3]$	$[340*10^3]$	$150*10^3$
1.35	$[23*10^3]$	$19*10^3$	1500	2100	960	1700	$180*10^3$	$37*10^3$	$[36*10^3]$	$81*10^3$	$19*10^3$	1200	930	7000	$44*10^3$	$[410*10^3]$	$[170*10^3]$	$[460*10^3]$	$210*10^3$
1.40	$[30*10^3]$	$25*10^3$	2000	2600	1200	2100	$230*10^3$	$47*10^3$	$[44*10^3]$	$100*10^3$	$25*10^3$	1600	1200	9000	$[57*10^3]$	$[530*10^3]$	$[220*10^3]$	$[600*10^3]$	$270*10^3$

Circ. = Circumferential, n= Number of the samples. Values in brackets correspond to the stretch values that exceed the test range.

*: The groups the samples belonged to were not identified in the stress-strain plot in the original paper. Therefore, the groups were combined.

**: Preoperative classification of the samples was used.

Table 6.4: Calculated tangential stiffness (in kPa) of average compression properties

Stretch	Maher (2009) Carotid Radial				Barrett (2009) Carotid Radial	Topoleski (1997) * Aortoiliac Radial				Salunke (2001) Aortoiliac Radial			
	Calcified	Mixed	Echolucent	All		Type 1 (Calcified)	Type 2 (Fibrous)	Type 3 (Atheromatous)	All	Calcified	Fibrous	Atheromatous	All
	n=16	n=23	n=5	n=44	n=48	n=1	n=1	n=1	n=3	n=5	n=7	n=6	n=18
1.00	0	0	15	0	33	<10	<10	<10	10	10	10	15	12
0.95	140	20	20	65	33	830	<10	<10	283	70	100	25	67
0.90	570	80	40	260	33	3300	<10	<10	1107	270	270	40	193
0.85	1300	190	65	570	34	7500	20	<10	2510	590	540	70	397
0.80	2300	330	100	1000	35	$[13*10^3]$	85	<10	4365	1000	900	100	661
0.75	3600	510	150	1600	36	$[21*10^3]$	240	<10	7083	1600	1300	140	997

n= Number of the samples. Values in brackets correspond to the stretch values that exceed the test range.

*: Values were obtained from a representative sample for each plaque type

A variety of strain and stress measures were used in the studies. Nominal (engineering or Cauchy) strain, Green-Lagrangian strain, and stretch were the most commonly used deformation measures. Stress data were reported either as engineering (nominal) stress or as Cauchy (true) stress. For consistency, we report stretch values (λ) and Cauchy stress values (σ) in this review. The following formulas were employed to calculate them from the original stress and deformation measures reported in the papers:

$$\lambda_i = \varepsilon_i + 1 \qquad \text{i=1, 2, 3 ;} \qquad (1)$$

$$\lambda_i = (2e_i + 1)^{0.5} \qquad \text{i=1, 2, 3 ;} \qquad (2)$$

$$\sigma_i = \lambda_i S_i \qquad \text{i=1, 2, 3 ;} \qquad (3)$$

where λ_i is the stretch, ε_i is nominal strain, e_i is Green-Lagrangian strain, and S_i is the nominal stress in the principal direction i.

After digitizing the experimental results, and calculating stretch and Cauchy stress values; we fitted a cubic polynomial function, as was previously applied by Loree et al. [94], to the stretch and Cauchy stress results using nonlinear curve fitting tool in MATLAB (R2010a, The MathWorks Inc.). Stress values were fitted for stretch values between 1 and 1.4 for tensile tests and between 1 and 0.75 for compression tests, even if this range exceeded the experimental stretch range. We calculated the tangential stiffness, defined as the derivative of the cubic function fitted to Cauchy stress-stretch relation, to compare the nonlinear properties of intima tissue at several stretch levels. The tangential stiffness values of the tensile and compressive studies are summarized in Table 6.3 and Table 6.4.

Coronary plaques

Tensile properties: Mechanical tensile properties of 25 coronary plaques were determined by Born&Richardson [31]. Axial and circumferential intima samples were subjected to uniaxial tension tests immediately after autopsy. The tests were performed at room temperature without preconditioning. The nominal stress-stretch results of 5 samples were graphically presented. Figure 6.2 illustrates the range of the measurements and the mean of the fitted data. Considerable variability in the results was observed. Stresses at stretch values below 1.05 and above 1.15 were not measured. We calculated the average tangential stiffness as 500 kPa at a stretch level of 1.05 and 7400 kPa at a stretch level of 1.20 (Table 6.3).
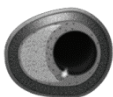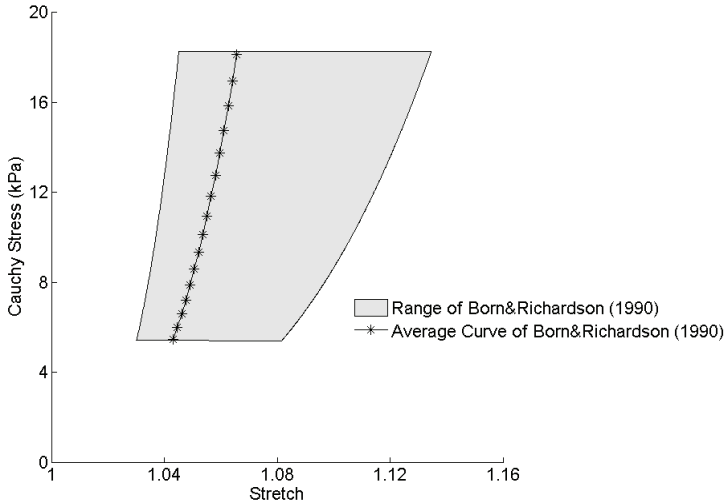
Figure 6.2: Test range and average response curve of the uniaxial tensile test results of Born&Richardson [31]. The range is defined by the stiffest and softest material response of the specimens tested.

Compressive properties: No studies on compressive mechanical properties of human coronary atherosclerotic intima complied with our inclusion criteria.

Carotid plaques

Tensile properties: Maher et al. [37] performed uniaxial tension tests on 16 carotid plaque specimens obtained from 10 patients. Tests were conducted in circumferential direction within two hours after endarterectomy. Based on pre-operative ultrasound imaging, the specimens were classified as calcified (n=8), echolucent (n=4) or mixed (n=4). There were no significant differences between the mechanical responses of the three groups. The range and the average response of all samples are shown in Figure 6.3. Stiffness values were comparable to coronary plaque stiffness values reported by Born&Richardson et al. [31]; however, the values in the low stretch region were larger. The average tangential stiffness modulus was 890 kPa at a stretch level of 1.05, and 7100 kPa at a stretch level of 1.2 (Table 6.3). Lawlor et al. [33] subjected surgically removed carotid plaques to uniaxial tension tests in circumferential direction, too. Based on pre-operative ultrasound imaging, plaques were divided into three groups: hard, mixed and soft. The results were not significantly different between the groups. The average tangential stiffness moduli off all samples were 290 kPa and 740 kPa at stretch levels of 1.05 and 1.20 (Table 6.3),

respectively. Compared to the carotid plaque measurements of Maher et al. [37], the results were significantly lower. This might be partly attributed to a lower number of hard (calcified) plaques included in the study. Only two of 14 plaques were identified as hard postoperatively whereas half of the plaques were calcified in the study of Maher et al. [37].

Figure 6.3: Test range and average response curve of the uniaxial tensile test results of Maher et al. [37] and Lawlor et al. [33]. The range is defined by the stiffest and softest material response of the specimens tested.

Compressive properties : Besides uniaxial tensile tests, Maher et al. [37] also performed unconfined compression tests in radial direction on carotid artery plaque sections. Forty-four plaque samples were obtained from 11 patients. The samples were classified as calcified (n=16), echolucent (n=5) and mixed (n=23) based on ultrasound imaging and were loaded up to stretch levels between 0.90 and 0.40. Calcified samples showed the stiffest response with a tangential stiffness of 140 kPa at a stretch level of 0.95 and 2300 kPa at a stretch level of 0.80. The echolucent samples showed the softest response with 20 kPa at a stretch level of 0.95 and 100 kPa at a stretch level 0.80 (Table 6.4). Large variability was observed within plaques and between patients.

Barrett et al. [30] studied radial compressive properties of fibrous caps dissected from carotid artery plaques by micro-indentation tests. The experiments were done within 3 hours after surgery. Heavily calcified plaques were excluded from the study. They used a finite element model with neo-Hookean strain energy

function to estimate the radial compressive properties of the specimens. Tangential stiffness values ranged from 21 to 300 kPa. The average stiffness was relatively constant and varied from 33 kPa at a stretch level of 0.95 to 35 kPa at a stretch level of 0.80 (Table 6.4). Although the tangential stiffness values are lower than the ones of the echolucent samples from Maher et al. on average [37], there is some overlap in the reported range of the test results from both papers (Figure 6.4).

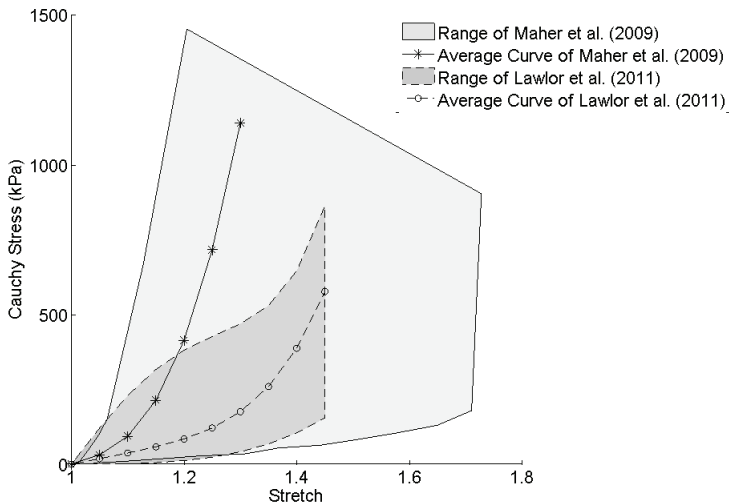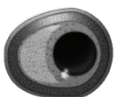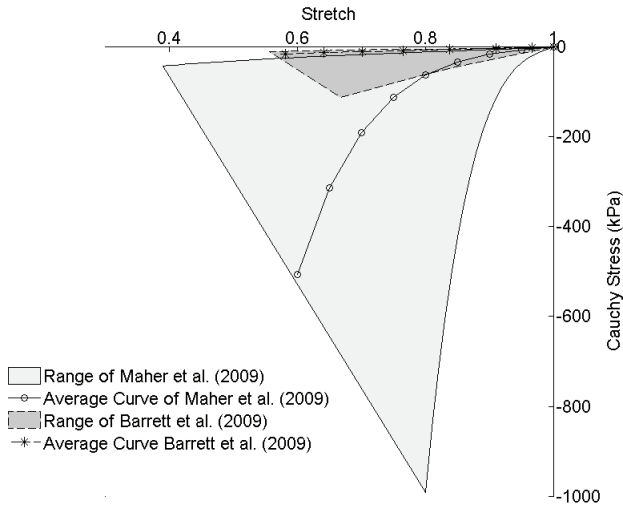**Figure 6.4: Test range and average response curve of the compressive test results of Maher et al. [37] and Barrett et al. [30]. The range is defined by the stiffest and softest material response of the specimens tested.**

Aortic plaques

Tensile properties: Loree et al. [94] studied the tensile properties of a specific part of the intima, being of fibrous caps dissected from aortic plaques. The tests were done in circumferential direction within 36 hours after death. 'Visibly uncomplicated' specimens (n=26) were mainly obtained from abdominal aortas from 21 autopsies. Based on histology, the samples were identified as cellular (n=12), hypo-cellular (n=9), or calcified (n=5). Large variation in test results was observed for all tissue types (Figure 6.5). Hypo-cellular samples were on average about five times stiffer than cellular samples (Table 6.3) Hypo-cellular and cellular samples had an average stiffness of 4900 kPa and 1100 kPa, respectively, at a stretch level of 1.05. The stiffness was 60000 kPa for hypo-cellular samples and 13000 kPa for cellular samples at stretch levels of 1.20. Calcified samples were softer (3000 kPa at stretch levels of 1.05 and 16000 kPa

at stretch level of 1.20) than hypo-cellular samples. However, there was no statistically significant difference in stiffness moduli of the three tissue types due to the large variation in each group. In an earlier study on tensile properties by Lendon et al. [35], a limited number of aortic plaque samples (2 ulcerated plaque caps, 2 non-ulcerated plaque caps and 2 nearby intima) were tested. The range of the test results was comparable to the ones of Loree et al. [94] (Figure 6.5). The non-ulcerated caps were stiffer than the ulcerated caps and adjacent intima although no significant difference was found due to the small sample size (Table 6.3). The tangential stiffness was 170 kPa at a stretch level of 1.05 and 2300 kPa at a stretch level of 1.20 if all samples were grouped together.
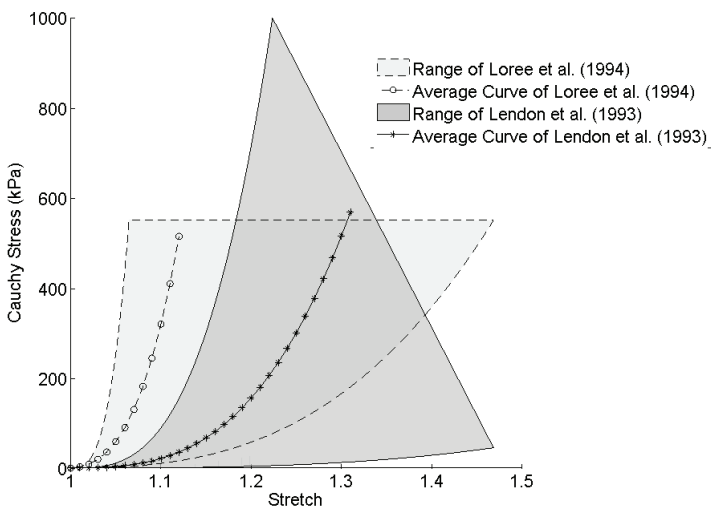
Figure 6.5: Test range and average response curve of the uniaxial tensile test results of Loree et al. [94] and Lendon et al. [35]. The range is defined by the stiffest and softest material response of the specimens tested.

Compressive properties: Although lack of the stress-strain results was one of our exclusion criteria, we made an exception for the following two papers since they were the only studies investigated compressive properties of aortic plaques. Lee et al. [34] evaluated the radial compressive properties by testing 27 fibrous caps from 14 abdominal aortas. Caps were classified as cellular (n=7), hypocellular (n=9), and calcified (n=11) based on histological examination. The tests were conducted at room temperature within 16 hours of death. The dynamic stiffness and phase angles of the test samples were evaluated by applying a static compressive stress of 9.3 kPa in the radial direction first and a dynamic stress with an amplitude of 0.5 kPa at different frequencies thereafter. The stiffness
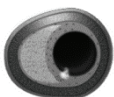
values increased with increasing frequency; however, the change was less than 10% between the frequencies 0.5, 1, and 2 Hz. As the stiffness was determined at a fixed load, the samples were subjected to different stretch levels. The average dynamic stiffness was 510 kPa for cellular, 900 kPa for hypocellular and 2200 kPa for calcified samples. In 1992, Lee et al. [97] studied the relation between the compressive mechanical properties and intravascular ultrasound classification of aortic plaques, utilizing a static measurement protocol. Forty-three atheroma caps were obtained from abdominal aortas. Nonfibrous samples had an average stiffness modulus of 40 kPa. The modulus for fibrous caps was 80 kPa and the one of calcified caps was 360 kPa. The corresponding stretch values were 0.75 for nonfibrous caps, 0.85 for fibrous caps and 0.97 for calcified caps. In general, the static stiffness values were about one order lower than the dynamic stiffness values reported in their previous paper [34].

Iliac and femoral plaques

Tensile properties: Holzapfel et al. [95] investigated the mechanical properties of atherosclerotic intima tissue of 9 iliac artery plaques under uniaxial tensile loading. The lesions were type V (fibroatheroma) or higher. They evaluated the properties of fibrous cap tissue near the luminal side (9 circumferential and 8 axial samples) and fibrous intima tissue near media (4 circumferential and 4 axial samples). The tests were conducted at 37°C after 5 cycles of preconditioning. The test results of axial samples from fibrous caps and from fibrous intima samples showed very similar ranges (Figure 6.6). For the circumferential samples, the overlap was smaller. Fibrous cap samples were about three times stiffer in axial direction than in circumferential direction (4200 versus 1600 kPa at stretch level of 1.05 and 56000 versus 16000 kPa at stretch level of 1.20). The fibrotic intima showed comparable values in both circumferential and axial directions over the whole stretch range (Table 6.3). In circumferential direction the fibrous intima samples were about 10 times stiffer than the fibrous cap samples.

Compressive properties: Topoleski et al. [147] investigated radial compressive behavior of aortoiliac plaques. Twenty-four non-ulcerated lesions were obtained from 6 autopsies and stripped from the remaining vessel wall. The samples underwent two 15-cycle loading phases with a 10-15 minute unloaded rest period in between. The main focus of the study was on repeatability and recoverability, which were introduced for the first time and are comparable to preconditioning. We extracted tangential stiffness values from the representative curves (Table 6.4). Atheromatous plaques showed the most compliant response (stiffness<10 kPa for stretch values between 1 and 0.75). Fibrous samples were stiffer, however, still much softer than calcified samples (830 kPa versus <10
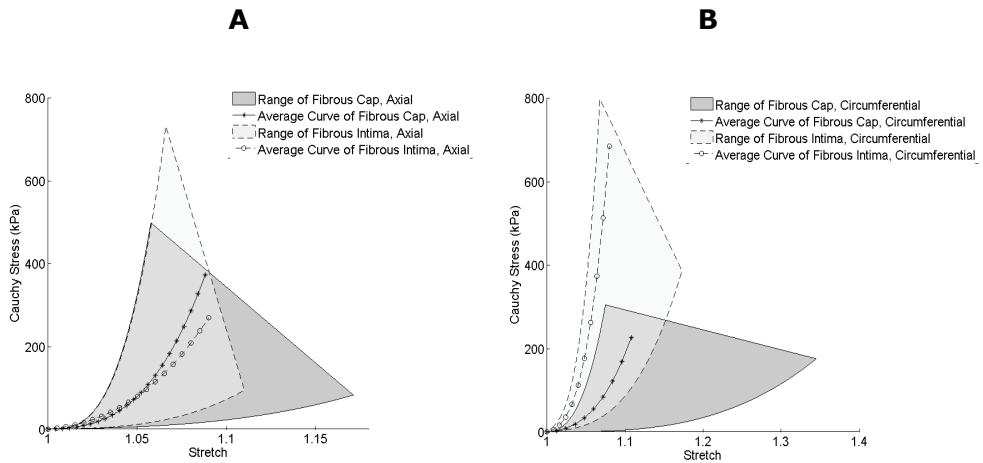
Figure 6.6: Test range and average response curve of the uniaxial tensile test results in axial (A) and circumferential (B) direction reported by Holzapfel et al. [95]. The range is defined by the stiffest and softest material response of the specimens tested.

kPa at a stretch level of 0.95 and 13000 kPa versus 85 kPa at stretch levels of 0.80). The same group further investigated the compressive stress-relaxation behavior of aortoiliac plaques in radial direction [148]. Twenty-three samples (5 calcified, 7 fibrous, 6 atheromatous) were obtained from post-mortem atherosclerotic plaques. After two 15-cycle loading phases, the samples were subjected to three stress-relaxation phases. Atheromatous tissue had a lower stiffness compared to calcified and fibrous tissue (25 kPa versus 70 at 0.95 stretch; 100 kPa versus 1000 and 900 kPa at 0.80 stretch). Compared to Topoleski et al. (1997), calcified tissue was more compliant while fibrous and atheromatous tissue had higher stiffness (Table 6.3).

Comparison of the experimental data

The studies reviewed were different in many aspects. Varying preconditioning protocols were used, the temperatures at which the experiments were conducted were different, and freshness of samples and their treatment until the experiments were diverse. Furthermore, the number of studies conducted for plaque samples from each vascular territory was limited. Firm conclusions and direct comparisons based on the reported experiments in these studies should therefore be regarded with caution. Keeping these limitations in mind, we compared the stiffness values obtained from the studies. In order to make a fair comparison, we fitted a third order polynomial to the experimental data of all
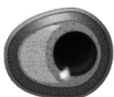
studies. The third order polynomial captured the nonlinearity of the experimental data nicely and fitted the data well. The circumferential tensile stiffness and the radial compressive stiffness values are compared in Figure 6.7. Since the loading directions were not reported in all studies, the stiffness values for the different directions were averaged (Table 6.5 and Table 6.6).
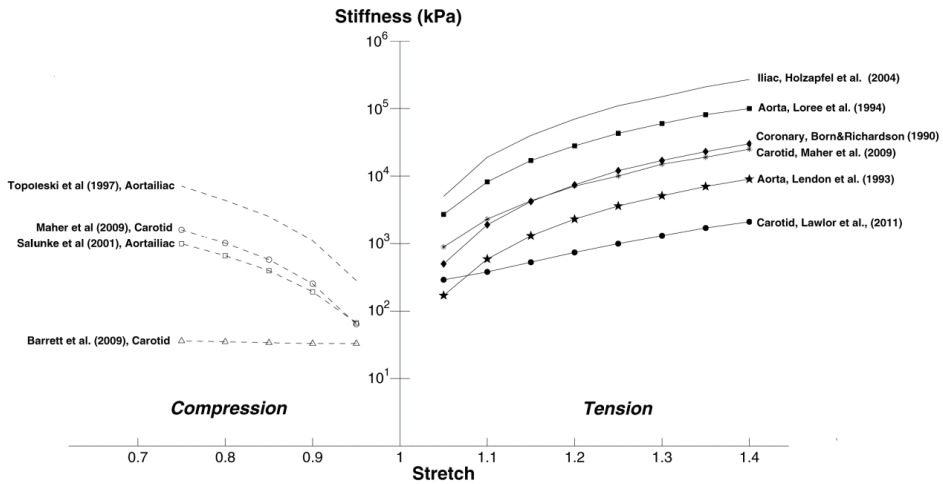
Figure 6.7: Comparison of tangential stiffness calculated from the data reported in the reviewed papers

From the comparison of the experimental studies presented above, we reached 5 main conclusions. First, all experiments reported non-linear strain hardening behavior of the plaques, regardless of the loading direction and vascular territory. For the samples subjected to circumferential tension, this behavior is generally attributed to the collagen fibers. For low strain values, collagen is mainly present in a wavy pattern and the fibers do not contribute to the loadingcapacity. Upon increasing strain, collagen fibers align and stretch. Since the collagen fibers are generally stiff, they lead to the non-linear increase in stiffness. The reason for non-linear behavior of plaque tissue under radial compression is much less clear.

Secondly, the results from each individual study demonstrated a great dispersion. Even the average values for plaques originating from the same vascular territory showed a considerable spread. This is illustrated when we compare the results from Maher et al. [37] and Lawlor et al. [33]. These studies followed comparable procedures to evaluate the circumferential tensile properties of carotid plaques but the resulting stiffness values at a stretch level of 1.2 differed almost an order of magnitude (7100 kPa versus 740 kPa).

Table 6.5: Parameter values (in kPa) of the cubic polynomial fitted to average response curve from the studies on tensile properties

Parameters	Maher (2009) Carotid				Salunke (2001) Aortoiliac			
	Calcified	Mixed	Echolucent	All	Calcified	Fibrous	Atheromatous	All
A	19000	2742	718	8424	8458	6068	538	4888
B	0	0	0	0	16	405	54	180
C	0	0	15	2	10	9	15	11

Table 6.6: Parameter values (in kPa) of the cubic polynomial fitted to average response curve from the studies on compressive properties

Parameters	Born & Richardson (1990)	Maher et al. (2009)	Lawlor et al. (2011)				Loree et al. (1994)				Lendon et al. (1993)				Holzapfel et al. (2004)				
	All	All	Hard	Mixed	Soft	All	Hypo-cellular	Cellular	Calcified	All	Non-ulcerated Cap	Ulcerated Cap	Adjacent Intima	All	Cap	Medial Intima	Cap	Medial Intima	All
A	61553	45700	3741	5051	2244	3661	462324	93035	51624	202925	50650	3182	2520	26916	106682	1085723	450518	1219748	551446
B	0	3440	0	255	0	109	11598	3273	23278	9938	0	0	0	0	6605	13398	7111	17758	9638
C	13	200	1193	129	62	252	267	87	332	193	0	74	0	37	129	499	103	387	221

Notes:

- A cubic polynomial function, $\sigma = A\varepsilon^3 + B\varepsilon^2 + C\varepsilon$, was fitted to the experimental results with A, B, C > 0 to ensure monotonic increasing function through the origin. σ is the Cauchy stress and ε is the true stress in the test direction.

- No curve was fitted to the experimental results of Barrett et al. (Barrett et al., 2009). Stiffness values were calculated from the Neo-Hookean material model presented in the paper with the assumption of isotropy.

- A higher order polynomial function had to be fitted to the results of Topoleski et al. (Topoleski et al., 1997) because the cubic polynomial function could poorly fit the results (R-values < 0.8). Moreover, not all the experimental results but only representative curves for each plaque classification were reported in the corresponding paper. Therefore, this study is not included in the Table 6.5.

The same holds for the radial compressive properties: the values for carotid specimens reported by Maher et al. [37] were much larger than the values reported by Barrett et al. [30] (1000 kPa versus 35 kPa for a stretch value of 0.8). Since the mechanical properties of the different plaque type can vary greatly, these results suggest that the plaque phenotypes used in these studies were probably different.

The third general conclusion is that the stiffness under extension in circumferential direction seems to be much higher than the compressive stiffness in radial direction (Figure 6.7). This is most clearly demonstrated by the study from Maher et al. [37], in which results for both circumferential tension and radial compression were reported for carotid plaques. The results indicate that circumferential stiffness under tension is one order of magnitude larger than the radial compressive stiffness. The contribution of collagen is probably responsible for this. The stiff collagen fibers can carry load under tension but are unlikely to bear load under compression, regardless of the fiber orientation. We have to mention though that the circumferential properties of carotid plaques reported by Lawlor et al. [33] indicate higher stiffness values than the compressive radial properties from Maher et al. [37].

Histological studies of coronary and carotid plaques suggest similar mechanical behavior for both plaque types. The circumferential tensile properties of atherosclerotic coronary intima tissue from Born&Richardson [31] are comparable to the ones measured by Maher et al [37] for carotid intimasconfirming the histological observations that plaque types from these territories are similar. However, the results from Born&Richardson [31] are based on a limited number of samples (n=5), and Lawlor et al. [33] reported much lower stiffness values. In general, the previously mentioned dispersion in the reported results prevents ordering stiffness values according to the vascular domain the plaques originate from. Although one would expect e.g. aortic and iliac plaques to be stiffer than carotid and coronary plaque based on histology, our fourth conclusion is that this expectation is not reflected by the experimental data.

Our final conclusion refers to the use of histological data. The benefit of including histological data when reporting on mechanical properties was illustrated by the study of Loree et al. [94]. The samples that they labeled as 'hypocellular' resemble plaque type VIII (fibrous plaque). Based on the composition of the plaque, the reported high stiffness values can be expected. However, it is not possible to relate material stiffness to the plaque composition for most of the studies since histological data were missing.

6.4   Biomechanical Modeling Implications

In the previous parts of this review, the pathology of atherosclerotic plaques was discussed from a mechanical perspective and the available experimental data that potentially can be used for macroscopic biomechanical modeling were reviewed. In this final part, we will try to sublimate these two parts -plaque pathology and atherosclerotic intima properties- and provide guidelines for future experimental protocols, evaluate implications for biomechanical modeling and finally discuss the clinical implications.

For mechanical testing of biological tissue, *preconditioning* was recognized by Fung et al. [149] as a requirement to obtain consistent results. Preconditioning is typically applied until tissue response becomes reproducible before recording the stress-strain behavior. Although generally accepted as an essential part of the testing procedure, preconditioning was not always performed or the protocol was not reported in the studies that we reviewed (see Table 6.2). The freshness of the tested samples also varied between the studies. In some studies, tests were conducted within few hours after the test samples had been obtained while in others, the samples were refrigerated (stored at 4°C) for a considerable time period until the experiments. To our knowledge, there is no experimental study available in literature that investigated the effect of refrigeration on mechanical properties of atherosclerotic plaques. The effect of freezing (e.g. at -80°C) on the mechanical properties of healthy arteries is ambiguous [150-153], although deep freezing seems to be preferable over refrigeration. The only study on freezing of diseased arterial segments [154] did not report any significant effect. This study also investigated the influence of testing temperature by conducting the experiments either at room temperature or at a physiological temperature of 37°C. No difference was reported between strain for diseased arteries measured at 23°C and 37°C [154]. Temperatures below room temperature, however, may have an impact on the mechanical behavior of lipids in the plaque, especially when cholesterol crystals are forming [155]. Based on the above, we strongly advise to execute and report preconditioning protocols. Furthermore, the samples should preferably be as fresh as possible and tested at 37°C.

All the above described effects possibly contribute to the large variety found in the reported data and their effects cannot be separated from the influence of heterogeneous character of diseased intima tissue on its material behavior. An important factor therein is the type of plaque the test sample is obtained from. In most studies, plaque characteristics were not mentioned at all or described inadequately. In all studies that classified the test specimens, one of the groups was 'calcified specimens. In these cases, calcified samples always showed stiffer
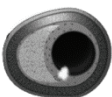
behavior than the other groups. However, comparing the results of calcified samples between studies showed large differences. The underlying cause may be in the different calcium content in the samples. A systematic approach to classify the plaques and samples, e.g. the classification scheme introduced by Stary et al. [8], would greatly add to the understanding of the differences and similarities of mechanical behavior of atherosclerotic intima from different vascular territories. Since the plaque type largely determines the mechanical properties of atherosclerotic intima and the available experimental data cannot be directly linked to the plaque type, it is currently not possible to identify which material model is appropriate for which plaque type. This implies that macroscopic modeling studies should include sensitivity analyses, such as [92], or employ several material models [64] to cover the wide range of reported atherosclerotic intima properties. The parameters given in Table 6.5 and Table 6.6 can be used to generate the appropriate stress-strain curves for this purpose.

Although a considerable number of studies have been performed on mechanical properties of atherosclerotic intima tissue, some data are still missing on the tensile or compressive properties for different vascular territories, especially for coronary arteries. This can mainly be attributed to tissue availability. Carotid artery plaque tissue is more available than plaque tissue from other vessels, as carotid plaques are removed surgically on high-risk indication. Coronary plaques are much harder to obtain for mechanical analysis as they are often treated by coronary angioplasty or by stent placement. Moreover, samples from coronary, aortic, femoral, and iliac arteries are mainly available after autopsy and are therefore logistically more challenging to obtain. It should also be kept in mind that unstructured –and therefore probably softer- samples are unfit for mechanical testing with the equipment used in most studies, resulting in a bias towards the stronger and stiffer plaque samples. Testing the intact arterial segments without compromising the integrity of the plaque is preferable and can be accomplished by means of e.g. inflation test using intravascular ultrasound [156-159] or optical techniques [160]. A drawback of this technique is that highly reliable displacement measurements are needed and that an inverse approach is required to determine the material properties. These ex vivo inflation experiments can also be used to further develop and optimize in vivo strain measurement techniques for material property estimation like intravascular palpography [10, 159] and MRI strain measurements in the carotid artery [161, 162].

A valuable source of samples for mechanical testing might be atherosclerotic plaques from animals. The most commonly used animal model to study

atherosclerosis is the genetically modified murine model. Mice with a genetic disorder in the lipid metabolism develop atherosclerotic plaques within weeks if put on a western diet. The plaques that these mice develop have features that resemble human vulnerable plaques to some extent. Especially the plaques that develop upstream of a surgically placed flow-altering device in the carotid artery are widely used [163]. In general, due to the small size, the mouse model is unfit for macroscopic mechanical testing although atomic force microscopy experiments were recently reported to study murine plaque properties [103]. Some types of rabbits also develop plaques when fed a high-fat diet, however, these plaques tend to be immature, fatty streak like lesions, and are therefore less suitable as atherosclerosis model [164] A more appropriate, but also more expensive model for atherosclerosis is the hypercholesterolaemic porcine model [165, 166]. After induction of diabetes and being fed a western diet, these mini-pigs develop plaques that share many features with human vulnerable plaques. Since the typical dimensions of the porcine vasculature are close to the dimensions of the human vasculature, these models are frequently used to evaluate intracoronary devices, including stents [167]. Although the atherosclerotic pig model is expensive, it is an ideal model for the development of new methods for mechanical characterization of atherosclerotic intima.

Determining the mechanical properties of atherosclerotic intima is essential for stress analyses of atherosclerotic plaques. However, determining the stress in a plaque is only half of the equation. We also need to know at which stress level the tissue ruptures. Lendon et al. [108] reported that fracture stress of ulcerated plaques was significantly lower than the one of non-ulcerated plaques (200±50 vs. 600±100 kPa) in atherosclerotic human aortas. Some of the experimental studies that determined the stiffness of atherosclerotic tissue also evaluated the point of tissue failure. Fracture stress of human aortic plaques was estimated as 480±220 kPa [94]. Holzapfel et al. measured ultimate tensile stress as 255±80 kPa in the circumferential direction and as 470±100 kPa in the axial direction for fibrous caps excised from atherosclerotic human iliac arteries [95]. Recently, Lawlor et al. reported a range between 130 and 780 kPa for the ultimate tensile stress of atherosclerotic human carotid plaques as 470±100 kPa by circumferential tensile tests [33]. A local inhomogeneity can strongly influence the failure behavior of plaque tissue, depending on the differences in stiffness and how intertwined the components are. For instance, micro calcifications (10-μm-diameter) are frequently observed in atherosclerotic plaques using high resolution in vitro CT imaging [71, 119]. When these micro calcifications are present in the fibrous cap, they may locally elevate stresses in the cap. Besides focusing on the mechanical properties of atherosclerotic tissue, determining the
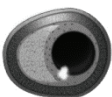
strength of the tissue with respect to the type of tissue, the plaque component and for instance the presence of micro calcifications or inflammatory cells is vital for future rupture risk assessment of atherosclerotic plaques.

Biomechanical plaque modeling has gained popularity as a research tool for predicting the effect of interventions [168-170] and for risk stratification [68, 171, 172]. The value of these models highly depends on the quality of the input data. Recent developments in imaging technology, such as carotid MRI, are promising: they combine tissue contrast with increasing resolution and provide data that can potentially serve as an input to generate reliable 3D plaque reconstructions. To predict the subsequent plaque stresses accurately, the material properties of diseased intima are required. This review demonstrates that the currently available experimental data are not sufficient to perform plaque specific biomechanical simulations. To reflect the variation in reported mechanical properties, sensitivity analyses seem to be indispensable, which implies that we need to report not only absolute stress values but also include confidence intervals. Whether macroscopic models suffice to describe the behavior of the complex and heterogeneous intima tissue is open question. When using biomechanical models for risk stratification, one also needs to include the expected variation in strength values. Although much work needs to be done, both from an experimental and numerical point of view, biomechanical plaque modeling has the potential to eventually provide essential support to clinicians for therapy planning and risk stratification.
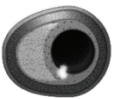
Chapter 7

Local Axial Compressive Mechanical Properties of Human Carotid Atherosclerotic Plaques

Characterization by Indentation Test and Finite Element Inverse Analysis

7.1   Introduction

Atherosclerotic plaque rupture is the main cause of ischemic stroke and myocardial infarction. Plaque rupture can lead to thrombus formation on the disrupted plaque surface and subsequent embolisation of thrombus into the distal vessels or to acute vessel occlusion. Rupture prone plaques are characterised by the presence of inflammatory cells, intraplaque haemorrhage and a lipid rich necrotic core (LRNC) covered by a thin fibrous cap. A reliable prediction model of cap rupture would have a big impact on the treatment of atherosclerosis and atherosclerosis-related diseases [173]. Currently, the used methods to estimate plaque rupture is merely based on geometrical parameters, whereas biomechanical models have shown to provide a better risk assessment [27, 64, 103, 174, 175]. However, the results of these models strongly depend on material properties of individual plaque components. Therefore, these models will benefit from specific knowledge of material properties of individual plaque components.

Experimental data on the mechanical properties of atherosclerotic tissue are scarce and show large variability, ranging from very soft (30-40 kPa, [30, 97]) to very stiff (in the order of 1 MPa, [34, 94, 95, 133]). Moreover, most of the data represent only the average global stiffness of the plaque tissue tested and do not distinguish between different plaque components.

Recently, an experimental technique was developed by Cox et al. [176, 177], combining micro-indentation tests on soft biological materials with confocal laser scanning microscope imaging. We apply this technique to investigate the compressive Young's moduli of different plaque components in the axial direction.

7.2   Methods

<u>Preparing plaque tissue</u>

Eight carotid artery endarterectomy specimens were obtained from eight symptomatic patients (2 female, 6 male, age 59 to 87). All plaques had ≥ 70 % stenosis and low calcium content on preoperative CT angiography. Approval was given by the Institutional Review Board of the Erasmus MC, and informed consent was obtained. The plaques were snap-frozen, using liquid nitrogen and stored at -80˚C. In a later stage, the plaques were sectioned, using a Leica cryotome at -20˚C. Slices of 200 μm thicknesses were obtained with 1 mm spacing in between for the indentation experiments (Figure 7.1).
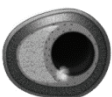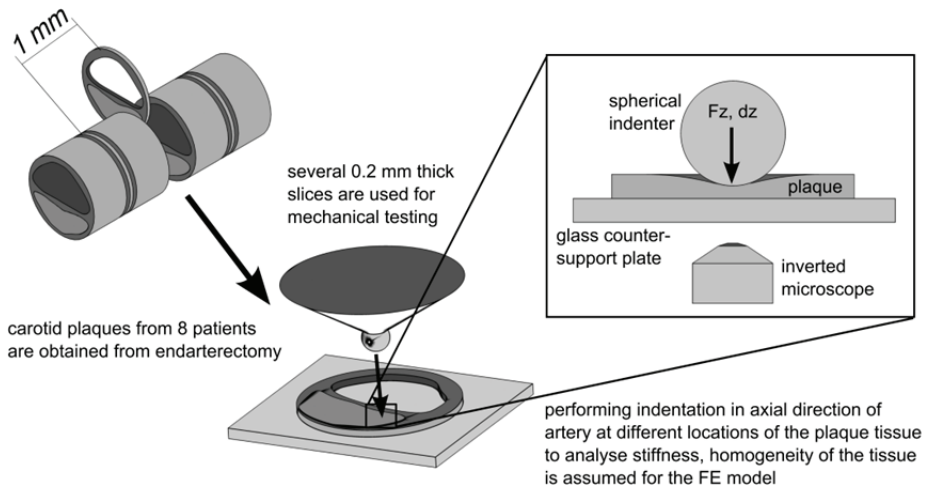
Figure 7.1: Sectioning of the plaque tissue with a cryotome to create 200 μm thick slices for mechanical testing. Depending on the axial length of the plaque, 6 to 13 slices were obtained. Adjacent slices were used for histology.

Distal and proximal to each test section, slices of 5 μm thickness were cut for histology. A Gomori trichrome staining was applied on these slices. This stains collagen green/blue, muscle cells red, and nuclei black/blue. The histological images were used to determine indentation locations by visual registration before the experiments.

Prior to the mechanical testing, the 200 μm thick sections were thawed at room temperature and stained overnight using a fluorescent CNA35-OG488 probe [178]. This fluorescent staining was applied to visualise the collagen architecture of the plaque tissue.

Indentation test and imaging

To analyse the local mechanical properties of a plaque tissue, an existing indentation test set-up [176] was adapted, using a surface force apparatus developed by Vaenkatesan et al. [179]. At each testing location at least three consecutive indentations were performed using a spherical indenter with a diameter of 2 mm. During indentation the force response and the indentation depth were recorded. As described in Cox et al. [180], the first indentation was considered as preconditioning and these results were not included. The measurements at the same indentation location were averaged. An inverted confocal laser scanning microscope (magnification 10x, excitation 488 nm, emission 500 nm high-pass), located underneath the set-up, was used to visualise the collagen structure, which were fluorescently stained (Figure 7.1 and

Figure 7.2 [178]). More detailed information regarding the indentation set-up can be found in Cox et al. [176].
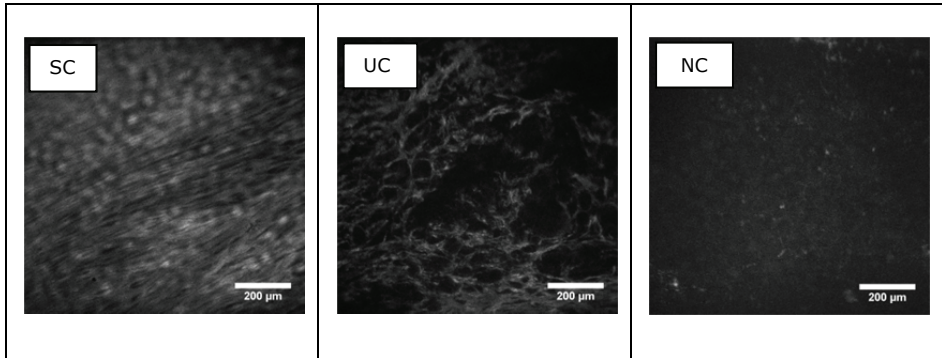
Figure 7.2: Examples of a dense structured collagen location (SC), a loose unstructured collagen location (UC) and a collagen poor lipid pool location (NC)

Data analysis

A 3D finite element model was created to simulate the indentation experiment, as previously described by Cox et al. [176]. The behaviour of the tissue was described with an isotropic incompressible Neo-Hookean model. The local shear modulus *G* at the test location was estimated by fitting the model to the experimental force-indentation depth curve. The force response of up to 30 % indentation of the tissue thickness was used for the parameter identification (Figure 7.3). Simulations confirmed that the circumferential strain at 30 % indentation of tissue thickness was about 20 %, which corresponds to the upper limit of physiological strain range. The contact radius between indenter and tissue was about 0.4 mm². To fit the experimental data to the simulated data, the least-square method was used. To compare the results obtained in this study with the results in literature the Young's modulus *E* was calculated from the shear modulus *G* with *E* = 3·*G.*

Measurement positions were classified by their indentation location and collagen structure. Based on the collagen structure, three different types of collagen architectures were distinguished using the confocal microscope (Figure 7.2). Following the approach of Timmins et al. [181], a customised MATLAB (R2010a, The MathWorks Inc.) script was generated to estimate the alignment index (*AI*) of the collagen fibres. The *AI* was given by

$$AI = \frac{\frac{\delta}{(\Delta+\delta)}}{\frac{\delta_{IR}}{(\Delta+\delta)_{IR}}} = \frac{\frac{\delta}{(\Delta+\delta)}}{\frac{40}{180}}$$
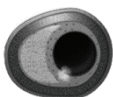
where δ described the sum of frequencies of fibres within ±20º of the preferred fibre alignment (PFA) and Δ was the sum of frequencies of the remaining fibres outside of this range. The sums of frequencies δ_{IR} and Δ_{IR} described the corresponding sum of frequencies for an ideal random (*IR*) distribution, where the fibre dispersion is isotropic. These sum of frequencies were per definition δ_{IR} = 40 and Δ_{IR} = 140.

To decide if the collagen distribution was structured or unstructured an arbitrary threshold of *AI* = 1.4 was chosen. Therefore, locations which showed a high amount of collagen fibres with a clear alignment (*AI* > 1.4) of the fibres were classified as dense structured collagen areas (SC). Positions with high amounts of collagen, but no clear alignment of the fibres (*AI* < 1.4), were characterised as loose unstructured collagen locations (UC). Collagen poor areas, primarily in the lipid rich necrotic core (LRNC) region, were classified as CP.
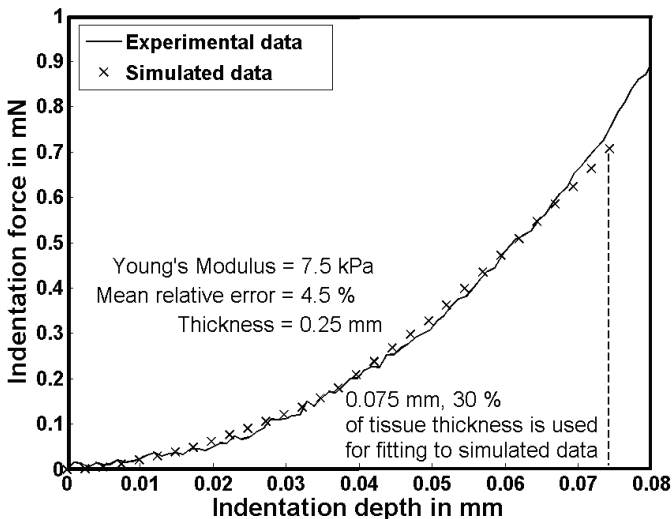
Figure 7.3: Fit of simulated data to experimental data. Least-square method was used to fit the experimental force-indentation data to a neo-Hookean material model, 30 % of the tissue thickness (here: 0.075 mm) was indented and used for fitting.

Each slice was indented at one to eight different locations. The locations were classified as middle of the fibrous cap, shoulder region of the fibrous cap, lipid rich necrotic core (LRNC) region and intima (remaining arterial wall regions, Figure 7.4).

Laser beam indicating the indentation position

Lipid core

Shoulder of fibrous cap

Middle of fibrous cap

Intima

1 mm
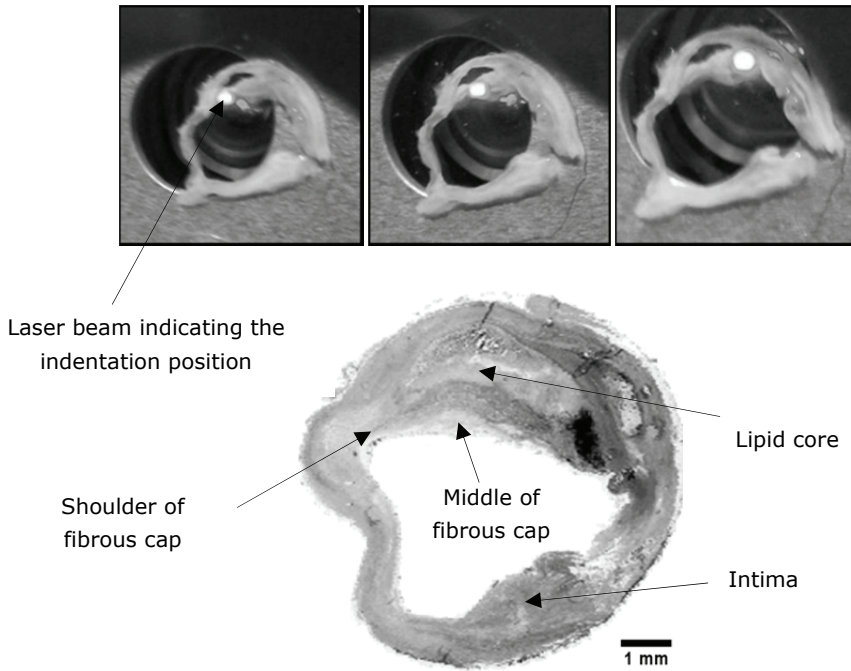
Figure 7.4: Histological slice (bottom).The top figures show the indentation positions indicated by the laser beam.

After the measurements the homogeneity at the tissue testing locations were examined based on the confocal images. Two observers (CKC and ACA), who were blinded to the stiffness results, conducted this evaluation. The following criteria led to the exclusion of the results from further analysis:

- Presence of debris or other foreign material, which were not identified as collagen fibres,
- Ruptured collagen fibres,
- Gap in the tissue which did not correspond to the structure of the surrounding tissue,
- Folded tissue, which can lead to slipping of the tissue influencing the stiffness results.

Statistical analysis was conducted to compare stiffness between indentation locations and between collagen types. The stiffness results showed a non-Gaussian distribution. The Kruskal-Wallis test (Dunn procedure) was applied using GraphPad Prism version 5.04 for Windows. A p-value < 0.05 was considered as significant result.
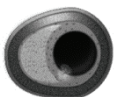
7.3   Results

<u>Representative plaque result</u>

In total, eight human carotid plaques were tested. Depending on the length of the plaque, 6 to 13 slices were obtained per plaque. At 284 locations, 574 measurements were performed. After examining the confocal images for homogeneity of test locations, 214 locations were used for further analysis. The average thickness of the tested plaque sections was 240 µm (±80 µm).

Representative results of one plaque are shown in Figure 7.5. On the left-hand side of Figure 7.5, a schematic representation of the plaque is shown where the common carotid artery bifurcates into internal (ICA) and external carotid artery (ECA). Among 9 slices obtained from the plaque, the most 3 proximal slices (slice 7 to 9 in Figure 7.5) contained both the internal and the external artery. The other slices only included the internal carotid artery. Above the illustration of the bifurcation, a schematic image of a slice is shown, where the different coloured areas represent the indentation locations. On the right-hand side of Figure 7.5, a table shows the Young's moduli in kPa. Corresponding to the schematic image of the slice, the different coloured columns represent the indentation locations. The collagen rich fibrous cap and intima locations, where further divided into dense structured collagen (SC) and loose unstructured collagen (UC). LRNC locations were collagen poor (CP). At slice 1 to 4 and at slice 6 a single location in the middle of the cap was measured. Slice 5 had a fibrous cap large enough to perform indentation tests at two different middle cap locations. Each value in the table represents the average of at least two consecutive measurements at the same location. For the middle of the cap all values were in the range from 15 to 53 kPa with an average of 41 kPa and standard deviation (SD) of 12 kPa. Moreover, based on the collagen dispersion, only SC regions were found in the middle of the cap. Most of the indentation locations at the shoulder of the cap were also found to be SC regions. Only at slice 2 and 8 UC regions were present. The Young's modulus of the shoulder regions ranged from 23 to 104 kPa. For this location the average value was 42 kPa, similar to the middle of the cap. At the intima regions, five SC and three UC locations were found. The Young's moduli varied from 7 to 114 kPa with an average of 40 kPa for SC and 80 kPa for UC. For this plaque only one CP location with a Young's modulus of 18 kPa was available for testing. To investigate the difference of mechanical properties in the longitudinal direction of a vessel, plaques were divided into three parts each consisting of three slices representing proximal, middle and distal regions of the plaque. This last column of the table shows the average values and the standard deviation of these three regions. For this particular plaque the proximal region is stiffer than the distal region.

Slice	SC Middle of cap	UC Middle of cap	SC Shoulder of cap	UC Shoulder of cap	SC Intima	UC Intima	CP	Average (StD) in kPa
1	52.2		42.6 36.5					43.8 (6.5)
2	15			36		94.4 113.5		48.5 (40.5)
3	33.7		22.6					28.2 (5.6)
4	45.3		29.3 51		7.4			33.3 (16.9)
5	52.9 41.9		30.2		57.1			45.5 (10.4)
6	44.4		34.2 31.3					34.7 (5.9)
7			103.5			33		62.9 (29.8)
8				64.9 37.1	51.1		17.5	42.7 (17.5)
9					20.4 64.4			42.4 (22)
Average (StD) in kPa	40.8 (12.1)		42.4 (23)	46 (13.4)	40.1 (22.2)	80.3 (34.3)	17.5 (0)	
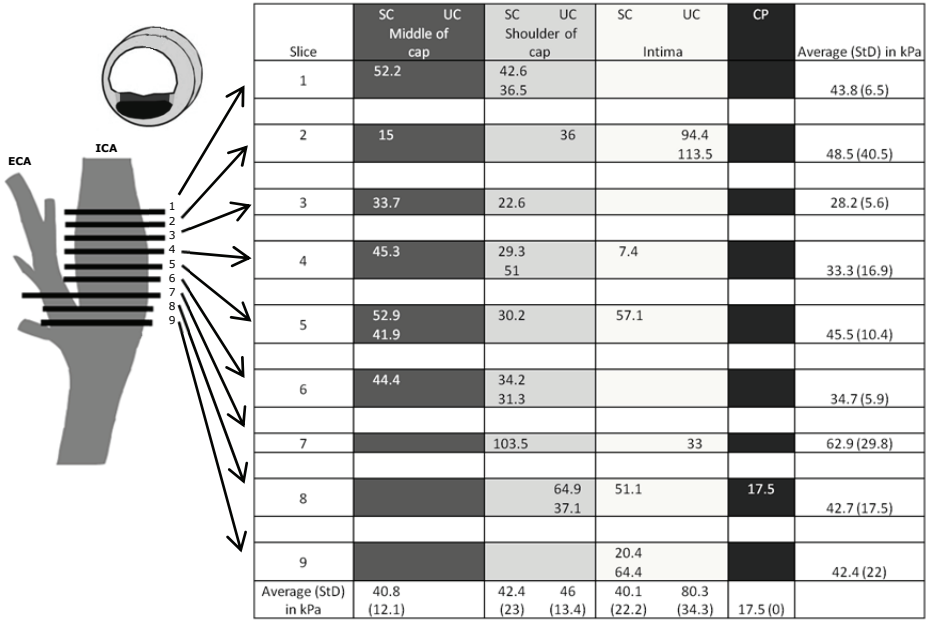
Figure 7.5: Results of a plaque at the bifurcation of common carotid into internal (ICA) and external carotid artery (ECA). The values in the table show the Young's moduli in kPa. SC (dense structured collagen), UC (loose unstructured collagen) and CP (collagen poor)

Collagen structure

There were 119 positions classified as SC, 75 positions as UC, and 20 positions as CP areas. No significant differences could be found between SC and UC (Figure 7.6). The collagen rich locations showed a high variation of stiffness results, ranging from 6 to 891 kPa. However, CP areas had a smaller range (9 to 143 kPa), and the results were significantly lower (median 16 kPa) compared to the SC locations (median 31 kPa) and UC (median 33 kPa) (Figure 7.6).
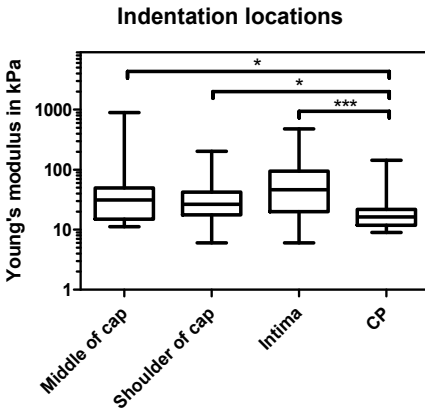
Figure 7.6: Box and whisker plots (minimum-maximum) of the Young's moduli of the different indentation locations and the significance of the values compared to each other, * p-value < 0.05, *** p-value < 0.001.

<u>Indentation locations</u>

Based on the histology images, indentation locations were chosen before performing the experiments. There were 43 indentation locations identified as middle of the fibrous cap, 61 as shoulder regions of the cap, 90 indentation locations as intima, and 20 as LRNC.

In Figure 7.7, the logarithmic scaled y-axis displays the Young's modulus in kPa, the x-axis shows the indentation location, middle of cap (median=31 kPa), shoulder of cap (median=27 kPa), intima (median=46 kPa), and LRNC locations (median=16 kPa). It was found that the fibrous cap and intim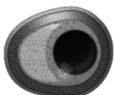a regions are significantly stiffer than the LRNC regions. No differences were observed between the middle and shoulder of cap, and the intima locations. All these results are summarised in Table 7.1.

Collagen structure
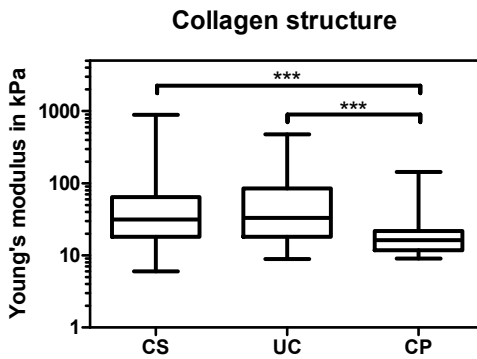
Figure 7.7: Box and whisker plots (minimum-maximum) of the Young's moduli, structured (SC), unstructured (UC) and collagen poor areas (CP), *** p-value < 0.001

Table 7.1: Summary of indentation test results. Mid: Middle of fibrous cap, Sh: Shoulder of cap, SC: Structured collagen, UC: Unstructured collagen, CP: collagen poor, Perc: Percentile

Location (#)	SC/Mid (29)	SC/Sh (36)	SC/Intima (54)	UC/Mid (14)	UC/Sh (25)	UC/Intima (36)	CP (20)	Avg.
Minimum	11.8	6	6	11.2	8.9	11.4	9	9.2
25% Perc.	18.4	18.2	16.8	13.5	14.8	30.1	11.8	17.7
Median	36.2	25.8	35.2	27.8	27	57.7	16.2	26.6
75% Perc.	53.7	42.5	94.6	33.8	46	108.7	21.6	33.8
Maximum	890.6	181.9	305.1	165.5	202.5	475.3	143.3	337.7

Inter- and intra-plaque variability, and longitudinal slices

The axial compressive Young's modulus of each plaque, excluding the collagen poor locations, are summarised in Figure 7.8. The results show that there is a large variation in Young's moduli within each plaque, especially for plaque 6 (11 to 891 kPa). Due to this variation, no significant differences between plaques were observed.
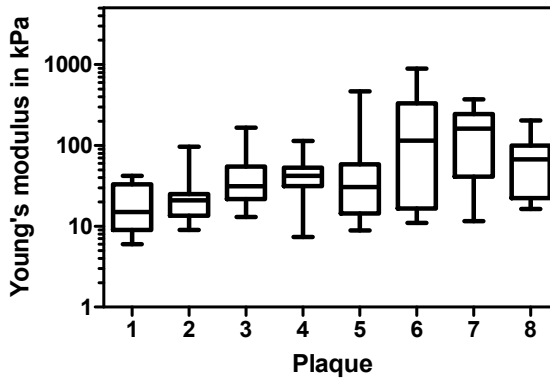
Figure 7.8: Box and whisker plots (minimum-maximum) of the Young's moduli of 8 human carotid atherosclerotic plaques, excluding collagen poor locations

The indentation tests were performed in axial direction of the artery on transversal slices. For one plaque, part of the tissue was sliced in the longitudinal direction and these longitudinal slices were used for testing. The resulting Young's moduli show no significant differences between the transversal and longitudinal slices (data not shown).

From proximal to distal, the results indicated no significant differences in Young's modulus. In three atherosclerotic plaques the fibrous cap at the proximal region showed higher stiffness than the distal region. However, in two cases the proximal site was softer than the distal side. For the remaining three plaques, numbers of indentation locations at the fibrous cap were not sufficient to make a comparison between proximal and distal regions.

7.4   Discussion

In this study we used an indentation test and inverse FE analysis to estimate the compressive Young's moduli of carotid atherosclerotic plaque tissue in axial direction. Assuming isotropic neo-Hookean behaviour, the Young's moduli were found in the range from 6 kPa to 891 kPa (median of 30 kPa) corresponding to values found in the literature. Collagen poor regions were softer than collagen
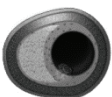
rich locations. However, no significant differences were observed between the Young's moduli of structured and unstructured collagen architectures. Moreover, no significant differences were found between the middle of the fibrous cap, the shoulder regions, and remaining intima locations. Therefore, the results indicate that the macroscopic behaviour of carotid atherosclerotic fibrous plaque tissue can be approximated by a single material model. However, it should be noted that the sample size (8 endarterectomy specimens) may not be sufficiently large to detect a statistical difference between the middle and shoulder regions of the fibrous cap, particularly since other patient-specific variables (age, gender, etc.) had not been controlled for.

A literature review revealed that there is a high variability of stiffness values of plaque tissue [30, 34, 36, 94, 95, 97, 120, 182, 183]. Our results are in the lower region of the range reported in literature and are consistent with the values obtained by Lee et al. [30, 97] and Barrett et al. [30] (Table 7.2). However, our results differ from the values obtained by other groups [30, 34, 36, 94, 95, 97, 120, 182, 183]. Possible explanations for this might be the different methods used to measure the mechanical properties of atherosclerotic plaque tissue (Table 7.2). In addition, the direction of measured stiffness also plays a role. The anisotropy of the tissue suggests that testing the stiffness of plaque tissue in different directions will lead to different results, although our values obtained from testing a small set of longitudinal slices were comparable to the results we obtained for transversal slices. Furthermore, different values might be the result of the measurements of different specimen types. Since the geometry of arteries at different locations varies and arteries from various locations experience different stresses and strains, it is suggested that the biomechanical properties of arteries from different location also vary. Differences between the values we obtained and the results of the other research groups might be also caused by the various methods used to classify the tissue. In our study we made the distinction between the test locations and collagen structure.

Table 7.2: Summary of indentation test results [kPa], excluding CP locations

Plaque # (# of values)	1 (11)	2 (27)	3 (26)	4 (27)	5 (52)	6 (11)	7 (19)	8 (21)	Avg.
Minimum	6	9	13	7.4	8.9	11	11.5	16.3	10.4
25% Perc.	9	13.5	21.8	31.3	14.4	16.6	41	22.3	21.2
Median	15	21	31.3	41.9	30.6	114.2	160.7	67.2	28
75% Perc.	33	25	54.8	52.9	58.3	331.7	243.7	99	52.3
Maximum	42	96	165.5	113.5	466.9	890.6	369.9	202.5	69

Measurements at same indentation positions led to a mean difference of 12 % (±14 %) showing that the indentation test method itself is reproducible. Taking the 25% and 75% percentile as range, the variability is similar to the range obtained by Barrett et al. [30] and Lee et al. [97]. It is smaller than the variability obtained by other research groups [94, 120, 133]. Since the range of values we found is similar for each plaque we tested and this is also observed by most research groups, the obtained range must reflect the variable nature of the mechanical properties of biological tissue.

It is suggested that, due to the different shear stress between the proximal and distal regions, different plaque morphology and therefore different stiffness results in those regions of the plaque can be expected [38, 184, 185]. Gijsen et al. [184] showed on human coronary arteries that the shear stress upstream is significantly higher than downstream. Dirksen et al. [185] found a significant difference between the cell compositions of proximal and distal parts of carotid plaques. Therefore, the results from literature suggest that also the stiffness of the fibrous cap proximal and distal of a plaque could be different. Using plaque tissue from carotid endarterectomy patients, it was possible to analyse the changes of stiffness from proximal to distal locations in five samples. No significant differences could be observed.

To analyse the influence of the collagen structure on the mechanical properties a confocal microscope was used to identify the collagen structure of the tested tissue location. The results show a wide spread of mechanical properties between plaques. Stiffness values of collagen poor locations, which are mostly found in the LRNC, have less variation than collagen rich regions. A statistical analysis using a non-parametric approach indicated that the collagen rich locations (structured and unstructured) are significantly stiffer than collagen poor locations. For collagen rich positions, no significant differences are found between the different collagen structures, suggesting that the architecture of collagen has no obvious effect on the Young's modulus. It is surprising that our results show no influence of the collagen structure on the stiffness results. Reasons for this might be the use of an isotropic model assuming homogeneity of the sample which might not reflect the actual mechanical behaviour of the tissue. In addition, it has to be noted that not only the collagen structure but also the amount of collagen influences the stiffness of the plaque tissue. The quantity of collagen was not measured during this study. Burleigh et al. [186] showed that plaque caps seem to require more quantities of collagen than neighbouring intima to maintain the same mechanical strength indicating that the collagen structure in the cap is less efficiently organised than in adjunct intima. The result of Burleigh et al. [186] suggests that for the stiffness of
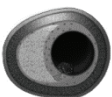
plaque caps the amount of collagen play a bigger role rather than the collagen structure. Therefore, the latter is probably the main reason why no significant difference between structured and unstructured collagen regions was observed.

For different indentation locations on each individual slice, it is observed that the fibrous cap tissue and intima tissue are significantly stiffer than the collagen poor regions which could be expected. However, no differences were found between the middle parts of the cap tissue, shoulder regions of the cap, and intima positions suggesting that one material model can be used to approximate the diseased intima and fibrous cap. On the other hand, considering the high variability of results, it is clear that finding a significant tendency is difficult.

A limitation of the study is the fact that the samples were frozen for logistical reasons. According to Schaar et al. [154], the influence of freezing on the mechanical properties of coronary arteries plays only a limited role. The freezing protocol applied in this study included dipping the sample in liquid nitrogen for snap freezing. This procedure is widely used to avoid ice-crystal formation. Hemmasizadeh et al. [152] used nano-indentation to show that snap-freezing and storage at -80ºC had no significant influence on the mechanical properties of porcine aortas. Therefore, the probability of damage of the collagen fibres due to ice-crystal formation was minimised. Furthermore, the indentation tests were performed at least twice at the same indentation location and the results were reproducible indicating that no damage to the tissue architecture occurred. The measurements were controlled by confocal microscopic visualization and also no damage to the tissue was observed. Moreover, the histological data was examined and indicated that no damage due to ice-crystallisation was present.

In literature the mechanical properties of atherosclerotic plaques are usually given only as Young's moduli. Furthermore, it is not always clear whether or not this is a Young's modulus determined at small strains, or a secant modulus of the slope of a curve at a certain strain level. Considering these reservations, the obtained values from this study were compared to the results in literature using $E = 3 \cdot G$, which is only valid at small strains.

The values of the lipid core regions appear to be higher than previously reported data [20]. A possible explanation might be that the mechanical tests were performed at room temperature. Testing at this temperature might affect the values for lipid core regions. The physiological mechanical properties of the lipid rich necrotic core at body temperature might be very different from their mechanical properties at room temperature. Therefore, these results should be dealt with caution when including them in simulations, since this may have a strong impact on the biomechanical stress analysis of plaques [187].

7.5   Conclusion

The system proved to be suitable to measure the local mechanical properties of plaque tissue. The compressive mechanical properties of human plaques in axial direction are lower than previously reported. Mechanical testing of fibrous cap tissue and surrounding intima tissue showed similar mechanical properties between these locations. They are significantly stiffer than collagen poor regions.
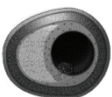
Chapter 8

Estimation of Material Properties of Atherosclerotic Intima in Porcine Iliac Arteries

Combination of Ultrasound Displacement Imaging and Inverse Finite Element Analysis

8.1   Introduction

Atherosclerosis is a systemic cardiovascular disease characterized by local thickening of vessel wall, referred to as atherosclerotic plaque. A subset of atherosclerotic plaques, called vulnerable plaques, is identified by a lipid core and a cap separating the lipid core from the lumen [39]. Rupture of the cap exposes the lipid content of the plaque to the blood and leads to intraluminal thrombosis. Thrombi induced by cap rupture are the predominant cause of myocardial infarction and stroke [4, 188]. Biomechanical studies showed that high stress regions corresponded to rupture locations [20, 21]. The rationale behind it is that a cap ruptures when local stresses at a certain location within the cap exceed the cap strength.

Plaque stresses can be computed with finite element (FE) models [121]. Material properties of plaque components, especially of intima, are essential for accurate stress computations [64]. Experimental data for material properties of atherosclerotic intima are scarce and span a wide range [189]. The large range can partly be attributed to the different testing methods used in the studies. Majority of these methods required test samples excised from plaque tissue. This compromises the structural integrity of the tissue. Thus, results from these experimental studies should be used with caution in the FE models for clinical application. Moreover, it is very likely that these results are biased towards stiff material properties as useable test samples from soft, unstructured tissues are hard to obtain and handle.

A methodology to overcome the aforementioned shortcomings is to measure the plaque deformation in intact plaques. In vivo deformation measurements or ex vivo inflation tests can serve to this purpose. Ex vivo inflation tests were widely used to estimate material properties of healthy vessels. Generally, the deformation of the outer border of the vessel wall is measured. The vessel is modeled as a thin walled cylinder and the material properties are obtained by analytical solutions (e.g. [190-192] among many others). For atherosclerotic plaques, determination of the material properties requires more advanced approaches such as inverse FE analysis since the morphology is very heterogeneous and complex.

With the inverse FE analysis, material properties can be estimated by varying material parameters in the simulations iteratively and fitting the computed data to measured deformations. A number of studies used this methodology for simulated inflation test results of realistic or idealized atherosclerotic plaque models [193-196]. Some other groups employed the methodology for real test measurements. Chandran and his colleagues estimated the Young's modulus of
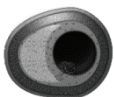
atherosclerotic porcine femoral and carotid arteries from the deformation of the lumen and the outer vessel wall borders, measured with intravascular ultrasound [197-199]. Liu et al. made use of in vivo magnetic resonance (MR) imaging for atherosclerotic human carotid arteries and employed the change of the lumen circumference over cardiac cycle for the stiffness estimation [161]. Both groups lacked the sufficient information from the images to delineate the individual plaque components and therefore, modeled the plaques as a single material. Beattie et al. used the methodology with more local deformation measures [120]. Human aortic rings with early stage intimal thickening were inflated by a balloon in ex vivo. The displacements on transversal wall cross sections were measured and bilinear elastic material model constants were estimated for plaque components. An important in vivo application of the methodology, with local deformation measures employed, is the intravascular ultrasound (IVUS) modulography [157]. IVUS modulography combines elastography [200] with inverse FE analysis and estimates the Young's modulus of plaque tissue. Baldewsing et al. demonstrated the clinical feasibility of this technique by testing one human coronary plaque in vivo [157].

Combination of ex vivo inflation tests or in vivo deformation measurements with inverse FE analysis is a potential approach to determine material properties of atherosclerotic plaque components. This method enables testing the plaques while they are intact and in the physiological (or close-to-physiological) environment. Previous studies that used the method either tested early atherosclerotic lesions or used global deformation measures such as lumen circumference change or modeled the entire plaque as a single material. For accurate stress analysis, we need to use local deformation measures from advanced plaques and model the plaques as a multi-component structure. This study aims to set up a pipeline to estimate the material properties of the components of advanced atherosclerotic plaques by combining local deformation measurements from ex vivo inflation tests and inverse FE analysis.

8.2   Methods

The methodology of the study consists of three main parts: ex vivo inflation tests, FE modeling, and estimation of the material properties (Figure 8.1). Briefly, atherosclerotic porcine iliac arteries were inflated in an ex vivo setup and displacements in the plaques were measured with high frequency ultrasound. FE models of the plaques were created to compute the displacements of the plaques during the inflation tests. Material properties of plaque components were estimated by rerunning the FE models with different material parameters

and evaluating the difference between the computed and measured displacements. The individual steps are explained below in details.

Ex vivo inflation tests

Atherosclerotic iliac arteries were collected from diabetic pigs (n=4) on a saturated fat/cholesterol diet. This animal model was discussed in detail elsewhere [201]. In short, streptozotocin-induced diabetic pigs (~45 kg) were fed supplemental (40% of dietary energy) saturated fat/cholesterol, unsaturated fat or starch for 10 weeks. The pigs showed substantial amount of atherosclerotic lesions in the arterial system.

Immediately after sacrificing the animals, iliac arteries were excised and snap-frozen in liquid nitrogen. Arteries were stored at -80° C. At the day of experimentation, the arteries were thawed to room temperature, cannulated and the side branches were closed. Before the test, the arteries were stretched 20% in the longitudinal direction [202] and preconditioned between 80 and 140 mmHg for ten-times by changing the pressure gradually. During the inflation experiments, pressure was increased stepwise from 0 mmHg to 140 mmHg with increments of 5 mmHg. The tests were conducted in a buffer bath at room temperature.

Deformation of the atherosclerotic vessel wall in the inflation test was imaged with a Vevo® 2100 ultrasound system (FUJIFILM VisualSonics, Inc., Toronto, Canada) using a high frequency linear transducer (32-56 MHz). Before the inflation experiments, a sweep in the longitudinal direction of the vessel was performed. 2D B-mode images were scanned to identify a location with a substantial atherosclerotic plaque, at least 10 mm away from the cannulae. Transversal cross-sectional B-mode ultrasound images and radiofrequency (RF) data were acquired at this location at each pressure step.

The RF data enabled to estimate the axial (along the ultrasound lines) and lateral (in the direction perpendicular to ultrasound lines) displacements on the plaque cross-section with high precision. The displacement estimation method was an iterative coarse-to-fine 2D cross-correlation based method and was explained in detail before [203-205]. Displacement estimation was carried out in three iterations. In each iteration tissue displacements between the frames corresponding to successive pressure steps were estimated by cross-correlating 2D kernels of RF data (frame n) with larger 2D "search"-kernels of RF data (frame n+1). The location of the peak of the normalized cross-correlation function for each kernel corresponds to the 2D tissue displacement. To estimate the location of the cross-correlation peak at subsample and sub-line level, a 2D parabolic function was fitted through the peak of the cross-correlation function
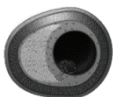
[206, 207]. The 2D displacements obtained in the first iteration were used as offset for the RF data of the search kernels in the second and third iteration. In iteration 2 and 3, kernel sizes were decreased in the axial direction to obtain displacement information more locally. The final kernel size was 60×715 μm^2 and the final search kernel size was 120×935 μm^2. Displacements were estimated for every 15 μm axially and for every 55 μm laterally.
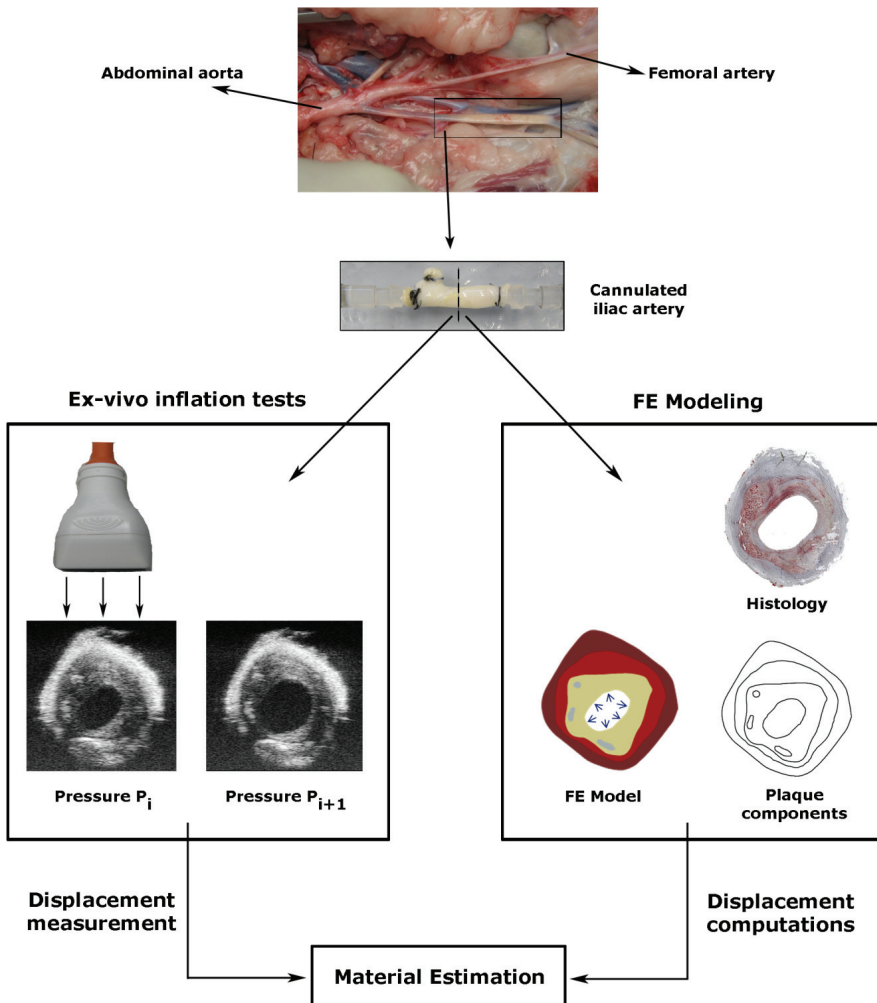

Figure 8.1: The methodology of the study consists of three main parts: ex vivo inflation tests, FE modeling, and estimation of the material properties
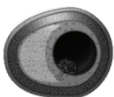
FE models

In this study, we used a new approach to obtain detailed plaque geometries for FE models. Figure 8.2 demonstrates the procedure. This approach employed both B-mode ultrasound images and histology. B-mode images provided the overall structural in the experiments (Figure 8.2.A) and histology images provided detailed information of different plaque components (Figure 8.2.B).

After the inflation tests, the arteries were fixed with formaldehyde for histology at 10 mmHg and 20% longitudinal prestretch. Five micron thick segments from the imaged plaque cross-section were used for ORO (Oil red O) staining counter stained with hematoxylin. In ORO staining, lipids and fatty acids appear red. The counter-staining hematoxylin stains the nuclei and calcium blue. This staining enabled us to delineate the adventitia, media, intima, calcium, lumen and the outer border of the vessel wall.

The contours of the plaque components delineated on histology images were mapped onto ultrasound images (Figure 8.2, from C to F) using the image registration software *elastix* [208]. First, the lumen contour and the outer vessel wall contour were manually drawn both on the ultrasound image obtained at 10 mmHg (Figure 8.2.C) and on the histology image (Figure 8.2.D). Subsequently, the contours on the images were mapped with *elastix*. Finally, the contours of the plaque components drawn on the histology image (Figure 8.2.E) were transformed onto the ultrasound image (Figure 8.2.F) by using the transformation matrix obtained in the previous step. The transformed histology contours were used to create 2D FE models of the plaques (Figure 8.2.G).

The generated FE models (ABAQUS, version 6.11) were used to simulate the plaque deformation during the inflation tests and solved under plane strain assumption. The possible nonlinearity in the material behavior of the plaque components can be modeled with different material models. We decided to use a simple nonlinear model, the incompressible Neo-Hookean model for all plaque components. Incompressible Neo-Hookean material model is characterized by the strain energy density function W defined as $W = C (I_1-3)$ where C is the shear modulus and I_1 is the first invariant of the left Cauchy-Green deformation tensor. Identical shear moduli were assigned to the adventitia and media. This material complex is referred to as "wall" in the rest of the paper. Calcium was assumed to be very stiff ($C=10^4$ kPa). A very soft and compressible solid buffer layer surrounding the plaque was created and zero-displacement boundary condition was applied to its outer border to prevent rigid body motion in the FE simulations. The models were pressurized intraluminally following the protocol of the experiment.
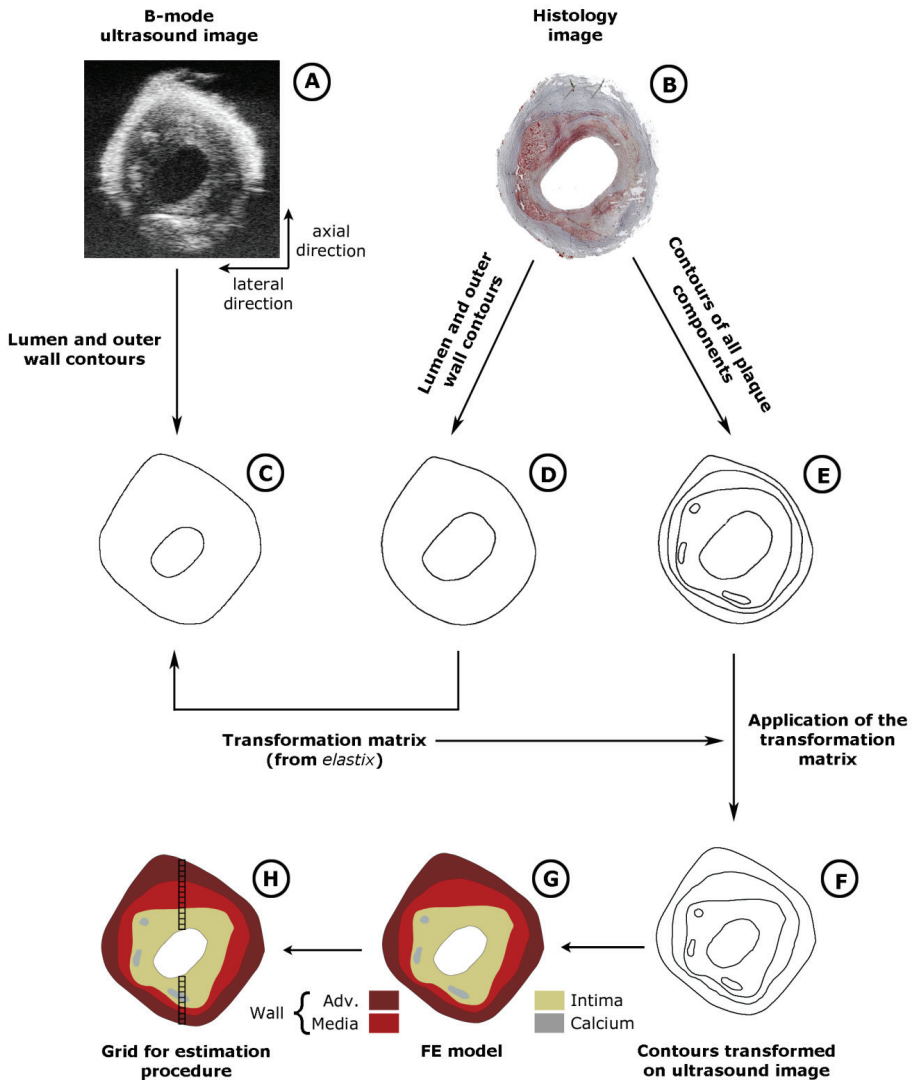
Figure 8.2: Illustration of the procedure for obtaining the geometry for FE models. Ultrasound RF (radiofrequency) data was used for displacement measurements. Axial (along the ultrasound lines) and lateral (in the direction perpendicular to ultrasound lines) directions are indicated next to the B-mode image. Plaque component borders drawn on histology images were transformed onto the B-mode ultrasound image by the image registration software *elastix* [208].

Estimation of Material Properties

Numerous minimization algorithms, such as Levenberg-Marquardt algorithm commonly used, are available for parameter estimation procedures. We decided to employ the Brute Force Method instead of a minimization algorithm to reveal the effect of the change in the material parameters. In the Brute Force Method, the parameters are altered in a range with a constant step size and all possible combinations of the parameters are simulated.

In the estimation procedure, shear moduli of the plaque wall and intima were varied in the FE models and the displacements were recomputed. The lower limits for the shear modulus were set to 1 kPa to force them to be positive, and the upper limit was chosen as 200 kPa for the wall and 100 kPa for the intima. The increments for the shear moduli were chosen as one thirtieth of the ranges. This resulted in 900 simulated displacement fields for each plaque model.

Most reliable displacement measurements are obtained from the central region of an ultrasound beam in axial direction. Therefore, displacements from this region of the plaques in the axial direction were used in the analysis. Plaques were located in the test setup such that the most relevant plaque part was in this region. A grid with 100 µm element size (∼ 6-times the axial and ∼ twice the lateral in-plane resolution of ultrasound data) was generated in this plaque region as illustrated in Figure 8.2.H.

The computed and measured displacements in each grid element were averaged. To cover the physiological pressure range, the displacements at the pressure steps of 80, 100, and 120 mmHg were used in the analysis. As proposed by Beattie et al. [120], an objective function, *F*, was defined

$$F = \sum_{i=1}^{3} \sum_{j=1}^{n} \left(Average\ computed\ dispacement_{i,j} - Average\ measured\ dispacement_{i,j} \right)^2 .$$

In the objection function, *F*, "*i*" represents the pressure step number, "*j*" the grid element number and "*n*" the total number of the grid elements. "*i*" takes the values 1, 2 and 3 corresponding to 80, 100, and 120 mmHg, respectively. The FE simulation with the minimum value of the objective function, *F*, was considered as the best match to the results. The shear moduli used in this FE provided the estimates of the material properties of the intima and the wall.

The corresponding Young's modulus values, *E*, of the estimated shear moduli were calculated with the formula, *E=6*C*, and reported in this chapter for an easy comparison to the results reported in literature.
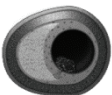
8.3   Results

Plaque histology

Of the four porcine iliac plaques, three plaques were eccentric and one plaque was concentric. Histology images revealed the heterogeneity of these plaques (Figure 8.3). In the healthy parts of the media, a multilayered structure with smooth muscle cells was clearly evident on the histology images (Figure 8.3, zoom-box in plaque 1). Degenerated regions of the media contained less smooth muscle cells than healthy parts (Figure 8.3, zoom-box in plaque 2). The adventitia was thinner than the media except plaque #2. The atherosclerotic intima contained extracellular lipids and collagen fibers (Figure 8.3, zoom-box in plaque 3). No lipid core or necrotic core was present in any of the plaques. All plaques contained calcium with varying sizes. The calcifications were localized usually near the intima-media interface (Figure 8.3, zoom-box in plaque 4). Overall, the iliac plaques resembled the human atherosclerotic plaque type III in the classification scheme of American Heart Association (AHA) [8].
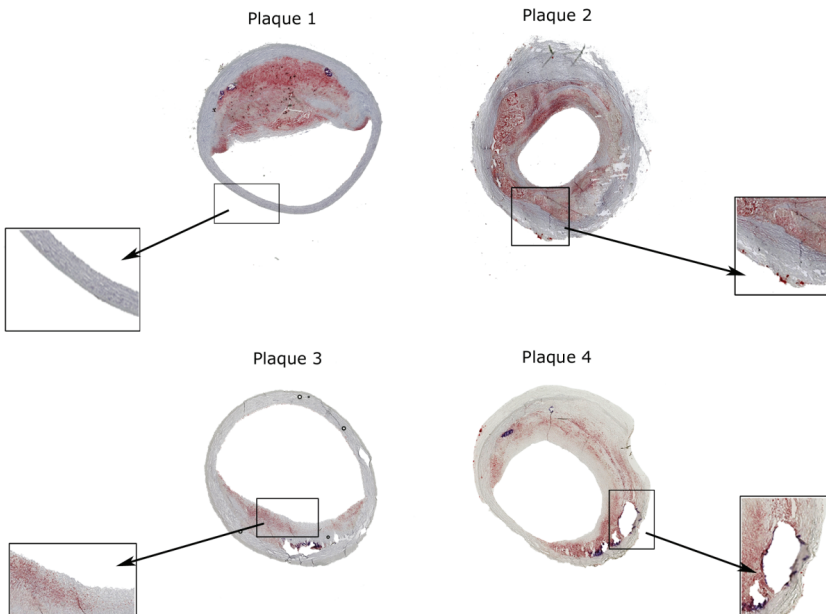
Figure 8.3: Histology images of the atherosclerotic plaques from porcine iliac arteries

Displacement measurements and computations: an illustrative example

Displacement measurements were successfully performed with high frequency ultrasound imaging. An example of the measured displacements (plaque #2) in the axial and lateral directions at 100 mmHg is shown in the upper panel of Figure 8.4. Axial displacements showed a smooth profile. Lateral displacement measurements were noisier than the axial displacements. The smoothest displacement measurements were obtained from the midsection of the plaque in the axial direction. The corresponding computed displacements (from the simulation with the best match) are shown in the lower panel of the figure.

The left panel in Figure 8.4 shows that the axial displacements in the upper half of the cross section were upwards, indicated by positive values. The lower half of the cross section displaced downwards, indicated by negative values. Similarly, the right panel of Figure 8.4 demonstrates that the right half of the plaque displaced to the right whereas the left half displaced in the opposite direction, to the left. This implies that the general deformation of the plaque was outwards in the radial direction, the expected deformation profile of a circular structure under inflation.

Figure 8.4: Measured (upper panel) and computed (lower panel) displacement maps in the axial direction (parallel to the ultrasound beam) in the left panel and lateral direction (perpendicular to the ultrasound beam) in the right panel for plaque #2 at 100 mmHg
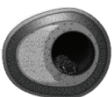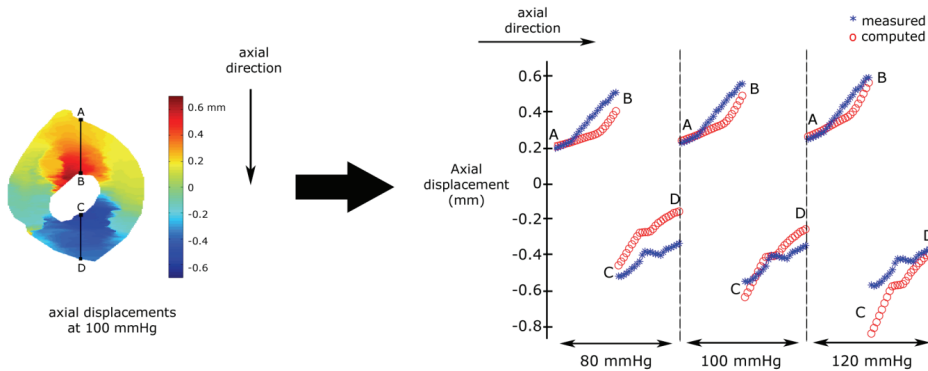
Figure 8.5: Measured (blue crosses) and computed (red circles) axial displacements in the midsection of plaque #2

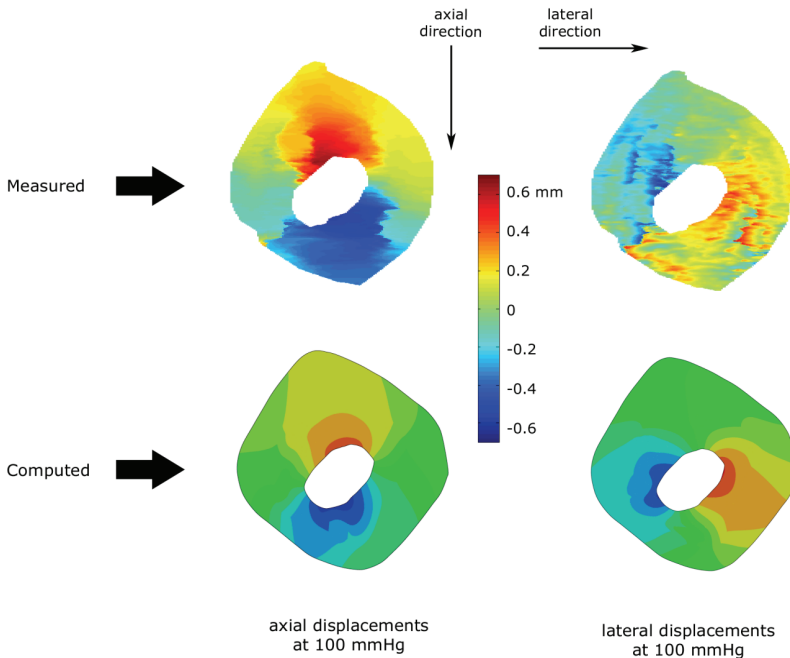Figure 8.5 represents the measured and computed axial displacements in the grid elements (lines A-B and C-D) at 80, 100 and 120 mmHg for plaque #2. For 80 mmHg, the displacement of point A was measured as +0.20 mm whereas point B displaced +0.52 mm. The relative displacement of B with respect to A (+0.32 mm) implies that the tissue between the two points was compressed. Relative displacement of B was +0.34 mm for 100 mmHg and +0.35 mm for 120 mmHg. Increase in relative displacement of point B from low to high pressure suggests that the tissue was more compressed with increasing pressure. Similar deformation profile was observed for the tissue between points C and D. Relative displacement of point C with respect to D was -0.29, -0.30, and -0.32 mm at 80, 100, 120 mmHg, respectively. This deformation behavior can be also visualized by the change of the thickness of the cross-section (Figure 8.6). The thickness of the upper half of the cross-section (length of the line A-B) was 2.87 mm at 10 mmHg and decreased to 2.55, 2.53, and 2.51 mm at 80, 100, and 120 mmHg, respectively. Similarly, the thickness of the lower half (length of the line C-D) decreased from 2.13 to 1.94, 1.93, and 1.91 mm.

The computed displacements displayed the same global trend as the measurements (Figure 8.5). The tissues between the points A and B, and between C and D were compressed. The displacements on the line A-B were underestimated by the FE simulation for all pressure steps. The displacements on the line C-D were overestimated for 80 mmHg and underestimated for 120 mmHg. For this plaque, the mean error of the computed and measured displacements was -0.015 mm with a standard deviation of 0.10 mm.
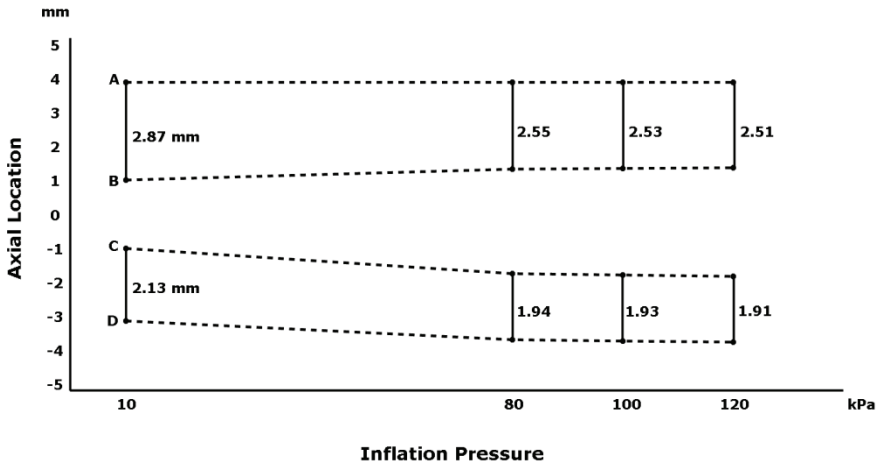
Figure 8.6: Thickness change of the plaque #2 along the lines A-B and C-D. Lumen center is at zero-axial location

Not only the general deformation patterns, but also local deformations were captured with both the ultrasound measurements and FE simulations. The plateau in the measured displacements between the points C and D (Figure 8.5) suggests that this region showed a relatively small deformation. This trend is also evident in the computed displacements. Inspection of the histology and ultrasound images confirmed the presence of calcium in this region (Figure 8.2). In a calcium region, one would expect the relative displacements to be almost zero. This deformation behavior of the calcium was captured by both the measurements and the FE simulations. The general deformation profiles of the other three plaques were similar to plaque #2.

Estimation procedure

The relative mean error (±SD) between the measured displacements and the displacements computed by the FE simulation with the best match was -0.014 (±0.10), -0.015 (±0.10), 0.0004 (±0.09), and 0.0015 (±0.13) mm for plaque #1,#2, #3 and #4, respectively. Measured and computed lumen areas are shown in Table 8.1. From 10 to 100 mmHg, the measured change was 245% on average, and ranged from 172% to 390%. In the simulations, the lumen area was always underestimated at 80 mmHg and overestimated at 120 mmHg. The difference between the measured and computed lumen areas at 100 mmHg was less than 13% for all plaques.
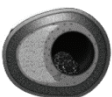
Table 8.1: Measured and computed lumen area (mm²)

	Plaque 1		Plaque 2		Plaque 3		Plaque 4	
	Meas.	Comp.	Meas.	Comp.	Meas.	Comp.	Meas.	Comp.
10 mmHg	11.0	-	3.5	-	6.2	-	4.0	-
80 mmHg	18.6	18.4	8.0	7.4	10.7	10.2	15.2	11.1
100 mmHg	18.9	21.2	8.4	8.9	11.1	11.8	15.6	13.8
120 mmHg	20.0	24.4	8.9	10.5	11.9	13.7	15.7	17.4

Material properties of intima and wall

The color graphs in Figure 8.7 show the results of the objective function, *F*, of the 900 simulations and demonstrate the effect of intima and wall stiffness. Stiffness values for intima and wall at the lower limit of the ranges (left bottom corner in the graphs) resulted in large errors since the soft intima and wall components caused overestimation of the deformations in the simulations. Higher stiffness values for intima and wall (right top corner in the graphs) also resulted in large errors since the simulations underestimated the measured deformations. There is a valley between these two regions in the graphs. The intima and wall stiffness combinations in the valleys resulted in low error values.
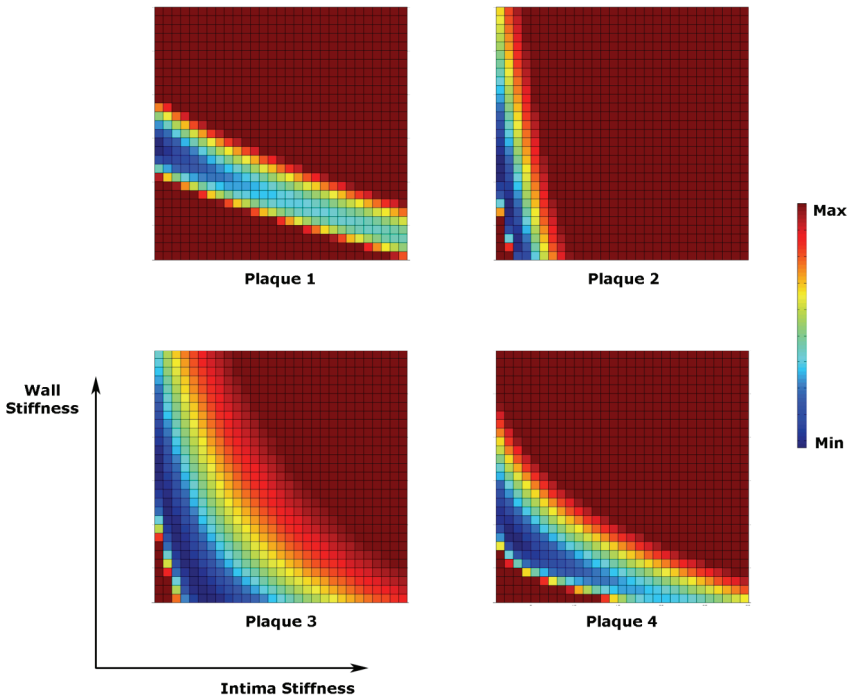
Figure 8.7: Color graphs for the results of the objective function, *F*, of the 900 simulations for all four plaques

A constant step size was used in the estimation procedure. Therefore, instead of the stiffness values of intima and wall in the simulation with the best match to measured deformation, the range of the stiffness values where the minimum value of the objective function, F, is located are reported (Table 8.2). Intima stiffness values were lower than 45 kPa for all four plaques. Wall stiffness values varied between 168 and 372 kPa.

Table 8.2: Range of the estimated stiffness (Young's modulus) values for the atherosclerotic intima and wall (kPa)

	Plaque 1	Plaque 2	Plaque 3	Plaque 4
Intima stiffness	<30	<30	<30	6-45
Wall stiffness	210-295	168-252	295-372	132-210

8.4   Discussion

We presented a hybrid experimental-numerical approach to determine atherosclerotic plaque properties. Compared to previous studies that combined either ex vivo inflation tests or in vivo deformation measurements with inverse FE analysis, our methodology has two main advantages. First advantage is the use of local displacement measurements. In this study, RF-correlation technique was applied to high frequency ultrasound data for the first time. The displacements were measured in high resolution. The displacement profiles in the axial direction were smooth, whereas, the displacements in the lateral direction were noisier. Ultrasound acquisition was fast and non-invasive. This makes the technique attractive for both ex vivo and in vivo applications. The second advantage of this study is the detailed plaque geometries of FE models. The novel method, where plaque component borders from histology images were mapped to ultrasound images, provided unprecedented details in plaque geometries. We used a 2-materials approach in our analysis; however, the method allows including more components in the FE models. Matching of the histology images and ultrasound images is critical in this method. Successful match can be confirmed with the visual inspection of the measured and computed displacement maps. The good agreement in the local deformations, such as the calcium location in plaque #2, further supports this.
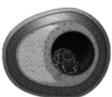
Three main issues in the methodology require further exploration. First, atherosclerotic plaques are considered to be nonlinear, heterogeneous and anisotropic. Neo-Hookean material models provided successful results. However, lumen area was underestimated at 80 mmHg and overestimated at 120 mmHg in the simulations. This indicates that more advanced, anisotropic material models with higher nonlinearity might capture the material behavior of plaque components better. We used a 2-materials approach in our analysis. It is possible to further divide a plaque into smaller regions (e.g. intima component into fibrous intima region and lipid rich intima region) using the histology images and estimate the material properties of these smaller regions for further refinement in the plaque stiffness results. Secondly, as the most reliable displacement measurements were expected from the central part of the ultrasound transducer in the axial direction, only the axial displacements from the midsection of the plaques were used in the analysis. Using a larger area, preferably entire plaque cross-section, would be more desirable. However, this would most likely introduce more artifacts and noise in the displacement measurements. The artifacts and noise level should be reduced for this analysis. Thirdly, we did not employ any minimization technique for the stiffness estimation procedure. Instead, we used the so called Brute Force Method. This provided us with valuable information about the influence of the material parameters on the errors in the estimation procedure. The valley in the error plots demonstrated that several parameter combinations might result in comparable low error values. Brute Force Method requires large computational effort. A robust, fast minimization technique (e.g. Levenberg-Marquardt algorithm) would decrease the computational burden. However, the risk of minimization techniques is that they might find a local minimum instead of the global minimum. Incorporating a minimization method in the estimation procedure requires investigation of the robustness of these methods by comparing them to the Brute Force Method results.

Preliminary data obtained from the application of the mixed experimental-numerical approach to porcine iliac plaques resulted in intima stiffness values in the lower range of literature [189]. The values are comparable to the atherosclerotic intima measurements of Chai et al. [209] and Barrett et al. [30] in human carotid arteries, and Lee et al. [97] in human abdominal aortas. The only experimental data on atherosclerotic intima properties in iliac arteries were reported by Holzapfel et al. [95] and Salunke et al. [148]. Both groups tested human arteries. Holzapfel et al. used uniaxial tension tests and reported intima properties that were two orders of magnitude stiffer than our results. Salunke et

al. measured the intima stiffness with unconfined compression tests. Their results were an order of magnitude higher than ours.

A direct comparison of our results to the results of the studies mentioned above should be treated cautiously as the physiological geometry is destroyed in these studies by excising the test samples from plaques. Moreover, the loading conditions were different than the ones in inflation tests. We ran additional FE simulations with the high stiffness values for the intima as reported by Holzapfel et al. and Salunke et al. Even without the vessel wall, the simulations resulted in lumen area changes that were lower than the values measured in our inflation tests. This illustrates that such high stiffness values for the intima of porcine iliac plaques we tested are unlikely.

Ex vivo inflation tests of atherosclerotic plaques are comparable to the in vivo deformation measurements as the excised vessel is still intact and the loading type is similar to the in vivo condition. In vivo stiffness measurements of atherosclerotic plaques were done by few research groups. Baldewsing et al. measured the stiffness of one human atherosclerotic coronary in vivo [157]. The modulagram results displayed stiffness values between 1 and 100 kPa. Our intima stiffness results are in the range of this paper. Liu et al. calculated the overall plaque stiffness of human carotid arteries from the in vivo plaque deformation measurements obtained by MRI [161]. They reported the mean stiffness value as 480 kPa and the range from 140 to 1440 kPa. Hamilton et al. estimated the stiffness of atherosclerotic porcine femoral arteries from intravascular ultrasound data [198]. Their average stiffness result was approximately 95 kPa. Also in this case, a direct comparison is difficult since plaques were modeled as a single material in these studies. We can however speculate that the combination of our intima stiffness (<45 kPa) and wall stiffness results (165-375 kPa) are comparable to their results.

8.5 Conclusion

This study provided the pipeline of a nondestructive method for determining the material properties of atherosclerotic plaque components where the samples were tested under physiological loading condition and in an environment similar to in vivo environment. This mixed experimental-numerical approach was successfully applied to four porcine iliac arteries with advanced atherosclerotic plaques. The methodology can be further used to test more samples with different plaque phenotypes to deepen our knowledge on plaque material properties.
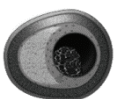
Chapter 9

General Discussion

Atherosclerosis is a systemic, inflammatory disease of the arterial system. The acute manifestations of atherosclerosis such as stroke and myocardial infarction are the main cause of morbidity and mortality worldwide. Atherosclerotic plaques can be divided into two categories: stable plaques and vulnerable plaques. The majority of stroke and myocardial infarction are associated with rupture of the cap of vulnerable plaques.

Discriminating vulnerable plaques from stable plaques is of high importance for predicting acute cardiovascular events. Therefore, characterization of vulnerable plaques is a very active research field. Numerous studies focused on identification of geometric plaque features and associated these features to vulnerable plaques and plaque rupture. Although these studies identified vulnerable plaques as the plaques with a thin cap and a large lipid core [15-18], not all plaques with these characteristics rupture. Moreover, not all plaques that rupture have these geometric features. Thus, further refinement of vulnerable plaque characterization is required.

From mechanical point of view, a plaque cap ruptures when the local stresses in the cap exceed the cap strength. Biomechanical models that compare cap stresses to cap strength may be of additional value for rupture risk assessment. Previous numerical studies showed the correspondence of high stress regions in the cap to rupture locations. Therefore, cap stresses might serve as a rupture risk predictor [20, 21].

Finite element (FE) analysis is a method frequently used to compute stresses in atherosclerotic plaques. Assessment of the stresses with FE plaque models relies on three important parameters: 1.) accurate representation of the loading, boundary and initial conditions, 2.) geometric features of atherosclerotic plaques, and 3.) the material properties of the plaque components.

The objective of this thesis was to determine the requirements for FE plaque models to compute plaque and cap stresses, to establish the influence of plaque geometry and material properties on cap stresses, and to estimate the material properties of atherosclerotic plaques.

9.1   Summary

<u>Requirements for FE Plaque Models</u>

FE stress analyses of atherosclerotic plaques are commonly based on in vivo images or histology images of pressure-fixed vessels. Until recently, the stresses at this deformed state, the initial stresses, were neglected in computational studies as there were no means to compute them. A numerical technique, the
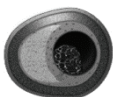
Backward Incremental (BI) method, was developed before to compute initial stresses in abdominal aortic aneurysms [55, 82]. Chapter 2 represented the implementation of the BI method to FE models of atherosclerotic plaques and the influence of initial stresses on cap stresses. On average the change in peak cap stress was approximately 5% when initial stresses were neglected. The effect depended on plaque geometry and varied between -55% to +50%. Plaques with a thin cap and a large lipid core showed an average decrease of approximately 10% in peak cap stress if initial stresses were incorporated. Plaques with a thick cap and a small lipid core also showed changes, however no general trend was observed. Despite the variation in the effect of initial stresses on cap stresses, the general trend of the relationship between the geometric features and cap stresses did not change when initial stresses were incorporated. This implies that parametric studies that are used to relate geometric plaque features to cap stresses do not require initial stress computations. However, since initial stresses influence absolute stresses in a rather unpredictable fashion, they have to be incorporated in the models for patient or plaque specific stress computations.

Initial stresses are not the only concern if in vivo images are used in FE plaque models. Atherosclerotic plaques are 3D structures and image based plaque models generally have a relatively low axial resolution compared to the in-plane resolution [80]. In chapter 3, the influence of axial sampling resolution on plaque and cap stresses was investigated based on high resolution histology data. The study employed 3D models with high axial resolution (0.5 mm), 3D models with low axial resolution (1 mm), and 2D models. Axial sampling rate did not change the general stress distribution and peak cap stress location, but it did affect the absolute cap stress values. The difference between 2D and high sampling 3D models ranged from -40% to +50%, and between 3D low and high sampling models from -15% to +35%. No systematic bias in the changes could be determined. All three groups showed similar trends for the influence of the cap thickness on peak cap stresses. It was concluded that 2D plaque models are appropriate to describe general relationships between geometric features and cap stresses, but 3D models with high axial resolution are necessary for reliable, plaque specific stress calculations.

Influence of Plaque Geometry and Intima Stiffness on Cap Stresses

Previous computational studies showed that a thin cap is a potential predictor for high cap stresses [25-27]. Large variation in cap thickness of ruptured plaques [28] implies that cap thickness is not the only relevant geometric feature. In chapter 4, the influence of geometric features on cap stresses was investigated

with an extensive parametric study, using idealized 2D FE models. With this parametric study, a wide range of possible plaque geometries were generated. The results of the FE models that employed intima stiffness values comparable to the ones used in previous computational plaque studies showed that cap thickness had indeed the strongest influence on cap stresses. Changing it from 0.25 mm to 0.05 mm doubled the peak cap stress. Lipid core thickness had also significant effect on peak cap stresses. Doubling the lipid core thickness elevated the cap stresses by 60%.

Recent experimental studies [30, 32] reported intima stiffness values lower than the values commonly used in biomechanical plaque modeling studies. In chapter 4, the influence of intima stiffness on cap stresses was studied by employing softer intima models. These models generally showed lower cap stresses than the stiff intima models. The effect of geometric parameters was different for soft intima models as well. Cap thickness was less influential (55% increase for soft intima models vs. 200% increase for stiff intima models if it was changed from 0.25 mm to 0.05 mm) and lipid core thickness had a stronger effect (100% increase for soft intima models vs. 60% increase for stiff intima models if it was changed from 0.6 mm to 1.4 mm). Moreover, lipid core angle was as influential as the cap thickness in soft intima models. Larger angles decreased the peak cap stresses up to 55%. The study demonstrated the importance of accurate intima stiffness for cap stress computations. If the intima is soft, cap thickness might be less influential on cap stresses, and lipid core thickness and angle might have a stronger impact.

In chapter 5, the influence of plaque geometry on cap stresses was further studied by using realistic plaque geometries. Additionally, geometric surrogates for high cap stresses were sought. The 2D FE models were based on histology images of human coronary plaques. The analysis confirmed the importance of cap thickness on peak cap stress. Contrary to the findings in chapter 4, lipid core size was not influential. This can be attributed to the more complex structure of realistic plaque geometry compared to the idealized geometries. Lumen radius emerged as a new risk factor for high cap stresses.

This study demonstrated that a combination of geometric plaque features can be used as a surrogate marker for peak cap stress. Based on the ratio of the lumen radius to the cap thickness –the two most effective geometric parameters obtained from the analysis-, a new model was proposed as a surrogate for cap stresses. It was shown that the human coronary plaques with a lumen radius to cap thickness ratio lower than 2.5 had cap stresses below 140 kPa and could be classified as low stress plaques. If the ratio was higher than 6.5, the plaques
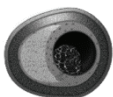
showed cap stresses higher than 300 kPa and could be classified as high stress plaques. This parameter might be used to separate plaques with low cap stresses from the plaques with high stresses based on imaging.

Material Properties of Atherosclerotic Intima

To have a better understanding of intima material properties, experimental studies with atherosclerotic human intima tissue were reviewed in chapter 6. The in vivo loading condition is the combination of circumferential tension and radial compression. Therefore, the studies that tested either one of the two loading conditions were included in the review. The experimental stiffness data show a large variation (between 30 and 250×10^3 kPa if all results combined). Circumferential tension results are approximately one order of magnitude stiffer than the radial compression results. This is most probably due to the fact that collagen fibers are recruited only under tension, not under compression. Yet, this cannot explain the huge variation. The variation can have several reasons. It might be expected that plaques from different vascular territories show different stiffness results. However, no clear correlation between stiffness results and the vascular territory could be found in the study. The large variation could originate from the difference in the progressive stage of atherosclerosis in the test samples. It is very likely that early stage plaques show different intima stiffness than advanced plaques. Therefore, including histological data and AHA classification is advised for future experimental studies. The chapter demonstrated the lack of adequate experimental data on atherosclerotic intima properties and the need for more and better documented experimental studies.

To explore the atherosclerotic intima properties, axial compressive properties of atherosclerotic human carotid plaques were investigated in chapter 7. The combination of the indentation tests and inverse FE analysis was used to estimate local intima properties. The stiffness results were related to collagen content and structure, and location of the test regions. Results showed a large variation (between 5 and 900 kPa) and the average values were in the lower range of the reported values in literature [189], comparable to the stiffness of the soft intima models in chapter 4. Collagen rich intima showed higher average stiffness values than the collagen poor intima (30 kPa vs. 15 kPa). No statistical difference was observed between structured and unstructured collagen regions, and between the cap region and the rest of the intima.

In chapter 8, a methodology that enables investigating the material behavior of atherosclerotic intima under more physiological conditions was demonstrated. Ultrasound deformation measurements from ex vivo inflation tests were successfully combined with inverse FE analysis. High resolution radiofrequency

data of noninvasive ultrasound imaging were used to measure the displacements on transversal plaque cross-sections during inflation tests. Detailed 2D FE models were obtained from a novel technique that combined histology data with the ultrasound images. The models were used to simulate plaque deformation in the tests. Intima stiffness of atherosclerotic plaques was estimated by fitting the computed displacements to measured displacements.

This study provided the pipeline of a nondestructive method for determining the material properties of atherosclerotic plaque components where the samples were tested under physiological loading condition and in an environment similar to in vivo environment. This mixed experimental-numerical approach was successfully applied to four porcine iliac arteries with advanced atherosclerotic plaques. Preliminary results confirmed low stiffness values for atherosclerotic intima.

9.2 Discussion and Future Perspective

Initial and Residual Stresses

We implemented a numerical method, BI method, to compute initial stresses in plaques. Another method, called Shrinkage method, was recently proposed by Huang et al. to compute initial stresses in atherosclerotic plaques [54]. This technique is based on uniformly shrinking the imaged geometry and pressurizing it to match the simulated circumference of the lumen to the imaged circumference. The group reported lower cap stresses in general when Shrinkage method was used.

Shrinkage method requires manual adaptations in the zero-pressure geometry to fit the simulated geometry to the imaged geometry. It is difficult to have a good fit of plaque geometries due to the complexity of morphology. BI method provides a straightforward calculation of initial stresses and a unique solution. Therefore, BI method is a more appropriate method to estimate initial stresses in atherosclerotic plaques. However, the method requires some programming to implement it to commercial FE packages. Shrinkage method can be useful if such programming efforts have to be avoided.

It is known that biological tissues are not stress-free even if no external load is applied [84]. The remaining stresses in the tissue at no-loading condition are called residual stresses. A widely used method to determine residual stresses in healthy arterial segments is the Opening Angle method [210]. With this method, a radial cut is made in the segment. The segment opens up into a C-shaped sector to release the residual stresses. The size of the opening is used as a measure for residual stresses. Residual stresses in atherosclerotic plaques are
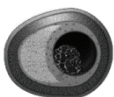
difficult to estimate as plaques are structurally nonuniform, asymmetric and heterogeneous. Based on the "opening angle" studies from healthy arterial walls, Williamson et al. [92] assumed uniform distribution of the residual stresses in their numerical models in the radial direction. The stress distribution did not show significant differences when residual stresses were incorporated. However, peak cap stresses decreased by approximately 25%. Ohayon et al. applied the Opening Angle method to atherosclerotic plaques [79]. They showed that the location of the peak cap stress did not shift significantly, but the peak cap stress values decreased by up to 75% when residual stresses were included. Although this group provided the first experimental study for the residual stresses in atherosclerotic plaques, it is unlikely that a single cut suffices to release the residual stresses in such a complex, heterogeneous and non-uniform structure.

Since no validated means of estimating residual stresses are available yet, the models in this thesis did not incorporate the residual stresses. A possible way to estimate residual stresses might be combining ex vivo inflation test and a destructive test such as uniaxial tension. First, an intact atherosclerotic vessel can be inflated in an ex vivo setup and by using the methodology described in chapter 8, and strain-stress relation of the intact plaque can be obtained. Then, a piece from the plaque can be excised and tested in e.g. a uniaxial tension setup. Since the residual stresses are released due to the removal of the piece from the plaque, the difference between the results of this destructive method and ex vivo inflation tests might provide an estimate of residual stresses.

If the aim of obtaining reliable stress maps is to compare them to strength maps and assess the rupture risk, another option to deal with residual stresses in atherosclerotic plaque modeling would be measuring strength from the experiments with the plaque still intact and the residual stresses not released. By doing so, both stress and strength maps will omit residual stresses leading to a fair comparison between the two, thus potentially improving rupture risk judgment.

Material Properties of Plaque Components

More plaques with different phenotypes and from different vascular territories need to be tested under physiological loading conditions in the future to build an extensive database for material properties of atherosclerotic plaque components. Even with carefully designed experiments, it is very likely that the results will show large variation, even for the samples obtained from the same vasculature and of similar phenotype due to the heterogeneity. Therefore, reporting not only the average stiffness value but also some measures reflecting the variation and the distribution in the results (standard deviation, range, percentile values, etc.)

is advisable. Large variation in atherosclerotic intima stiffness suggests that plaque specific properties are required for plaque specific stress computations.

In vivo, plaque specific stiffness estimation can be done by combining in vivo deformation measurement techniques with inverse FE analysis such as intravascular ultrasound (IVUS) modulography [157]. IVUS modulography combines elastography [200] with inverse FE analysis to estimate the Young's modulus of the plaque tissue. Baldewsing et al. demonstrated the clinical feasibility of this technique by testing human coronary plaques in vivo [157]. Recent developments in ultrasound imaging such as compounding [205] and shear wave imaging [211] show that this methodology might be feasible for application on carotid arteries in the near future.

Plaque Geometry and Imaging Requirements

The findings of previous studies and this thesis demonstrated that cap thickness, lipid core size, and lumen radius and curvature are risk factors for high cap stresses. Deep lying layers such as media and adventitia did not show substantial effects on cap stresses in our studies. These findings suggest that high precision imaging of the lumen, cap and lipid core combined with general geometric description of the plaque including the outer vessel and lumen borders are required. For coronaries, combination of optical coherence tomography and intravascular ultrasound imaging might provide such detailed geometries. For carotid arteries, since the vessel is close to the skin, imaging studies are mainly focused on noninvasive techniques such as magnetic resonance imaging and ultrasound imaging. Yet, these imaging modalities cannot achieve the high resolution and/or the contrast required to delineate plaque components accurately. Therefore, discriminating high rupture-risk plaques based on non-invasive plaque imaging does not seem possible in the near future. However, stable, low risk plaques are easier to identify since their geometric features are more recognizable and easier to measure than vulnerable phenotype. Identification of stable plaques is important to prevent unnecessary interventions.

Biomechanical Perspective of Plaque Rupture

Stress maps of atherosclerotic caps are necessary for rupture risk assessment, but this is only half of the equation. The other half is the cap strength. A limited number of research groups tested the strength of atherosclerotic intima tissue using destructive techniques [95, 108]. Similar to the mechanical properties of atherosclerotic intima, experimental data on strength results showed a wide range. A better technique to estimate cap strength would be ex vivo inflation
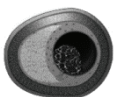
tests as these tests use intact vessels and resemble the physiological loading condition. By increasing the intraluminal pressure gradually, a cap rupture could be induced. A good technique to image the vessel and the rupture in real time is ultrasound imaging due to its fast acquisition. An extra-vascular high frequency ultrasound transducer would provide high resolution images. However, this technique will enable obtaining the images on a single transversal cross-section. To obtain the 3D vessel geometry and not to miss the rupture location, the transducer can be attached to a 3D step motor that would sweep the transducer in the longitudinal vessel direction. Dedicated contrast agents can further help to delineate the lumen contour if needed. Relating the test results to plaque type and pathology should be done to understand the likely variation in strength results. These tests might also help to understand the in vivo plaque rupture event as rupture will be induced by intraluminal pressure increase.

9.3   Final Conclusions

This thesis provided important steps forward to understand risk factors of high cap stresses and to obtain reliable stress maps of atherosclerotic plaques, an inevitable requirement for rupture risk assessment. It was demonstrated that a better understanding of the material properties of atherosclerotic intima is required for accurate biomechanical plaque modeling. The variability in material properties and plaque geometry suggests that plaque specific material properties and modeling are needed, and uncertainties in material properties and imaging of the geometric features should be incorporated in the models. For plaque specific models, 3D models with initial stresses should be used, and the geometries should be obtained from imaging techniques capable of providing cap and lipid core geometry in detail on transversal cross-section, and high resolution in the axial direction. These requirements have to be fulfilled and only then we will be able to generate biomechanical plaque models for reliable rupture risk assessment.

References

[1] Lusis AJ. Atherosclerosis. Nature. 2000;407:233-41.

[2] Moreno PR, Purushothaman KR, Fuster V, O'Connor WN. Intimomedial interface damage and adventitial inflammation is increased beneath disrupted atherosclerosis in the aorta: implications for plaque vulnerability. Circulation. 2002;105:2504-11.

[3] WHO. The Atlas of Heart Disease and Stroke. 2004.

[4] Falk E, Shah PK, Fuster V. Coronary plaque disruption. Circulation. 1995;92:657-71.

[5] Harrison MJ, Marshall J. Angiographic appearance of carotid bifurcation in pateints with completed stroke, transient ischaemic attacks, and cerebral tumour. Br Med J. 1976;1:205-7.

[6] Criqui MH, Coughlin SS, Fronek A. Noninvasively diagnosed peripheral arterial disease as a predictor of mortality: results from a prospective study. Circulation. 1985;72:768-73.

[7] WHO. World Health Statistics 2012. World Health Organization; 2012.

[8] Stary HC. Natural history and histological classification of atherosclerotic lesions: an update. Arterioscler Thromb Vasc Biol. 2000;20:1177-8.

[9] Stary HC. Atlas of Atherosclerosis Progression and Regression. Second Edition ed: Parthenon Publishing; 2003.

[10] Schaar JA, Regar E, Mastik F, McFadden EP, Saia F, Disco C, et al. Incidence of high-strain patterns in human coronary arteries: assessment with three-dimensional intravascular palpography and correlation with clinical presentation. Circulation. 2004;109:2716-9.

[11] Jang IK, Tearney GJ, MacNeill B, Takano M, Moselewski F, Iftima N, et al. In vivo characterization of coronary atherosclerotic plaque by use of optical coherence tomography. Circulation. 2005;111:1551-5.

[12] Ohayon J, Finet G, Gharib AM, Herzka DA, Tracqui P, Heroux J, et al. Necrotic core thickness and positive arterial remodeling index: emergent biomechanical factors for evaluating the risk of plaque rupture. Am J Physiol-Heart C. 2008;295:H717-H27.

[13] Chu B, Kampschulte A, Ferguson MS, Kerwin WS, Yarnykh VL, O'Brien KD, et al. Hemorrhage in the atherosclerotic carotid plaque: a high-resolution MRI study. Stroke. 2004;35:1079-84.

[14] Naghavi M, Libby P, Falk E, Casscells SW, Litovsky S, Rumberger J, et al. From vulnerable plaque to vulnerable patient: a call for new definitions and risk assessment strategies: Part II. Circulation. 2003;108:1772-8.

[15] Virmani R, Burke AP, Farb A, Kolodgie FD. Pathology of the vulnerable plaque. J Am Coll Cardiol. 2006;47:C13-8.

[16] Virmani R, Burke AP, Kolodgie FD, Farb A. Pathology of the thin-cap fibroatheroma: a type of vulnerable plaque. J Interv Cardiol. 2003;16:267-72.

[17] Virmani R, Burke AP, Kolodgie FD, Farb A. Vulnerable plaque: the pathology of unstable coronary lesions. J Interv Cardiol. 2002;15:439-46.

[18] Kolodgie FD, Burke AP, Farb A, Gold HK, Yuan J, Narula J, et al. The thin-cap fibroatheroma: a type of vulnerable plaque: the major precursor lesion to acute coronary syndromes. Curr Opin Cardiol. 2001;16:285-92.

[19] Sadat U, Teng Z, Gillard JH. Biomechanical structural stresses of atherosclerotic plaques. Expert Rev Cardiovasc Ther. 2010;8:1469-81.

[20] Cheng GC, Loree HM, Kamm RD, Fishbein MC, Lee RT. Distribution of circumferential stress in ruptured and stable atherosclerotic lesions. A structural analysis with histopathological correlation. Circulation. 1993;87:1179-87.

[21] Richardson PD, Davies MJ, Born GV. Influence of plaque configuration and stress distribution on fissuring of coronary atherosclerotic plaques. Lancet. 1989;2:941-4.

[22] Samady H, Eshtehardi P, McDaniel MC, Suo J, Dhawan SS, Maynard C, et al. Coronary artery wall shear stress is associated with progression and transformation of atherosclerotic plaque and arterial remodeling in patients with coronary artery disease. Circulation. 2011;124:779-88.

[23] Wentzel JJ, Chatzizisis YS, Gijsen FJ, Giannoglou GD, Feldman CL, Stone PH. Endothelial shear stress in the evolution of coronary atherosclerotic plaque and vascular remodelling: current understanding and remaining questions. Cardiovasc Res. 2012;96:234-43.

[24] Hoskins PR, Hardman D. Three-dimensional imaging and computational modelling for estimation of wall stresses in arteries. Br J Radiol. 2009;82 Spec No 1:S3-17.

[25] Ohayon J, Teppaz P, Finet G, Rioufol G. In-vivo prediction of human coronary plaque rupture location using intravascular ultrasound and the finite element method. Coron Artery Dis. 2001;12:655-63.

[26] Loree HM, Kamm RD, Stringfellow RG, Lee RT. Effects of fibrous cap thickness on peak circumferential stress in model atherosclerotic vessels. Circ Res. 1992;71:850-8.

[27] Finet G, Ohayon J, Rioufol G. Biomechanical interaction between cap thickness, lipid core composition and blood pressure in vulnerable coronary plaque: impact on stability or instability. Coronary Artery Dis. 2004;15:13-20.

[28] Virmani R, Kolodgie FD, Burke AP, Farb A, Schwartz SM. Lessons from sudden coronary death: a comprehensive morphological classification scheme for atherosclerotic lesions. Arterioscler Thromb Vasc Biol. 2000;20:1262-75.

[29] Ohayon J, Finet G, Gharib AM, Herzka DA, Tracqui P, Heroux J, et al. Necrotic core thickness and positive arterial remodeling index: emergent biomechanical factors for evaluating the risk of plaque rupture. Am J Physiol Heart Circ Physiol. 2008;295:H717-27.

[30] Barrett SR, Sutcliffe MP, Howarth S, Li ZY, Gillard JH. Experimental measurement of the mechanical properties of carotid atherothrombotic plaque fibrous cap. J Biomech. 2009;42:1650-5.

[31] Born GVR, Richardson PD. Mechanical properties of human atherosclerotic lesions. In: Glagov S, Newman WP, Schaffa SA, editors. Pathobiology of the Human Atherosclerotic Plaque. New York: Springer Verlag New York, Inc.; 1990. p. 413-23.

[32] Chai C-K, Akyildiz AC, Speelman L, Gijsen FJH, Oomens CWJ, Sambeek MRHMv, et al. Local axial compressive mechanical properties of human carotid atherosclerotic plaques - characterisation by indentation test and finite element inverse analysis. Journal of Biomechanics. 2013;46:1759-66.

[33] Lawlor MG, O'Donnell MR, O'Connell BM, Walsh MT. Experimental determination of circumferential properties of fresh carotid artery plaques. J Biomech. 2011;44:1709-15.

[34] Lee RT, Grodzinsky AJ, Frank EH, Kamm RD, Schoen FJ. Structure-dependent dynamic mechanical behavior of fibrous caps from human atherosclerotic plaques. Circulation. 1991;83:1764-70.

[35] Lendon CL, Davies MJ, Richardson PD, Born GV. Testing of small connective tissue specimens for the determination of the mechanical behaviour of atherosclerotic plaques. J Biomed Eng. 1993;15:27-33.

[36] Loree HM, Tobias BJ, Gibson LJ, Kamm RD, Small DM, Lee RT. Mechanical properties of model atherosclerotic lesion lipid pools. Arterioscler Thromb. 1994;14:230-4.

[37] Maher E, Creane A, Sultan S, Hynes N, Lally C, Kelly DJ. Tensile and compressive properties of fresh human carotid atherosclerotic plaques. J Biomech. 2009;42:2760-7.

[38] Slager CJ, Wentzel JJ, Gijsen FJ, Thury A, van der Wal AC, Schaar JA, et al. The role of shear stress in the destabilization of vulnerable plaques and related therapeutic implications. Nat Clin Pract Cardiovasc Med. 2005;2:456-64.

[39] Schaar JA, Muller JE, Falk E, Virmani R, Fuster V, Serruys PW, et al. Terminology for high-risk and vulnerable coronary artery plaques. Report of a meeting on the vulnerable plaque, June 17 and 18, 2003, Santorini, Greece. Eur Heart J. 2004;25:1077-82.

[40] Yuan C, Zhang SX, Polissar NL, Echelard D, Ortiz G, Davis JW, et al. Identification of fibrous cap rupture with magnetic resonance imaging is highly associated with recent transient ischemic attack or stroke. Circulation. 2002;105:181-5.

[41] Hamdan A, Assali A, Fuchs S, Battler A, Kornowski R. Imaging of vulnerable coronary artery plaques. Catheter Cardiovasc Interv. 2007;70:65-74.

[42] Taylor DC, Strandness DE, Jr. Carotid artery duplex scanning. J Clin Ultrasound. 1987;15:635-44.

[43] Wintermark M, Jawadi SS, Rapp JH, Tihan T, Tong E, Glidden DV, et al. High-resolution CT imaging of carotid artery atherosclerotic plaques. AJNR Am J Neuroradiol. 2008;29:875-82.

[44] Gao H, Long Q, Das SK, Sadat U, Graves M, Gillard JH, et al. Stress analysis of carotid atheroma in transient ischemic attack patients: evidence for extreme stress-induced plaque rupture. Annals of Biomedical Engineering. 2011;39:2203-12.

[45] Glagov S, Weisenberg E, Zarins CK, Stankunavicius R, Kolettis GJ. Compensatory enlargement of human atherosclerotic coronary arteries. N Engl J Med. 1987;316:1371-5.

[46] Ambrose JA, Tannenbaum MA, Alexopoulos D, Hjemdahl-Monsen CE, Leavy J, Weiss M, et al. Angiographic progression of coronary artery disease and the development of myocardial infarction. J Am Coll Cardiol. 1988;12:56-62.

[47] Little WC, Constantinescu M, Applegate RJ, Kutcher MA, Burrows MT, Kahl FR, et al. Can coronary angiography predict the site of a subsequent myocardial infarction in patients with mild-to-moderate coronary artery disease? Circulation. 1988;78:1157-66.

[48] Huang H, Virmani R, Younis H, Burke AP, Kamm RD, Lee RT. The impact of calcification on the biomechanical stability of atherosclerotic plaques. Circulation. 2001;103:1051-6.

[49] Tang D, Yang C, Mondal S, Liu F, Canton G, Hatsukami TS, et al. A negative correlation between human carotid atherosclerotic plaque progression and plaque wall stress: in vivo MRI-based 2D/3D FSI models. J Biomech. 2008;41:727-36.

[50] Gao H, Long Q. Effects of varied lipid core volume and fibrous cap thickness on stress distribution in carotid arterial plaques. J Biomech. 2008;41:3053-9.

[51] Kock SA, Nygaard JV, Eldrup N, Frund ET, Klaerke A, Paaske WP, et al. Mechanical stresses in carotid plaques using MRI-based fluid-structure interaction models. J Biomech. 2008;41:1651-8.

[52] Li ZY, Tang T, J UK-I, Graves M, Sutcliffe M, Gillard JH. Assessment of carotid plaque vulnerability using structural and geometrical determinants. Circ J. 2008;72:1092-9.

126

[53] Burke AP, Farb A, Malcom GT, Liang YH, Smialek J, Virmani R. Coronary risk factors and plaque morphology in men with coronary disease who died suddenly. N Engl J Med. 1997;336:1276-82.

[54] Huang X, Yang C, Yuan C, Liu F, Canton G, Zheng J, et al. Patient-specific artery shrinkage and 3D zero-stress state in multi-component 3D FSI models for carotid atherosclerotic plaques based on in vivo MRI data. Mol Cell Biomech. 2009;6:121-34.

[55] Speelman L, Bosboom EM, Schurink GW, Buth J, Breeuwer M, Jacobs MJ, et al. Initial stress and nonlinear material behavior in patient-specific AAA wall stress analysis. J Biomech. 2009;42:1713-9.

[56] Holzapfel GA. Nonlinear solid mechanics : a continuum approach for engineering. Chichester ; New York: Wiley; 2000.

[57] Holzapfel GA, Sommer G, Gasser CT, Regitnig P. Determination of layer-specific mechanical properties of human coronary arteries with nonatherosclerotic intimal thickening and related constitutive modeling. Am J Physiol-Heart C. 2005;289:H2048-H58.

[58] Bluestein D, Alemu Y, Avrahami I, Gharib M, Dumont K, Ricotta JJ, et al. Influence of microcalcifications on vulnerable plaque mechanics using FSI modeling. J Biomech. 2008;41:1111-8.

[59] Wenk JF. Numerical modeling of stress in stenotic arteries with microcalcifications: a parameter sensitivity study. J Biomech Eng. 2011;133:014503.

[60] Holzapfel GA, Stadler M, Schulze-Bauer CA. A layer-specific three-dimensional model for the simulation of balloon angioplasty using magnetic resonance imaging and mechanical testing. Annals of Biomedical Engineering. 2002;30:753-67.

[61] Kiousis DE, Wulff AR, Holzapfel GA. Experimental studies and numerical analysis of the inflation and interaction of vascular balloon catheter-stent systems. Annals of Biomedical Engineering. 2009;37:315-30.

[62] Redgrave JN, Gallagher P, Lovett JK, Rothwell PM. Critical cap thickness and rupture in symptomatic carotid plaques: the oxford plaque study. Stroke. 2008;39:1722-9.

[63] Tang D, Teng Z, Canton G, Yang C, Ferguson M, Huang X, et al. Sites of rupture in human atherosclerotic carotid plaques are associated with high structural stresses: an in vivo MRI-based 3D fluid-structure interaction study. Stroke. 2009;40:3258-63.

[64] Akyildiz AC, Speelman L, van Brummelen H, Gutierrez MA, Virmani R, van der Lugt A, et al. Effects of intima stiffness and plaque morphology on peak cap stress. Biomed Eng Online. 2011;10:25.

[65] Gao H, Long Q, Graves M, Gillard JH, Li ZY. Study of reproducibility of human arterial plaque reconstruction and its effects on stress analysis based on multispectral in vivo magnetic resonance imaging. J Magn Reson Imaging. 2009;30:85-93.

[66] Sadat U, Teng Z, Young VE, Li ZY, Gillard JH. Utility of magnetic resonance imaging-based finite element analysis for the biomechanical stress analysis of hemorrhagic and non-hemorrhagic carotid plaques. Circ J. 2011;75:884-9.

[67] Vengrenyuk Y, Carlier S, Xanthos S, Cardoso L, Ganatos P, Virmani R, et al. A hypothesis for vulnerable plaque rupture due to stress-induced debonding around cellular microcalcifications in thin fibrous caps. Proc Natl Acad Sci U S A. 2006;103:14678-83.

[68] Teng Z, Sadat U, Ji G, Zhu C, Young VE, Graves MJ, et al. Lumen irregularity dominates the relationship between mechanical stress condition, fibrous-cap thickness, and lumen curvature in carotid atherosclerotic plaque. J Biomech Eng. 2011;133:034501.

[69] Creane A, Maher E, Sultan S, Hynes N, Kelly DJ, Lally C. Finite element modelling of diseased carotid bifurcations generated from in vivo computerised tomographic angiography. Comput Biol Med. 2010;40:419-29.

[70] Rambhia SH, Liang X, Xenos M, Alemu Y, Maldonado N, Kelly A, et al. Microcalcifications increase coronary vulnerable plaque rupture potential: a patient-based micro-CT fluid-structure interaction study. Annals of Biomedical Engineering. 2012;40:1443-54.

[71] Maldonado N, Kelly-Arnold A, Vengrenyuk Y, Laudier D, Fallon JT, Virmani R, et al. A mechanistic analysis of the role of microcalcifications in atherosclerotic plaque stability: potential implications for plaque rupture. Am J Physiol-Heart C. 2012;303:H619-H28.

[72] Sadat U, Teng Z, Young VE, Graves MJ, Gaunt ME, Gillard JH. High-resolution magnetic resonance imaging-based biomechanical stress analysis of carotid atheroma: a comparison of single transient ischaemic attack, recurrent transient ischaemic attacks, non-disabling stroke and asymptomatic patient groups. Eur J Vasc Endovasc Surg. 2011;41:83-90.

[73] Sadat U, Li ZY, Young VE, Graves MJ, Boyle JR, Warburton EA, et al. Finite element analysis of vulnerable atherosclerotic plaques: a comparison of mechanical stresses within carotid plaques of acute and recently symptomatic patients with carotid artery disease. J Neurol Neurosurg Psychiatry. 2009;81:286-9.

[74] Chau AH, Chan RC, Shishkov M, MacNeill B, Iftimia N, Tearney GJ, et al. Mechanical analysis of atherosclerotic plaques based on optical coherence tomography. Annals of Biomedical Engineering. 2004;32:1494-503.

[75] Kural MH, Cai M, Tang D, Gwyther T, Zheng J, Billiar KL. Planar biaxial characterization of diseased human coronary and carotid arteries for computational modeling. J Biomech. 2012;45:790-8.

[76] Baldewsing RA, de Korte CL, Schaar JA, Mastik F, van der Steen AF. Finite element modeling and intravascular ultrasound elastography of vulnerable plaques: parameter variation. Ultrasonics. 2004;42:723-9.

[77] Vengrenyuk Y, Kaplan TJ, Cardoso L, Randolph GJ, Weinbaum S. Computational stress analysis of atherosclerotic plaques in ApoE knockout mice. Annals of Biomedical Engineering. 2010;38:738-47.

[78] Speelman L, Akyildiz AC, den Adel B, Wentzel JJ, van der Steen AF, Virmani R, et al. Initial stress in biomechanical models of atherosclerotic plaques. J Biomech. 2011;44:2376-82.

[79] Ohayon J, Dubreuil O, Tracqui P, Le Floc'h S, Rioufol G, Chalabreysse L, et al. Influence of residual stress/strain on the biomechanical stability of vulnerable coronary plaques: potential impact for evaluating the risk of plaque rupture. Am J Physiol Heart Circ Physiol. 2007;293:H1987-96.

[80] Yuan C, Kerwin WS. MRI of atherosclerosis. J Magn Reson Imaging. 2004;19:710-9.

[81] Gasser TC, Ogden RW, Holzapfel GA. Hyperelastic modelling of arterial layers with distributed collagen fibre orientations. J R Soc Interface. 2006;3:15-35.

[82] de Putter S, Wolters BJ, Rutten MC, Breeuwer M, Gerritsen FA, van de Vosse FN. Patient-specific initial wall stress in abdominal aortic aneurysms with a backward incremental method. J Biomech. 2007;40:1081-90.

[83] Ohayon J, Finet G, Treyve F, Rioufol G, Dubreuil O. A three-dimensional finite element analysis of stress distribution in a coronary atherosclerotic plaque: In-vivo prediction of plaque rupture location. Biomechanics Applied to Computer Assisted Surgery. 2005:225-41

[84] Cilla M, Pena E, Martinez MA. 3D computational parametric analysis of eccentric atheroma plaque: influence of axial and circumferential residual stresses. Biomechanics and Modeling in Mechanobiology. 2012;11:1001-13.

[85] Tang D, Yang C, Zheng J, Woodard PK, Sicard GA, Saffitz JE, et al. 3D MRI-based multicomponent FSI models for atherosclerotic plaques. Ann Biomed Eng. 2004;32:947-60.

[86] Naghavi M, Libby P, Falk E, Casscells SW, Litovsky S, Rumberger J, et al. From vulnerable plaque to vulnerable patient: a call for new definitions and risk assessment strategies: Part I. Circulation. 2003;108:1664-72.

[87] Tang D, Teng Z, Canton G, Hatsukami TS, Dong L, Huang X, et al. Local critical stress correlates better than global maximum stress with plaque morphological features linked to atherosclerotic plaque vulnerability: an in vivo multi-patient study. Biomed Eng Online. 2009;8:15.

[88] Tang D, Yang C, Zheng J, Woodard PK, Saffitz JE, Petruccelli JD, et al. Local maximal stress hypothesis and computational plaque vulnerability index for atherosclerotic plaque assessment. Ann Biomed Eng. 2005;33:1789-801.

[89] Finet G, Ohayon J, Rioufol G. Biomechanical interaction between cap thickness, lipid core composition and blood pressure in vulnerable coronary plaque: impact on stability or instability. Coron Artery Dis. 2004;15:13-20.

[90] Kiousis D, Rubinigg S, Auer M, Holzapfel G. A methodology to analyze changes in lipid core and calcification onto fibrous cap vulnerability: The human atherosclerotic carotid bifurcation as an illustratory example. J Biomech Eng. 2009;131:121002-10.

[91] Lee RT, Schoen FJ, Loree HM, Lark MW, Libby P. Circumferential stress and matrix metalloproteinase 1 in human coronary atherosclerosis. Implications for plaque rupture. Arterioscler Thromb Vasc Biol. 1996;16:1070-3.

[92] Williamson SD, Lam Y, Younis HF, Huang H, Patel S, Kaazempur-Mofrad MR, et al. On the sensitivity of wall stresses in diseased arteries to variable material properties. J Biomech Eng. 2003;125:147-55.

[93] Versluis A, Bank AJ, Douglas WH. Fatigue and plaque rupture in myocardial infarction. J Biomech. 2006;39:339-47.

[94] Loree HM, Grodzinsky AJ, Park SY, Gibson LJ, Lee RT. Static circumferential tangential modulus of human atherosclerotic tissue. J Biomech. 1994;27:195-204.

[95] Holzapfel GA, Sommer G, Regitnig P. Anisotropic mechanical properties of tissue components in human atherosclerotic plaques. J Biomech Eng. 2004;126:657-65.

[96] Holzapfel GA, Sommer G, Gasser CT, Regitnig P. Determination of layer-specific mechanical properties of human coronary arteries with nonatherosclerotic intimal thickening and related constitutive modeling. Am J Physiol Heart Circ Physiol. 2005;289:H2048-58.

[97] Lee RT, Richardson SG, Loree HM, Grodzinsky AJ, Gharib SA, Schoen FJ, et al. Prediction of mechanical properties of human atherosclerotic tissue by high-frequency intravascular ultrasound imaging. An in vitro study. Arterioscler Thromb. 1992;12:1-5.

[98] Joshi AK, Leask RL, Myers JG, Ojha M, Butany J, Ethier CR. Intimal thickness is not associated with wall shear stress patterns in the human right coronary artery. Arterioscler Thromb Vasc Biol. 2004;24:2408-13.

[99] Pessanha BS, Potter K, Kolodgie FD, Farb A, Kutys R, Mont EK, et al. Characterization of intimal changes in coronary artery specimens with MR microscopy. Radiology. 2006;241:107-15.

[100] Gradus-Pizlo I, Bigelow B, Mahomed Y, Sawada SG, Rieger K, Feigenbaum H. Left anterior descending coronary artery wall thickness measured by high-frequency transthoracic and epicardial echocardiography includes adventitia. Am J Cardiol. 2003;91:27-32.

[101] von Birgelen C, Klinkhart W, Mintz GS, Papatheodorou A, Herrmann J, Baumgart D, et al. Plaque distribution and vascular remodeling of ruptured and nonruptured coronary plaques in the same vessel: an intravascular ultrasound study in vivo. J Am Coll Cardiol. 2001;37:1864-70.

[102] Speelman L, Bosboom EM, Schurink GW, Hellenthal FA, Buth J, Breeuwer M, et al. Patient-specific AAA wall stress analysis: 99-percentile versus peak stress. Eur J Vasc Endovasc Surg. 2008;36:668-76.

[103] Tracqui P, Broisat A, Toczek J, Mesnier N, Ohayon J, Riou L. Mapping elasticity moduli of atherosclerotic plaque in situ via atomic force microscopy. J Struct Biol. 2011;174:115-23.

[104] Kumar RK, Balakrishnan KR. Influence of lumen shape and vessel geometry on plaque stresses: possible role in the increased vulnerability of a remodelled vessel and the "shoulder" of a plaque. Heart. 2005;91:1459-65.

[105] Corrado E, Rizzo M, Coppola G, Fattouch K, Novo G, Marturana I, et al. An update on the role of markers of inflammation in atherosclerosis. J Atheroscler Thromb.17:1-11.

[106] Chen WQ, Zhang M, Ji XP, Ding SF, Zhao YX, Chen YG, et al. Usefulness of high-frequency vascular ultrasound imaging and serum inflammatory markers to predict plaque rupture in patients with stable and unstable angina pectoris. Am J Cardiol. 2007;100:1341-6.

[107] Nair A, Kuban BD, Tuzcu EM, Schoenhagen P, Nissen SE, Vince DG. Coronary plaque classification with intravascular ultrasound radiofrequency data analysis. Circulation. 2002;106:2200-6.

[108] Lendon CL, Davies MJ, Born GV, Richardson PD. Atherosclerotic plaque caps are locally weakened when macrophages density is increased. Atherosclerosis. 1991;87:87-90.

[109] Tearney GJ, Yabushita H, Houser SL, Aretz HT, Jang IK, Schlendorf KH, et al. Quantification of macrophage content in atherosclerotic plaques by optical coherence tomography. Circulation. 2003;107:113-9.

[110] Hoshino T, Chow LA, Hsu JJ, Perlowski AA, Abedin M, Tobis J, et al. Mechanical stress analysis of a rigid inclusion in distensible material: a model of atherosclerotic calcification and plaque vulnerability. Am J Physiol Heart Circ Physiol. 2009;297:H802-10.

[111] WHO. Cause-specific mortality: regional estimates for 2008. 2011.

[112] Falk E. Pathogenesis of atherosclerosis. J Am Coll Cardiol. 2006;47:C7-12.

[113] Teng Z, Sadat U, Li Z, Huang X, Zhu C, Young VE, et al. Arterial luminal curvature and fibrous-cap thickness affect critical stress conditions within atherosclerotic plaque: an in vivo MRI-based 2D finite-element study. Ann Biomed Eng.38:3096-101.

[114] Dolla WJ, House JA, Marso SP. Stratification of risk in thin cap fibroatheromas using peak plaque stress estimates from idealized finite element models. Med Eng Phys. 2012;34:1330-8.

[115] Li ZY, Howarth SP, Tang T, Gillard JH. How critical is fibrous cap thickness to carotid plaque stability? A flow-plaque interaction model. Stroke. 2006;37:1195-9.

[116] Wong KK, Thavornpattanapong P, Cheung SC, Sun Z, Tu J. Effect of calcification on the mechanical stability of plaque based on a three-dimensional carotid bifurcation model. BMC Cardiovasc Disord. 2012;12:7.

[117] Maehara A, Mintz GS, Bui AB, Walter OR, Castagna MT, Canos D, et al. Morphologic and angiographic features of coronary plaque rupture detected by intravascular ultrasound. J Am Coll Cardiol. 2002;40:904-10.

[118] Teng Z, Sadat U, Li Z, Huang X, Zhu C, Young VE, et al. Arterial luminal curvature and fibrous-cap thickness affect critical stress conditions within atherosclerotic plaque: an in vivo MRI-based 2D finite-element study. Ann Biomed Eng. 2010;38:3096-101.

[119] Vengrenyuk Y, Cardoso L, Weinbaum S. Micro-CT based analysis of a new paradigm for vulnerable plaque rupture: cellular microcalcifications in fibrous caps. Mol Cell Biomech. 2008;5:37-47.

[120] Beattie D, Xu C, Vito R, Glagov S, Whang MC. Mechanical analysis of heterogeneous, atherosclerotic human aorta. J Biomech Eng. 1998;120:602-7.

[121] Nieuwstadt HA, Akyildiz AC, Speelman L, Virmani R, van der Lugt A, van der Steen AF, et al. The influence of axial image resolution on atherosclerotic plaque stress computations. J Biomech. 2013;46:689-95.

[122] Richardson PD. Biomechanics of plaque rupture: Progress, problems, and new frontiers. Ann Biomed Eng. 2002;30:524-36.

[123] Teng Z, Sadat U, Li Z, Huang X, Zhu C, Young VE, et al. Arterial luminal curvature and fibrous-cap thickness affect critical stress conditions within atherosclerotic plaque: an in vivo MRI-based 2D finite-element study. Ann Biomed Eng. 2010;38:3096-101.

[124] Matsumoto T, Nagayama K. Tensile properties of vascular smooth muscle cells: bridging vascular and cellular biomechanics. J Biomech. 2012;45:745-55.

[125] Matsumoto T, Goto T, Furukawa T, Sato M. Residual stress and strain in the lamellar unit of the porcine aorta: experiment and analysis. J Biomech. 2004;37:807-15.

[126] Nagayama K, Nagano Y, Sato M, Matsumoto T. Effect of actin filament distribution on tensile properties of smooth muscle cells obtained from rat thoracic aortas. J Biomech. 2006;39:293-301.

[127] Rekhter MD. Collagen synthesis in atherosclerosis: too much and not enough. Cardiovasc Res. 1999;41:376-84.

[128] Fung YC. Biomechanics: Mechanical properties of living tissues. 2nd ed: Sronger-Verlag; 1993.

[129] Bruel A, Ortoft G, Oxlund H. Inhibition of cross-links in collagen is associated with reduced stiffness of the aorta in young rats. Atherosclerosis. 1998;140:135-45.

[130] Lillie MA, Gosline JM. Mechanical properties of elastin along the thoracic aorta in the pig. J Biomech. 2007;40:2214-21.

[131] Smith EB, Slater RS. The microdissection of large atherosclerotic plaques to give morphologically and topographically defined fractions for analysis. 1. The lipids in the isolated fractions. Atherosclerosis. 1972;15:37-56.

[132] Small DM. George Lyman Duff memorial lecture. Progression and regression of atherosclerotic lesions. Insights from lipid physical biochemistry. Arteriosclerosis. 1988;8:103-29.

[133] Ebenstein DM, Coughlin D, Chapman J, Li C, Pruitt LA. Nanomechanical properties of calcification, fibrous tissue, and hematoma from atherosclerotic plaques. J Biomed Mater Res A. 2009;91:1028-37.

[134] Stary HC, Blankenhorn DH, Chandler AB, Glagov S, Insull W, Jr., Richardson M, et al. A definition of the intima of human arteries and of its atherosclerosis-prone regions. A report from the Committee on Vascular Lesions of the Council on Arteriosclerosis, American Heart Association. Circulation. 1992;85:391-405.

[135] Stary HC, Chandler AB, Dinsmore RE, Fuster V, Glagov S, Insull W, Jr., et al. A definition of advanced types of atherosclerotic lesions and a histological classification of

atherosclerosis. A report from the Committee on Vascular Lesions of the Council on Arteriosclerosis, American Heart Association. Circulation. 1995;92:1355-74.

[136] Stary HC, Chandler AB, Glagov S, Guyton JR, Insull W, Jr., Rosenfeld ME, et al. A definition of initial, fatty streak, and intermediate lesions of atherosclerosis. A report from the Committee on Vascular Lesions of the Council on Arteriosclerosis, American Heart Association. Circulation. 1994;89:2462-78.

[137] Carr S, Farb A, Pearce WH, Virmani R, Yao JS. Atherosclerotic plaque rupture in symptomatic carotid artery stenosis. J Vasc Surg. 1996;23:755-65; discussion 65-6.

[138] de Weert TT, Cretier S, Groen HC, Homburg P, Cakir H, Wentzel JJ, et al. Atherosclerotic plaque surface morphology in the carotid bifurcation assessed with multidetector computed tomography angiography. Stroke. 2009;40:1334-40.

[139] Barnett HJ, Taylor DW, Eliasziw M, Fox AJ, Ferguson GG, Haynes RB, et al. Benefit of carotid endarterectomy in patients with symptomatic moderate or severe stenosis. North American Symptomatic Carotid Endarterectomy Trial Collaborators. N Engl J Med. 1998;339:1415-25.

[140] Virmani R, Ladich ER, Burke AP, Kolodgie FD. Histopathology of carotid atherosclerotic disease. Neurosurgery. 2006;59:S219-27; discussion S3-13.

[141] Redgrave JN, Lovett JK, Gallagher PJ, Rothwell PM. Histological assessment of 526 symptomatic carotid plaques in relation to the nature and timing of ischemic symptoms: the Oxford plaque study. Circulation. 2006;113:2320-8.

[142] Virmani R, Kolodgie FD, Burke AP, Finn AV, Gold HK, Tulenko TN, et al. Atherosclerotic plaque progression and vulnerability to rupture: angiogenesis as a source of intraplaque hemorrhage. Arterioscler Thromb Vasc Biol. 2005;25:2054-61.

[143] Dalager S, Paaske WP, Kristensen IB, Laurberg JM, Falk E. Artery-related differences in atherosclerosis expression: implications for atherogenesis and dynamics in intima-media thickness. Stroke. 2007;38:2698-705.

[144] Herisson F, Heymann MF, Chetiveaux M, Charrier C, Battaglia S, Pilet P, et al. Carotid and femoral atherosclerotic plaques show different morphology. Atherosclerosis. 2011;216:348-54.

[145] van Dijk RA, Virmani R, von der Thusen JH, Schaapherder AF, Lindeman JH. The natural history of aortic atherosclerosis: a systematic histopathological evaluation of the peri-renal region. Atherosclerosis. 2010;210:100-6.

[146] PDAY. Natural history of aortic and coronary atherosclerotic lesions in youth. Findings from the PDAY Study. Pathobiological Determinants of Atherosclerosis in Youth (PDAY) Research Group. Arterioscler Thromb. 1993;13:1291-8.

[147] Topoleski LD, Salunke NV, Humphrey JD, Mergner WJ. Composition- and history-dependent radial compressive behavior of human atherosclerotic plaque. J Biomed Mater Res. 1997;35:117-27.

[148] Salunke NV, Topoleski LD, Humphrey JD, Mergner WJ. Compressive stress-relaxation of human atherosclerotic plaque. J Biomed Mater Res. 2001;55:236-41.

[149] Fung YC. Biorheology of soft tissues. Biorheology. 1973;10:139-55.

[150] Stemper BD, Yoganandan N, Stineman MR, Gennarelli TA, Baisden JL, Pintar FA. Mechanics of fresh, refrigerated, and frozen arterial tissue. J Surg Res. 2007;139:236-42.

[151] Chow MJ, Zhang Y. Changes in the mechanical and biochemical properties of aortic tissue due to cold storage. J Surg Res. 2010;171:434-42.

[152] Hemmasizadeh A, Darvish K, Autieri M. Characterization of Changes to the Mechanical Properties of Arteries due to Cold Storage Using Nanoindentation Tests. Ann Biomed Eng. 2012;40:1434-42.

[153] Venkatasubramanian RT, Grassl ED, Barocas VH, Lafontaine D, Bischof JC. Effects of freezing and cryopreservation on the mechanical properties of arteries. Ann Biomed Eng. 2006;34:823-32.

[154] Schaar JA, de Korte CL, Mastik F, van der Steen AF. Effect of temperature increase and freezing on intravascular elastography. Ultrasonics. 2002;40:879-81.

[155] Abela GS, Aziz K, Vedre A, Pathak DR, Talbott JD, Dejong J. Effect of cholesterol crystals on plaques and intima in arteries of patients with acute coronary and cerebrovascular syndromes. Am J Cardiol. 2009;103:959-68.

[156] Behler RH, Nichols TC, Zhu H, Merricks EP, Gallippi CM. ARFI imaging for noninvasive material characterization of atherosclerosis. Part II: toward in vivo characterization. Ultrasound Med Biol. 2009;35:278-95.

[157] Baldewsing RA, Danilouchkine MG, Mastik F, Schaar JA, Serruys PW, van der Steen AF. An inverse method for imaging the local elasticity of atherosclerotic coronary plaques. IEEE Trans Inf Technol Biomed. 2008;12:277-89.

[158] Baldewsing RA, Mastik F, Schaar JA, Serruys PW, van der Steen AF. Young's modulus reconstruction of vulnerable atherosclerotic plaque components using deformable curves. Ultrasound Med Biol. 2006;32:201-10.

[159] Schaar JA, De Korte CL, Mastik F, Strijder C, Pasterkamp G, Boersma E, et al. Characterizing vulnerable plaque features with intravascular elastography. Circulation. 2003;108:2636-41.

[160] Beattie D, Xu G, Vito R, Glagov S, Whang WG. Mechanical analysis of heterogeneous, atherosclerotic human aorta. Journal of Biomechanical Engineering-Transactions of the Asme. 1998;120:602-7.

[161] Liu H, Canton G, Yuan C, Yang C, Billiar K, Teng Z, et al. Using in vivo Cine and 3D multi-contrast MRI to determine human atherosclerotic carotid artery material properties and circumferential shrinkage rate and their impact on stress/strain predictions. J Biomech Eng. 2012;134:011008.

[162] Beaussier H, Naggara O, Calvet D, Joannides R, Guegan-Massardier E, Gerardin E, et al. Mechanical and structural characteristics of carotid plaques by combined analysis with echotracking system and MR imaging. JACC Cardiovasc Imaging. 2011;4:468-77.

[163] Cheng C, Tempel D, van Haperen R, van der Baan A, Grosveld F, Daemen MJ, et al. Atherosclerotic lesion size and vulnerability are determined by patterns of fluid shear stress. Circulation. 2006;113:2744-53.

[164] Segers D, Helderman F, Cheng C, van Damme LC, Tempel D, Boersma E, et al. Gelatinolytic activity in atherosclerotic plaques is highly localized and is associated with both macrophages and smooth muscle cells in vivo. Circulation. 2007;115:609-16.

[165] Thim T, Hagensen MK, Drouet L, Bal Dit Sollier C, Bonneau M, Granada JF, et al. Familial hypercholesterolaemic downsized pig with human-like coronary atherosclerosis: a model for preclinical studies. EuroIntervention. 2010;6:261-8.

[166] Granada JF, Kaluza GL, Wilensky RL, Biedermann BC, Schwartz RS, Falk E. Porcine models of coronary atherosclerosis and vulnerable plaque for imaging and interventional research. EuroIntervention. 2009;5:140-8.

[167] Kim JS, Wallace-Bradley D, Alviar CL, Conditt G, Milewski K, Afari ME, et al. Correlation of angiographic late loss with neointimal proliferation in stents evaluated by OCT and histology in porcine coronary arteries. JACC Cardiovasc Imaging. 2011;4:1002-10.

[168] Gijsen FJ, Migliavacca F, Schievano S, Socci L, Petrini L, Thury A, et al. Simulation of stent deployment in a realistic human coronary artery. Biomed Eng Online. 2008;7:23.

[169] Mortier P, Holzapfel GA, De Beule M, Van Loo D, Taeymans Y, Segers P, et al. A Novel Simulation Strategy for Stent Insertion and Deployment in Curved Coronary Bifurcations: Comparison of Three Drug-Eluting Stents. Ann Biomed Eng. 2010;38:88-99.

[170] Morlacchi S, Chiastra C, Gastaldi D, Pennati G, Dubini G, Migliavacca F. Sequential structural and fluid dynamic numerical simulations of a stented bifurcated coronary artery. J Biomech Eng. 2012;133:121010.

[171] Wu Z, Yang C, Tang D. In vivo serial MRI-based models and statistical methods to quantify sensitivity and specificity of mechanical predictors for carotid plaque rupture: location and beyond. J Biomech Eng. 2011;133:064503.

[172] Li Z-Y, Howarth SPS, Tang T, Graves MJ, U-King-Im J, Trivedi RA, et al. Structural analysis and magnetic resonance imaging predict plaque vulnerability: A study comparing symptomatic and asymptomatic individuals. J Vasc Surg. 2007;45:768-75.

[173] Rothwell PM, Warlow CP. Prediction of benefit from carotid endarterectomy in individual patients: a risk-modelling study. European Carotid Surgery Trialists' Collaborative Group. Lancet. 1999;353:2105-10.

[174] Hayenga HN, Trache A, Trzeciakowski J, Humphrey JD. Regional atherosclerotic plaque properties in ApoE-/- mice quantified by atomic force, immunofluorescence, and light microscopy. J Vasc Res. 2011;48:495-504.

[175] Salunke NV, Topoleski LD. Biomechanics of atherosclerotic plaque. Crit Rev Biomed Eng. 1997;25:243-85.

[176] Cox MAJ, Driessen NJB, Boerboorn RA, Bouten CVC, Baaijens FPT. Mechanical characterization of anisotropic planar biological soft tissues using finite indentation: Experimental feasibility. Journal of Biomechanics. 2008;41:422-9.

[177] Cox MAJ, Driessen NJB, Bouten CVC, Baaljens FPT. Mechanical characterization of anisotropic planar biological soft tissues using large indentation: A computational feasibility study. Journal of Biomechanical Engineering-Transactions of the Asme. 2006;128:428-36.

[178] Krahn KN, Bouten CVC, van Tuijl S, van Zandvoort MAMJ, Merkx M. Fluorescently labeled collagen binding proteins allow specific visualization of collagen in tissues and live cell culture. Analytical Biochemistry. 2006;350:177-85.

[179] Vaenkatesan V, Li ZL, Vellinga WP, de Jeu WH. Adhesion and friction behaviours of polydimethylsiloxane - A fresh perspective on JKR measurements. Polymer. 2006;47:8317-25.

[180] Cox MAJ, Kortsmit J, Driessen N, Bouten CVC, Baaijens FPT. Tissue-Engineered Heart Valves Develop Native-like Collagen Fiber Architecture. Tissue Eng Pt A. 2010;16:1527-37.

[181] Timmins LH, Wu QF, Yeh AT, Moore JE, Greenwald SE. Structural inhomogeneity and fiber orientation in the inner arterial media. Am J Physiol-Heart C. 2010;298:H1537-H45.

[182] Kanai H, Hasegawa H, Ichiki M, Tezuka F, Koiwa Y. Elasticity imaging of atheroma with transcutaneous ultrasound: preliminary study. Circulation. 2003;107:3018-21.

[183] de Korte CL, Pasterkamp G, van der Steen AF, Woutman HA, Bom N. Characterization of plaque components with intravascular ultrasound elastography in human femoral and coronary arteries in vitro. Circulation. 2000;102:617-23.

[184] Gijsen FJ, Wentzel JJ, Thury A, Mastik F, Schaar JA, Schuurbiers JC, et al. Strain distribution over plaques in human coronary arteries relates to shear stress. Am J Physiol Heart Circ Physiol. 2008;295:H1608-14.

[185] Dirksen MT, van der Wal AC, van den Berg FM, van der Loos CM, Becker AE. Distribution of inflammatory cells in atherosclerotic plaques relates to the direction of flow. Circulation. 1998;98:2000-3.

[186] Burleigh MC, Briggs AD, Lendon CL, Davies MJ, Born GVR, Richardson PD. Collagen Type-I and Type-Iii, Collagen Content, Gags and Mechanical Strength of Human Atherosclerotic Plaque Caps - Span-Wise Variations. Atherosclerosis. 1992;96:71-81.

[187] Tang DL, Yang C, Zheng J, Woodard PK, Saffitz JE, Sicard GA, et al. Quantifying effects of plaque structure and material properties on stress distributions in human atherosclerotic plaques using 3D FSI models. Journal of Biomechanical Engineering-Transactions of the Asme. 2005;127:1185-94.

[188] Virmani R, Finn AV, Kolodgie FD. Carotid plaque stabilization and progression after stroke or TIA. Arterioscler Thromb Vasc Biol. 2009;29:3-6.

[189] Akyildiz AC, Speelman L, Gijsen FJ. Mechanical properties of human atherosclerotic intima tissue. Journal of Biomechanics. 2013;accepted.

[190] Fung YC, Liu SQ. Determination of the mechanical properties of the different layers of blood vessels in vivo. Proc Natl Acad Sci U S A. 1995;92:2169-73.

[191] Kim J, Baek S. Circumferential variations of mechanical behavior of the porcine thoracic aorta during the inflation test. J Biomech. 2011;44:1941-7.

[192] Pandit A, Lu X, Wang C, Kassab GS. Biaxial elastic material properties of porcine coronary media and adventitia. Am J Physiol Heart Circ Physiol. 2005;288:H2581-7.

[193] Khalil AS, Chan RC, Chau AH, Bouma BE, Mofrad MR. Tissue elasticity estimation with optical coherence elastography: toward mechanical characterization of in vivo soft tissue. Ann Biomed Eng. 2005;33:1631-9.

[194] Karimi R, Zhu T, Bouma BE, Mofrad MR. Estimation of nonlinear mechanical properties of vascular tissues via elastography. Cardiovasc Eng. 2008;8:191-202.

[195] Franquet A, Avril S, Le Riche R, Badel P. Identification of heterogeneous elastic properties in stenosed arteries: a numerical plane strain study. Comput Methods Biomech Biomed Engin. 2011;15:49-58.

[196] Le Floc'h S, Ohayon J, Tracqui P, Finet G, Gharib AM, Maurice RL, et al. Vulnerable atherosclerotic plaque elasticity reconstruction based on a segmentation-driven optimization procedure using strain measurements: theoretical framework. IEEE Trans Med Imaging. 2009;28:1126-37.

[197] Chandran KB, Mun JH, Choi KK, Chen JS, Hamilton A, Nagaraj A, et al. A method for in-vivo analysis for regional arterial wall material property alterations with atherosclerosis: preliminary results. Med Eng Phys. 2003;25:289-98.

[198] Hamilton AJ, Kim H, Nagaraj A, Mun JH, Yan LL, Roth SI, et al. Regional material property alterations in porcine femoral arteries with atheroma development. J Biomech. 2005;38:2354-64.

[199] Nagaraj A, Kim H, Hamilton AJ, Mun JH, Smulevitz B, Kane BJ, et al. Porcine carotid arterial material property alterations with induced atheroma: an in vivo study. Med Eng Phys. 2005;27:147-56.

[200] Cespedes EI, de Korte CL, van der Steen AF, von Birgelen C, Lancee CT. Intravascular elastography: principles and potentials. Semin Interv Cardiol. 1997;2:55-62.

[201] Koopmans SJ, Dekker R, Ackermans MT, Sauerwein HP, Serlie MJ, van Beusekom HM, et al. Dietary saturated fat/cholesterol, but not unsaturated fat or starch, induces C-reactive protein associated early atherosclerosis and ectopic fat deposition in diabetic pigs. Cardiovasc Diabetol. 2011;10:64.

[202] Learoyd BM, Taylor MG. Alterations with age in the viscoelastic properties of human arterial walls. Circ Res. 1966;18:278-92.

[203] Lopata RG, Nillesen MM, Hansen HH, Gerrits IH, Thijssen JM, de Korte CL. Performance evaluation of methods for two-dimensional displacement and strain estimation using ultrasound radio frequency data. Ultrasound Med Biol. 2009;35:796-812.

[204] Chen H, Shi H, Varghese T. Improvement of elastographic displacement estimation using a two-step cross-correlation method. Ultrasound Med Biol. 2007;33:48-56.

[205] Hansen HHG, Idzenga T, de Korte CL. Noninvasive Vascular Strain Imaging: from Methods to Application. Current Medical Imaging Reviews. 2012;8:37-45.

[206] Cespedes I, Huang Y, Ophir J, Spratt S. Methods for Estimation of Subsample Time Delays of Digitized Echo Signals. Ultrasonic Imaging. 1995;17:142-71.

[207] Lopata RGP, Nillesen MM, Hansen HHG, Gerrits IH, Thijssen JM, de Korte CL. Performance Evaluation of Methods for Two-Dimensional Displacement and Strain Estimation Using Ultrasound Radio Frequency Data. Ultrasound in Medicine and Biology. 2009;35:796-812.

[208] Klein S, Staring M, Murphy K, Viergever MA, Pluim JPW. elastix: A Toolbox for Intensity-Based Medical Image Registration. Ieee Transactions on Medical Imaging. 2010;29:196-205.

[209] Chai C-K, Akyildiz AC, Speelman L, Gijsen FJH, Oomens CWJ, Sambeek MRHMv, et al. Local axial compressive mechanical properties of human carotid atherosclerotic plaques - characterisation by indentation test and finite element inverse analysis. Journal of BIomechanics. 2013.

[210] Fung YC. What Are the Residual-Stresses Doing in Our Blood-Vessels. Annals of Biomedical Engineering. 1991;19:237-49.

[211] Couade M, Pernot M, Prada C, Messas E, Emmerich J, Bruneval P, et al. Quantitative Assessment of Arterial Wall Biomechanical Properties Using Shear Wave Imaging. Ultrasound in Medicine and Biology. 2010;36:1662-76.

Summary

Atherosclerosis is a systemic, inflammatory disease of the arterial system. It is characterized by local lipid accumulation in the vessel wall, which is called atherosclerotic plaque. A significant number of strokes and myocardial infarctions are associated with rupture of atherosclerotic plaques.Rupture occurs in the fibrous cap of the plaque, which separates the lipid rich core of the plaque from the lumen.

Only a portion of these atherosclerotic plaques rupture and characterization of the rupture prone plaques is of high importance for predicting acute cardiovascular events. From a mechanical point of view, a fibrous cap ruptures when the local stresses in the cap exceed the cap strength. Biomechanical models that compare cap stresses to cap strength can be of substantial value for rupture risk assessment. Previous numerical studies showed that high stress regions in the fibrous cap corresponded to the rupture locations. Therefore, cap stresses might serve as a rupture risk predictor.

Finite element (FE) analysis is a method frequently used to compute stresses in atherosclerotic plaques. Stress computations with FE plaque models relies on three important parameters: 1.) accurate representation of the loading, boundary and initial conditions, 2.) geometric features of the atherosclerotic plaque, and 3.) the material properties of the plaque components.

The objective of this thesis was to determine the requirements for FE plaque models to compute plaque and cap stresses for future rupture risk assessment, to establish the influence of plaque geometry and material properties on cap stresses, and to estimate the material properties of atherosclerotic plaques.

FE stress analyses of atherosclerotic plaques are commonly based on pressurized geometries. Until recently, the stresses at this deformed state, the initial stresses, were neglected in computational studies, as there were no

means to compute them. In chapter 2, a numerical technique, the Backward Incremental method, was implemented to FE plaque models and the influence of initial stresses on cap stresses was studied. The effect depended on plaque geometry and varied between -55% to +50%. It was concluded that initial stresses are a requirement in the FE plaque models for accurate stress computations. However, the relationship between the geometric features and cap stresses did not change when initial stresses were incorporated. This implies that parametric studies, that relate geometric plaque features to cap stresses, do not require initial stress computations.

In chapter 3, the influence of axial sampling resolution of plaque imaging on plaque and cap stresses was investigated based on high resolution histology data. The axial sampling did not change the general stress distribution and peak cap stress location, but it did affect the absolute cap stress values. No systematic bias in the changes could be determined. Similar trends for the influence of the cap thickness on peak cap stresses were observed for different axial sampling rate. It was concluded that 2D plaque models are appropriate to describe general relationships between geometric features and cap stresses, but 3D models with high axial resolution are necessary for reliable, plaque specific stress calculations.

In chapter 4, the influence of geometric features and intima stiffness on cap stresses was investigated with an extensive parametric study, using idealized 2D FE models. For relatively stiff intima models, cap thickness and lipid core thickness were the most important geometric features. A thinner cap and/or a thick lipid core elevated the peak cap stress. For relatively soft intima models, cap thickness was less influential and the lipid core thickness had a stronger effect on the cap stresses. Moreover, the angle of the lipid core was just as influential as the cap thickness for the soft intima models. The study demonstrated the effect of plaque geometry of the cap and lipid core, and intima stiffness on cap stresses.

In chapter 5, the influence of plaque geometry on cap stresses, and how this depends on intima stiffness, was further studied by using realistic plaque geometries. The 2D FE models were based on histology images of human coronary plaques. The analysis confirmed the importance of cap thickness. Contrary to the findings in chapter 4, lipid core size was not influential, which could be attributed to the more complex structure of the realistic plaque geometries compared to the idealized geometries. The lumen radius emerged as a new risk factor for high cap stresses, as a larger lumen elevated the stresses. The study further demonstrated that a surrogate marker, defined as ratio of the

lumen radius over the cap thickness, can be used to separate low stress plaques from high stress plaques.

In chapter 6, experimental studies that tested atherosclerotic human intima tissue were reviewed. The main conclusion was that experimental data are scarce and cover a wide stiffness range (30 to 250x10^3 kPa). In general, tensile properties were stiffer than the compressive properties. However, no successful correlation of the stiffness data to the vascular territory or to the plaque type could be made. This study demonstrated the lack of adequate experimental data on atherosclerotic intima properties, and the need for more and better documented experimental studies.

Axial compressive properties of atherosclerotic human carotid plaques were investigated in chapter 7. The combination of indentation tests and inverse FE analysis was used to estimate local intima properties. The stiffness results showed a large variation (between 5 and 900 kPa) and the average values were in the lower range of the reported values in literature. Collagen rich intima showed a higher average stiffness value than collagen poor intima (30 kPa vs. 15 kPa). No statistical difference was observed between structured and unstructured collagen regions, or between the different regions of atherosclerotic intima.

In chapter 8, a methodology was proposed to investigate the material behavior of atherosclerotic intima under more physiological conditions. High resolution radiofrequency data of noninvasive ultrasound imaging were used to measure the displacements during artery inflation tests. 2D FE models were obtained from a novel technique combining histology data with ultrasound images. The models were used to simulate the plaque deformation as measured in the inflation tests. The intima stiffness of the atherosclerotic plaques was estimated by comparing the measured and computed displacements. This study provided a nondestructive method for determining the material properties of atherosclerotic plaque components under physiological loading conditions and in an environment similar to in vivo environment. Preliminary data confirm relatively low stiffness values for atherosclerotic intima.

The studies presented in this thesis provided important steps forward to understand the risk factors of high cap stresses and to obtain reliable stress data of atherosclerotic plaques, which is an inevitable requirement for future plaque rupture risk assessment. It was demonstrated that a better understanding of the material properties of the atherosclerotic intima is required for accurate biomechanical plaque modeling. The variability in material properties and plaque geometry suggests that plaque specific material properties and modeling are

needed. The uncertainties in material properties and imaging of the geometric features should be incorporated in the models. For plaque specific risk analysis, 3D models with initial stresses should be used and the geometries should be obtained from imaging techniques capable of providing cap and lipid core geometry in detail on transversal cross-sections, and high resolution in the axial direction. These requirements have to be fulfilled and only then we will be able to generate biomechanical plaque models for reliable rupture risk assessment.

Samenvatting

Atherosclerose is een systematische, inflammatoire ziekte van het vaatstelsel. De ziekte wordt gekenmerkt door plaatselijke vet ophopingen in de vaatwand, welke atherosclerotische plaques worden genoemd. Een groot deel van de beroertes en hartinfarcten wordt veroorzaakt door het scheuren van een atherosclerotische plaque. Dit gebeurt met name door het scheuren van de fibreuze kap van een atherosclerotische plaque, welke de vetrijke kern van de plaque scheidt van het lumen.

Slechts een deel van de atherosclerotische plaques scheuren en het karakterisen van deze kwetsbare plaques is belangrijk voor het voorspellen van acute cardiovasculaire symptomen. Mechanisch gezien scheurt een fibreuze kap op het moment dat de lokale wandspanningen in de kap hoger zijn dan de sterkte van de kap. Biomechanische modellen waarmee kap spanningen vergeleken worden met kap sterkte kunnen van substantiële waarde zijn bij de risicobeoordeling van plaque ruptuur. Numerieke studies hebben aangetoond dat hoge spanningregio's in de kap goed overeenkomen met de locatie van de ruptuur. Daarom zou kap spanning wellicht gebruikt kunnen worden als een voorspeller voor ruptuur risico.

Eindige elementen (EE) analyse is een methode die vaak wordt gebruikt om spanningen in atherosclerotische plaques te berekenen. Het berekenen van spanningen door middel van EE plaque modellen berust op drie belangrijke parameters: 1.) de nauwkeurige weergave van de drukverdeling, de initiële voorwaarden en de randvoorwaarden, 2.) de geometrische kenmerken van de atherosclerotische plaque, en 3.) de materiaaleigenschappen van de plaque componenten.

Het doel van dit proefschrift was om de eisen met betrekking tot EE plaque modellen te bepalen voor toekomstige ruptuur risico-evaluaties, om de invloed van de plaque geometrie en de materiaaleigenschappen op kap spanningen vast te stellen, en om de materiaaleigenschappen van atherosclerotische plaques te schatten. Spanningsberekeningen van atherosclerotische plaques zijn veelal

gebaseerd op geometrieën onder druk. Tot voor kort werden de spanningen in deze vervormde toestand, de initiële spanningen, verwaarloosd in numerieke studies, omdat er geen methodes beschikbaar waren om ze te berekenen. In hoofdstuk 2, werd een numerieke techniek geïmplementeerd, de Backward Incremental methode, op EE plaque modellen en de invloed van de initiële spanningen op kap spanningen werd bestudeerd. De invloed was afhankelijk van de plaque geometrie en varieerde van -55% tot +50%. Er werd geconcludeerd dat de initiële spanningen in EE plaque modellen noodzakelijk zijn voor nauwkeurige spanning berekeningen. Echter, de relatie tussen geometrische kenmerken en kap spanningen veranderde niet. Parametrische studies die de invloed van de plaque geometrie op kap spanningen bestuderen zullen de initiële spanningen dus niet hoeven berekenen.

In hoofdstuk 3 werd de invloed onderzocht van de axiale resolutie van plaque beeldvorming op de plaque en kap spanningen, op basis van hoge resolutie histologie data. De axiale resolutie heeft geen effect op de algemene verdeling van de spanningen en de locatie van de maximale kap spanning, maar beïnvloedt wel de absolute kap spanningswaarden. Er is geen systematische afwijking gevonden in het effect van de axiale resolutie op de kap spanningswaarden. Vergelijkbare relaties tussen de kap dikte en de maximale kap spanning zijn waargenomen voor de verschillende axiale resolutie modellen. Er werd geconcludeerd dat 2D plaque modellen volstaan voor het bepalen van algemene relaties tussen geometrische kenmerken en kap spanningen, maar dat 3D modellen met een hoge axiale resolutie nodig zijn voor betrouwbare, plaque specifieke spanning berekeningen.

In hoofdstuk 4 werd de invloed van geometrische kenmerken van de plaque en de stijfheid van de intima op de kap spanningen onderzocht met een uitgebreide parametrische studie, op basis van geïdealiseerde 2D EE modellen. Voor relatief stijve intima modellen waren de fibreuze kap dikte en de dikte van de vetrijke kern de belangrijkste geometrische kenmerken. Een dunnere kap en een dikkere vetrijke kern verhoogde de kap spanning. Voor relatief zachte intima modellen was de kap dikte minder invloedrijk en had de vetrijke kern dikte een sterker effect op de kap spanningen. De hoek van de vetrijke kern was net zo invloedrijk als de kap dikte in de zachte intima modellen. Met deze studie is aangetoond dat stijfheid van de intima een belangrijke rol speelt in het berekenen van de juiste spanningen en dat de stijfheid van intima van een plaque daarom goed moet worden bepaald.

In hoofdstuk 5 werd verder onderzocht wat de invloed was van de geometrie van de plaque op de kap spanningen en hoe dit afhangt van de intima stijfheid,

op basis van realistische plaque geometrieën. De 2D EE modellen waren gebaseerd op histologische secties van humane coronaire plaques. De analyse bevestigde dat de kap dikte een belangrijke parameter is in de spanningsanalyse. In tegenstelling tot de bevindingen in hoofdstuk 4, was de grootte van de vetrijke kern niet van invloed op de kap spanning, wat kon worden toegeschreven aan de complexe structuur van de realistische plaque geometriën ten opzichte van de geïdealiseerde geometrieën. De diameter van het lumen was ook een risicofactor voor hoge kap spanningen in de realischtische geometriën, omdat een groter lumen leidde tot hogere kap spanningen. De studie toonde verder aan dat een surrogaat parameter, gedefiniëerd als de verhouding van de lumendiameter en de kap dikte, kan worden gebruikt om plaques met lage kap spanning scheiden van plaques met hoge kap spanning.

In hoofdstuk 6 zijn experimentele studies uit de literatuur beoordeeld, die de stijfheid van atherosclerotische humane intima hadden bepaald. De belangrijkste conclusie was dat de experimentele gegevens zeldzaam zijn en een breed scala van stijfheden bestrijkt (30 tot 250x103 kPa). In het algemeen waren de gerapporteerde stijfheden bepaald met trekexperimenten hoger dan de stijfheden bepaald met compressie experimenten. Echter, er kon geen relatie aangetoond worden tussen de intima stijfheid en het vasculaire gebied waar de plaque vandaan kwam, of het type plaque dat getest was. Het hoofdstuk benadrukte het ontbreken van voldoende experimentele gegevens over atherosclerotische intima eigenschappen, en de behoefte aan meer en betere gedocumenteerde experimentele studies.

De eigenschappen van atherosclerotische humane plaques werden onderzocht in hoofdstuk 7, met behulp van axiale compressie experimenten. De combinatie van compressie experimenten en inverse EE analyse werd gebruikt om de lokale intima eigenschappen te schatten. De resultaten toonden een grote variatie in intima stijfheid (tussen 5 en 900 kPa) en de gemiddelde waarden waren in het onderste bereik van de gerapporteerde literatuur waarden. Collageen rijke intima was gemiddeld stijver dan collageen arme intima (30 kPa versus 15 kPa). Er was geen statistisch significant verschil tussen gestructureerde en ongestructureerde collageen regios, of tussen de verschillende regios van atherosclerotische intima.

In hoofdstuk 8 werd een methode gepresenteerd om het materiaalgedrag van de atherosclerotische intima te onderzoeken, onder meer fysiologische omstandigheden. Hoge resolutie radiofrequentie data van invasieve echografie werden gebruikt om de vervorming tijdensinflatie van een arterie met plaque te

meten. 2D EE modellen werden verkregen met een nieuwe techniek die histologie and echografie beelden met elkaar combineert. De modellen simuleerden de vervorming van de plaque, zoals gemeten in de inflatie experimenten. De intima stijfheid van atherosclerotische plaques werd geschat door het vergelijken van de gemeten en de berekende vervormingen. Dit onderzoek demonstreerde een niet-destructieve werkwijze waarmee de materiaaleigenschappen van een atherosclerotische plaque kan worden bepaald, onder fysiologische omstandigheden en in een omgeving vergelijkbaar met de in vivo omgeving.

In conclusie, met de studies in dit proefschrift zijn belangrijke stappen voorwaarts gemaakt om risicofactoren van hoge kap spanningen te begrijpen en om betrouwbare spannings data van atherosclerotische plaques te verkrijgen, wat een onvermijdelijke voorwaarde is voor ruptuur risicobeoordeling. Er werd aangetoond dat een beter begrip van de materiaaleigenschappen van de atherosclerotische intima is vereist voor het nauwkeuriger modelleren van atherosclerotische plaques. De variabiliteit in materiaaleigenschappen en plaque geometrie vereist plaque specifieke materiaaleigenschappen en modellering. Onzekerheden in materiaaleigenschappen en geometrische eigenschappen moeten in EE plaque modellen worden opgenomen. Voor plaque specifieke risico analyse dienen 3D-modellen met initiële spanningen gebruikt te worden, waarbij de geometrieën worden verkregen met beeldvormingstechnieken die de geometrie van de fibreuze kap en de vetrijke kern in detail kunnen weergeven met een hoge resolutie, in de transversale en axiale richting. Aan deze eisen moet worden voldaan voordat we in staat zijn om biomechanische plaque modellen te genereren voor betrouwbare ruptuur risicobeoordeling.

Acknowledgement

"Some people think power is all about money or running big companies with hundreds of employees. If you are not interested in such a power, ladies and gentlemen, if you are curious about power and force just as Leonardo da Vinci was, I invite you to the science of mechanics. It is a long and tough journey. Please, never give up on the way and hold on to it."

(Adapted from a speech of Prof. Dr. Mustafa Inan, 1911-1967, former head of the Mechanical Engineering Department of Istanbul Technical University)

The historical words of Prof. Dr. Mustafa Inan to his students summarize very well my major motivation for being a researcher: I am curious about power and force the way Leonardo was. This curiosity translated into a desire and led me to a quest for explanations to biomechanical phenomena. The book you hold in your hands contains some of the first steps -hopefully preceding many others in the future- in this quest of mine.

This book would not exist without the help and support of some other people, thus, I owe them a big "THANK YOU!'.

First, I would like to thank **Ton**, not only for being my promoter but also for the excellent work environment he provides us, as the head of the Biomedical Engineering Department of Erasmus MC. Ton, it was a privilege for me to do my PhD in your very successful group!

I also owe a huge thank to you, **Frank**. Both for your great scientific input to my PhD work and for your positive and comforting attitude to your students… I am very glad that you were my supervisor throughout these years.

Next, I want to thank my PhD committee. **Aad** and **Harald**, thank you so much for all your contribution to my work via our fruitful discussions. **Jenny**, it was an honor for me to have you in my committee.

About the Author

Ali Çağdaş Akyıldız was born on November 23, 1982 in Istanbul, Turkey. He completed his high school education in the Mathematics & Science Division of Istanbul Lisesi in 2001. In the same year he started his undergraduate study in the Department of Mechanical Engineering at Bogazici University. After obtaining his Bachelor of Science degree in 2006, he enrolled in the Master Program of the same department. He obtained his Master of Science degree in 2008 with his dissertation entitled "*Modeling of Micropipette Aspiration of Flaccid Human Red Blood Cells Using Finite Elements".* In 2009, he joined the Biomechanics Research Group of the Biomedical Engineering Department at Erasmus University Medical Center as a Ph.D. student. His Ph.D. project focused on biomechanical modeling of atherosclerotic plaques and its result is now in your hands.

Publications

Akyildiz AC, Speelman L, van Brummelen H, Gutiérrez MA, Virmani R, van der Lugt A, van der Steen AF, Wentzel JJ, Gijsen FJ, *Effects of Intima Stiffness and Plaque Morphology on Peak Cap Stress*, Biomed Eng Online., 2011;10:25

Speelman L, **Akyildiz AC**, den Adel B, Wentzel JJ, van der Steen AF, Virmani R, van der Weerd L, Jukema JW, Poelmann RE, van Brummelen EH, Gijsen FJ. *Initial stress in biomechanical models of atherosclerotic plaques*, J Biomech., 2011; 44(13):2376-82

Nieuwstadt HA, **Akyildiz AC**, Speelman L, Virmani R, van der Lugt A, van der Steen AF, Wentzel JJ, Gijsen FJ. *The influence of axial image resolution on atherosclerotic plaque stress computations*, J Biomech., 2012; 44(13):2376-82

Chai C-K, **Akyildiz AC**, Speelman L, Gijsen FJ, Oomens CWJ, van Sambeek MRHM, van der Lugt A, Baaijens FPT. *Local axial compressive mechanical properties of human carotid atherosclerotic plaques: characterisation by indentation test and finite element inverse analysis*, J Biomech. 2013; 46:1759-1766

Akyildiz AC, Speelman L, Gijsen FJ. *Mechanical properties of human atherosclerotic intima tissue*, J Biomech., 2013, accepted for publication

Walsh MT, Cunnane EM, Mulvihill JJ, **Akyildiz AC**, Gijsen FJ, Holzapfel GA. *Uniaxial tensile approaches for characterization of atherosclerotic plaques*, J Biomech., 2013, accepted for publication

Akyildiz AC, Speelman L, Nieuwstadt HA, van Brummelen H, Virmani R, van der Lugt A, van der Steen AF, Wentzel JJ, Gijsen FJ. *Influence of Plaque Morphology on Peak Cap Stress in Human Coronary Arteries*, submitted

PhD Portfolio

Courses

8th PhD course "in-vivo NMR" (Radboud University)	2009
Pathophysiology in Ischemic Heart Disease (COEUR)	2009
Cardiovascular Imaging and Diagnostics	2010
Summer School on Modeling and Mechanobiology (Graz University)	2010
NIHES-Introduction to Data Analysis (ESP03)	2010
NIHES-Regression Analysis (ESP09)	2010
Biomedical English Writing and Communication	2011

Seminars and Workshops

Workshop Animal Imaging by AMIE: From Mouse to Man	2009
Vascular Imaging: Atherosclerosis and Biomechanics (COEUR)	2009
PhD Day (COEUR)	2010
Extracellular Matrix in Vascular Disease (COEUR)	2010
Detection of early atherosclerosis (COEUR)	2010
Heart valve implantation (COEUR)	2011
Translating Coronary Physiology and Biophysics to Clinical Applications	2012

Teaching activities

Lecturing in Minor Program 2010	2010
Supervising a BSc student	2010
Supervising a BSc student	2011
Lecturing in Minor Program 2011	2011
Supervising a MSc student	2012
Supervising a MSc student	2013

Podium Presentations

Coeur Seminar: Vascular Imaging in Atherosclerosis and Biomechanics	2010
6th World Congress of Biomechanics	2010
3rd Dutch Biomedical Engineering Conference	2011
ASME 2012 Summer Bioengineering Conference	2012
ASME 2013 Summer Bioengineering Conference	2013

Poster Presentations

4th International Symposium on Biomechanics in Vascular Biology and Cardiovascular Disease	2009
ASME 2010 Summer Bioengineering Conference	2010
5th International Symposium on 'Biomechanics in Vascular Biology and Cardiovascular Disease	2010
Artery11 Symposium	2011
ASME 2011 Summer Bioengineering Conference	2011
6th International Symposium on 'Biomechanics in Vascular Biology and Cardiovascular Disease	2011
ASME 2012 Summer Bioengineering Conference	2012
7th International Symposium on 'Biomechanics in Vascular Biology and Cardiovascular Disease	2012
4th Dutch Biomedical Engineering Conference	2013
8th International Symposium on 'Biomechanics in Vascular Biology and Cardiovascular Disease	2013